

論文 / 著書情報
Article / Book Information

題目(和文)	強誘電体における電気光学効果の起源と解釈
Title(English)	Origin and interpretation of electro-optic effect in ferroelectrics
著者(和文)	武田浩太郎
Author(English)	Koutarou Takeda
出典(和文)	学位:博士(工学), 学位授与機関:東京工業大学, 報告番号:甲第8652号, 授与年月日:2012年3月26日, 学位の種別:課程博士, 審査員:鶴見 敬章
Citation(English)	Degree:Doctor (Engineering), Conferring organization: Tokyo Institute of Technology, Report number:甲第8652号, Conferred date:2012/3/26, Degree Type:Course doctor, Examiner:
学位種別(和文)	博士論文
Type(English)	Doctoral Thesis

Origin and Interpretation of Electro-optic Effect in Ferroelectrics

Kotaro Takeda

Tokyo Institute of Technology
Graduate school of Science and Engineering
Department of Metallurgy and Ceramics Science

Origin and Interpretation of
Electro-optic Effect in Ferroelectrics

by

Kotaro Takeda

Submitted to the Department of Metallurgy and Ceramics Science in

fulfillment of the requirement for the degree of

Doctor of Philosophy in Inorganic Materials

at the

TOKYO INSTITUTE OF TECHNOLOGY

January 2011

© Tokyo Institute of Technology 2011. All right reserved.

Author

Kotaro Takeda

Department of Metallurgy and Ceramics Science

Certificated by

Professor Takaaki Tsurumi

Professor kazuo Shinozaki

Professor Akira Nakajima

Associate Professor Hiroaki Takeda

Associate Professor Masahiro Miyauchi

Contents

Chapter 1. Introduction	1
1.1 Preface	1
1.2 Electro-optic effect	2
1.3 Transparent EO ceramics	7
1.3.1 Lithium niobate	8
1.3.2 Lanthanum added lead zirconate titanate	8
1.3.3 Potassium tantalite niobate	10
1.3.4 Strontium barium niobate	11
1.4 Relaxation of driving efficiency in EO modulator	12
1.5 Pioneer work for origin of EO effect	15
1.6 Objective and organization of thesis	17
Chapter 2. Electro-optic effect and piezoelectric resonance	27
2.1 Introduction	27
2.1.1 Influence of piezoelectric effect to EO effect	27
2.1.2 Objective	29
2.2 Experimental procedure	29
2.2.1 Measurement system for EO effect	29
2.2.2 Measurement of piezoelectric effect around piezoelectric resonance frequency	31
2.2.3 Evaluation of EO effect	32
2.3 Result and discussion	33
2.3.1 Evaluation of EO coefficient in LN single crystal	33
2.3.2 Contribution to EO effect due to piezoelectric effect	35
2.3.3 Frequency dependence of EO coefficient	35
2.3.4 Analysis on EO effect around piezoelectric resonance	37
2.3.4.1 Retardation caused by the clamped Pockels effect	37
2.3.4.2 Retardation caused by the change of light path length	38
2.3.4.3 Retardation caused by the photo-elastic effect	39
2.3.4.4 Contribution to EO effect due to the phase lag	42
2.4 Summary of chapter 2	48

Chapter 3. Electric field dependence of birefringence and dielectric permittivity51

3.1	Introduction	51
3.1.1	Dielectric tunability and electro-optic effect	51
3.1.2	Objective	53
3.2	Experimental procedure	53
3.2.1	Sample preparation	53
3.2.2	Characterization of BST thin film	53
3.2.3	Formation of micro-sized planar electrodes	55
3.2.4	Measurement of dielectric tunability	56
3.2.5	Measurement system for EO effect	60
3.2.6	Evaluation of EO effect	62
3.3	Result and Discussion	62
3.3.1	Epitaxy and lattice distortion of BST film	62
3.3.2	Electric property of BST film	64
3.3.3	Dielectric tunability of BST thin film	66
3.3.4	Polarizing direction dependence of EO effect	68
3.3.5	Comparison of electric field dependence of birefringence and dielectric permittivity	76
3.4	Summary of chapter 3	79

Chapter 4. Relaxation and frequency dependence of electro-optic coefficient85

4.1	Introduction	85
4.1.1	Relaxation of dielectric permittivity and driving efficiency in EO modulators	85
4.1.2	Objective	87
4.2	Experimental procedure	87
4.2.1	Measurement of dielectric permittivity at low frequency	87
4.2.2	Methodology of micro-sized planar electrodes method	88
4.2.3	Designing of micro-sized planar electrodes	90
4.3	Result and discussion	94
4.3.1	Determination for dielectric permittivity up to GHz	94
4.3.2	Expansion of equation for EO effect	99

4.3.3 Calculation of driving efficiency due to EO effect	102
4.4 Summary of chapter 4	104

Chapter 5. Lattice distortion and variation of birefringence

.....	109
5.1 Introduction	109
5.1.1 EO coefficient g in dielectrics	109
5.1.2 Objective	112
5.2 Experimental procedure	112
5.2.1 Measurement of EO effect	112
5.2.2 Measurement of Electrostrictive effect	113
5.2.3 Measurement of polarization	114
5.3 Result and discussion	114
5.3.1 Expectation for origin of EO effect	114
5.3.2 Expansion of equation for EO coefficient g	115
5.3.3 Verification for expanded equation	117
5.3.3.1 Clausius-Mossotti relation and photo-elastic coefficient	117
5.3.3.2 Calculation of photo-elastic coefficient by expanded equation	120
5.3.3.3 Relation between electrostrictive coefficient and electron density	119
5.4 Origin of EO effect and principle for development of material with high EO property	124
5.5 Summary of chapter 5	125

Chapter 6. Electro-optic effect of Bi-based relaxor129

6.1 Introduction	129
6.1.1 Features for high EO property	129
6.1.2 Objective	130
6.2 Experimental procedure	130
6.2.1 Fabrication of 67BNT33BKT	130
6.2.2 Measurement of EO effect	131
6.2.3 Measurement of electrostrictive effect	132
6.2.4 Measurement of polarization	132

6.2.5	Measurement of dielectric dispersion	132
6.3	Result and discussion	133
6.3.1	Characterization of 67BNT33BKT	133
6.3.2	EO coefficient of 67BNT33BKT	137
6.3.3	Photo-elastic coefficients of 67BNT33BKT	139
6.3.4	Frequency dependence of EO coefficient of 67BNT33BKT	142
6.4	Summary of chapter 6	144
Chapter 7. Summary		149
List of Publication		153
Acknowledgement		155

Chapter 1

Introduction

1.1 Preface

The electro-optic (EO) effect, which is the change of refractive index with an external applied electric field^{1,2}, is manifested in certain materials which show tremendous promise of applications. Compared with other devices, the ceramic EO components, in general, possess advantages in terms of their response speed (GHz), low driving voltage³⁻⁷. Since the 1960s the EO effect of ferroelectrics has been investigated rather extensively⁸⁻¹⁴, and various EO devices have been developed such as laser beam deflectors^{3,15-19}, variable focus lenses^{4,20,21}, and optical modulators²²⁻³². Especially we focused on the optical modulator that is key device to achieve the next high speed information network. The present driving method in optical modulators such as DPSK, QPSK and 256QAM require higher EO coefficient than LN single crystal although conventional optical modulator employed Lithium niobate (LN) single crystal³³⁻³⁶. Therefore alternative material with higher EO coefficient was required to achieve high speed optical modulators. However, the alternative EO material has not been developed yet because we only had little experimental rules to develop materials with high EO coefficient. To build the principle for development of alternative EO materials, elucidation for origin of EO effect is necessary. This dissertation tried to elucidate the mechanism of EO effect to build the principle for development of material with high EO property.

Following section describe present trend and problems of optical modulator and EO materials, pioneer work for elucidation to origin of EO effect, and motivation of this study.

1.2 Electro-optic effect

Since light is an alternating electromagnetic wave with electric and magnetic field variation directions mutually perpendicular to one another, the electric field induces an electric polarization in a dielectric crystal and the light it self is influenced by the crystal. The alternative frequency of the light is so high (PHz = 10^{15} Hz) that only the electronic polarization can follow the electric field change, and the relative permittivity of an optically transparent crystal is small, not exceeding 10. The relative permittivity ϵ at this frequency is related to the refractive index n by the following equation:

$$\epsilon = n^2 \quad (1.1)$$

When an external electric field is applied to the crystal, ion displacement is induced, deforming the shape of the electron cloud, and consequently the refractive index is changed. This phenomenon is called the EO effect. Generally, the refractive index is treated as a symmetrical second-rank tensor quantity and is represented geometrically by the optical indicatrix as shown in Fig. 1(a) that is described by

$$\frac{x^2}{n_1^2} + \frac{y^2}{n_2^2} + \frac{z^2}{n_3^2} = 1, \quad (1.2)$$

where n_1, n_2, n_3 are the principal refractive indices^{1,2}. With the application of an electric field, the change in refractive index is given by an expansion expression:

$$\frac{1}{n_{ij}(E)^2} + \frac{1}{n_{ij}(0)^2} = \sum r_{ijk} E_k + \sum R_{ijkl} E_k E_l. \quad (1.3)$$

Here $n(E)$ and $n(0)$ are the refractive indices at E and zero field, respectively, and r_{ijk} is the linear EO coefficient called Pockels coefficient and R_{ijkl} is the quadratic EO coefficient called Kerr coefficient.

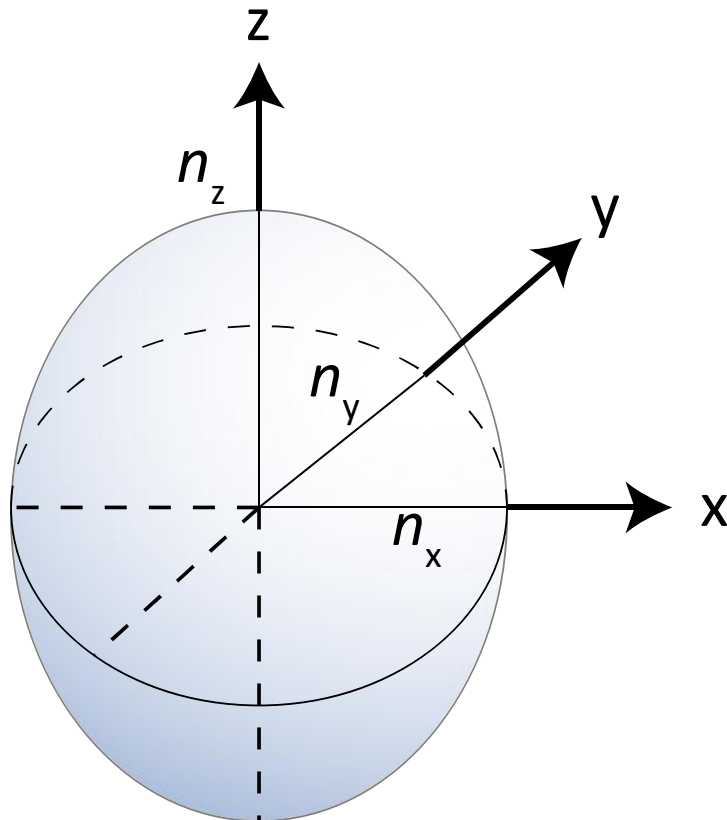


Fig. 1.1(a) Model of Optical indicatrix

Considering the ferroelectric phase of perovskite crystal (4mm) as an example, the optical indicatrix indicates uniaxial ellipsoid as shown in Fig. 1(b). The refractive indices along isotropic direction n_1 and n_2 are called ordinary refractive indices described as n_o . The refractive index along z axis n_3 is called extraordinary refractive index described as n_e .

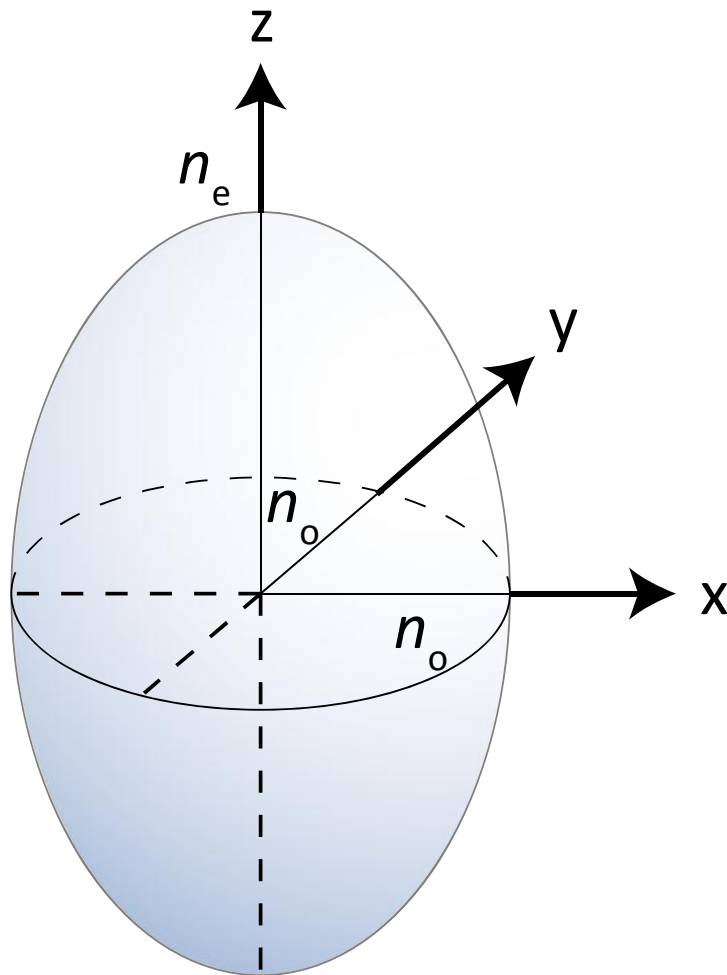


Fig. 1.1(b) Model of Optical indicatrix in uniaxial crystal

The Pockels coefficients are represented in the following matrix:

$$\begin{matrix} 0 & 0 & 0 & 0 & r_{15} & 0 \\ 0 & 0 & 0 & r_{15} & 0 & 0 \\ r_{31} & r_{31} & r_{33} & 0 & 0 & 0 \end{matrix} \quad (1.4)$$

so that the refractive indicatrix under electric field applied the z direction is expressed as:

$$\frac{x^2 + y^2}{n_0^2(1 - \frac{n_0^2}{2} r_{31} E_z)^2} + \frac{z^2}{n_e^2(1 - \frac{n_e^2}{2} r_{33} E_z)^2} = 1. \quad (1.5)$$

When light is transmitted along the y direction, the variation of birefringence by EO effect ($\delta(\Delta n)$) is given by

$$\delta(\Delta n) = \delta n_e - \delta n_o = n_e(-\frac{n_e^2}{2} r_{33} E_z) - n_o(-\frac{n_o^2}{2} r_{31} E_z) = -\frac{n_e^3 r_c}{2} E_z \quad (1.6)$$

$$r_c = r_{33} - (\frac{n_o}{n_e})^3 r_{31} \quad (1.7)$$

Generally, the EO effect is not evaluated by variation of refractive indices but by variation of birefringence.

The refractive index change under an external electric field is explained intuitively as follows. When an electric field E_z is applied to a cubic perovskite crystal, the crystal is elongated along the z-axis and contracted along both the x and y axes. Consequently, the material's density or compactness will be decreased along the z axis and densified along the x and y axes, leading to decrease in the refractive index n_z and an increase of the indices n_x and n_y as shown in Fig. 1.1(c). (Note that the refractive index is proportional to the electron density or ion

compactness along the polarized light electric field direction which is perpendicular to the light propagation direction.)

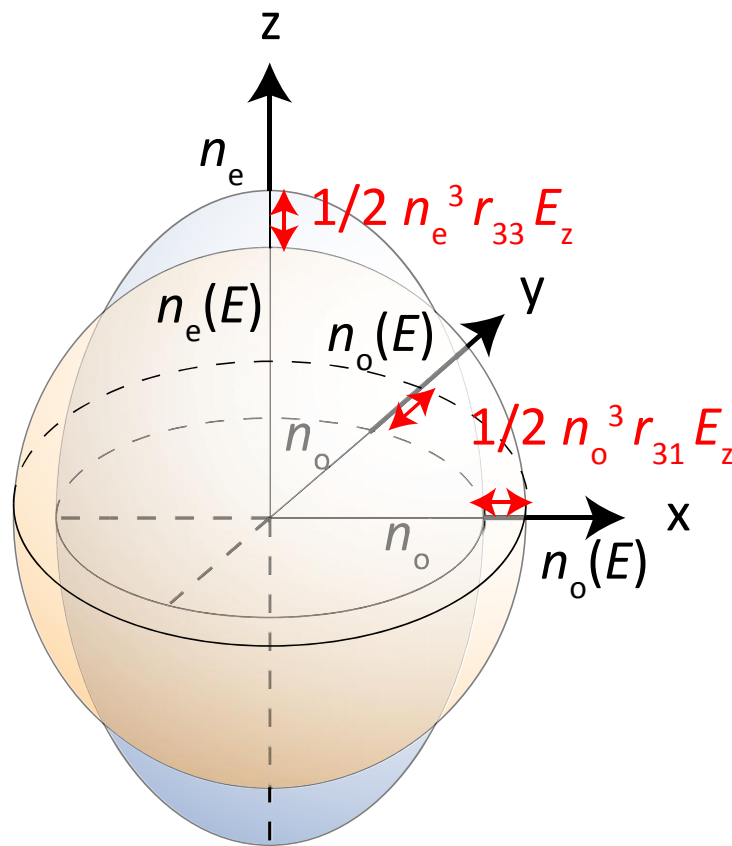


Fig. 1.1(c) Model of Optical indicatrix in uniaxial crystal. Blue ellipsoid indicates optical indicatrix without electric field. Red ellipsoid indicates optical indicatrix with applying external electric field. Red equations indicate the differences of refractive index caused by EO effect.

Placing the crystal between crossed polarizer and analyzer arranged at 45° angle with respect to the z axis, the output light intensity is modulated as a function of applied voltage as shown in Fig. 1.2. This is the principle behind the operation of a longitudinal optical modulator.

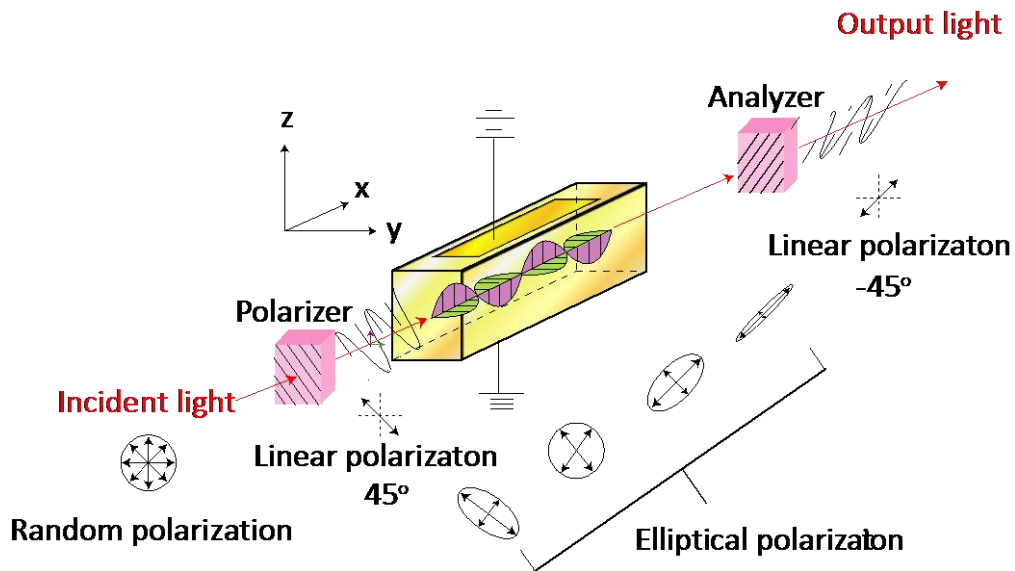


Fig. 1.2 Model of modulation by EO effect. A linear polarized light is separated in each crystal directions and modulated by each EO effect. So output light does not show same polarization from incident light.

1.3 Transparent EO ceramics

Along with the development of various EO devices, various EO materials have been developed. This section describes the fundamental electro-optic properties of conventional EO materials.

1.3.1 Lithium niobate

Lithium niobate (LiNbO_3 , LN) single crystals are the most popular EO materials and widely applied for optical modulator³⁷⁻⁴⁰. It has trigonal crystal system, which lacks inversion symmetry and displays ferroelectricity, Pockels effect, piezoelectric effect, photo-elasticity. It generally has good transparency in a wavelength range extending from the visible to infrared⁴¹⁻⁴³, and does not exhibit chirping that is wavelength shift by passing through the EO materials. They show relatively high EO coefficient (Pockels coefficient $r_c = 16 \times 10^{-12}$ m/V). However, as mentioned above, the present driving method in optical modulators such as DPSK, QPSK and 256QAM require higher EO coefficient. Therefore the development of alternative EO materials with more high EO efficiency will be required in more high speed modulators.

1.3.2 Lanthanum added lead zirconate titanate

Lanthanum added lead zirconate titanate ($\text{Pb}_{1-x}\text{La}_x\text{Zr}_{1-y}\text{Ti}_y\text{O}_3$, PLZT) are transparent polycrystalline ceramics and thin films studied as optical, electrical, mechanical materials because of their attracted properties⁴⁴⁻⁵¹. The polycrystalline microstructure of a ferroelectric ceramics can also exhibit the electro-optic effect if it is sintered to pore-free state to make it transparent. Figure 1.3 shows the phase diagram of the system⁵², on which is indicated the electro-optic effects manifested for various phase regions. The electro-optic coefficients of the PLZT system are much larger than the values in conventional EO crystals⁵³⁻⁵⁶ such as LiNbO_3 ³⁷⁻⁴⁰ and $\text{Ba}_{1-x}\text{Sr}_x\text{TiO}_3$ ⁵⁷⁻⁶² as shown in Table 1.1, which means that the modulator size is shorter for the PLZT. However, they don't have good

transparency in a wavelength range extending from the visible to infrared⁶³⁻⁶⁵, and lead toxicity is a serious matter concern for mass production. Therefore, they have not been replaced from LN modulator though they indicate high EO properties.

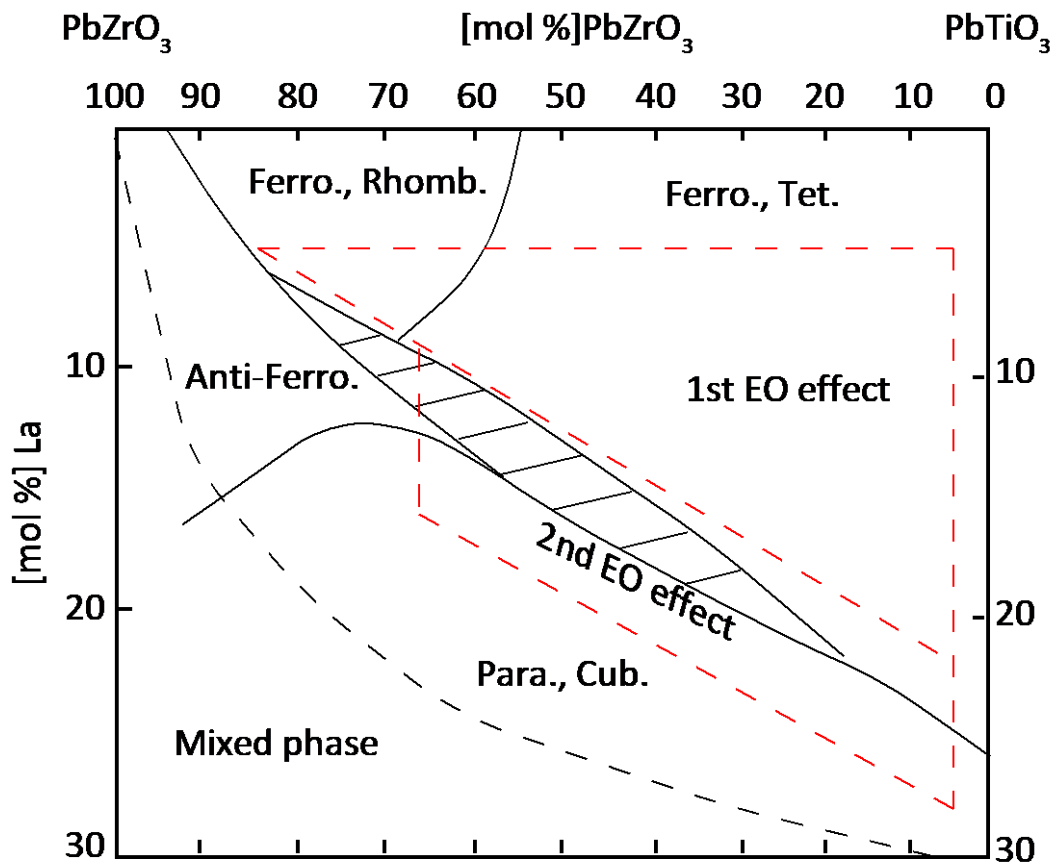


Fig. 1.3 Relation between PLZT composition and structure and electro-optic application.

Table 1.1 EO coefficient of conventional EO materials. (a) Pockels coefficient, (b) Kerr coefficient.

(a)		
Material	r_c ($\times 10^{-12}$ m/V)	Ref.
LiNbO ₃	0.16	37-40
KH ₂ PO ₄	0.52	106-108
Pb _{0.8} La _{0.2} Zr _{0.65} Ti _{0.35} O ₃	5.23	53-56,108
(Sr _{0.75} Na _{0.25})Nb ₂ O ₆	13.5	76-82,108

(b)		
Material	R_c ($\times 10^{-16}$ m/V)	Ref.
Ba _{0.5} Sr _{0.5} TiO ₃	0.42	57-62
Pb _{0.9} La _{0.1} Zr _{0.65} Ti _{0.35} O ₃	0.8	53-56,108
Pb _{0.91} La _{0.09} Zr _{0.65} Ti _{0.35} O ₃	3.8	53-56,108
KTa _{0.65} Nb _{0.35} O ₃	48	66-69,108

1.3.3 Potassium tantalite niobate

Potassium tantalite niobate (KTa_{0.65}Nb_{0.35}O₃, KTN) single crystals exhibit a large EO effect ($R_c = 4.8 \times 10^{-15}$ m²/V²) around the paraelectric to ferroelectric phase transition temperature T_c ⁶⁶⁻⁶⁹. The variation in the Ta/Nb ratio enables us to change T_c in a -273 to 435 °C temperature range. The crystal composition was adjusted to Ta/Nb = 1.85 which yielded a T_c of about 35 °C. The crystal temperature was kept at 5 °C above T_c to obtain a large EO effect. Though KTN has attractive EO property, no KTN-based waveguides had yet been reported because it is very difficult to grow optical quality KTN single crystals due to their inherent

characteristics⁷⁰⁻⁷². Recently, high-quality and large-size KTN crystals were prepared by S. Yagi⁷³. This large-size and high quality KTN single crystals were expected as alternative EO materials. Actually the optical beam deflectors^{3,74,75} and variable focusing lens⁴ using KTN single crystals were reported. However, the KTN single crystals are not appropriate applying to EO modulator because of their high dielectric permittivity. KTN single crystals indicates large dielectric permittivity ($\epsilon_r = 30000$) at 5 °C above T_c to obtain a large EO effect. A material with high permittivity is difficult to match the characteristic impedance to signal generator so that it needs the insulator layer to control the impedance of optical modulator^{33,34}.

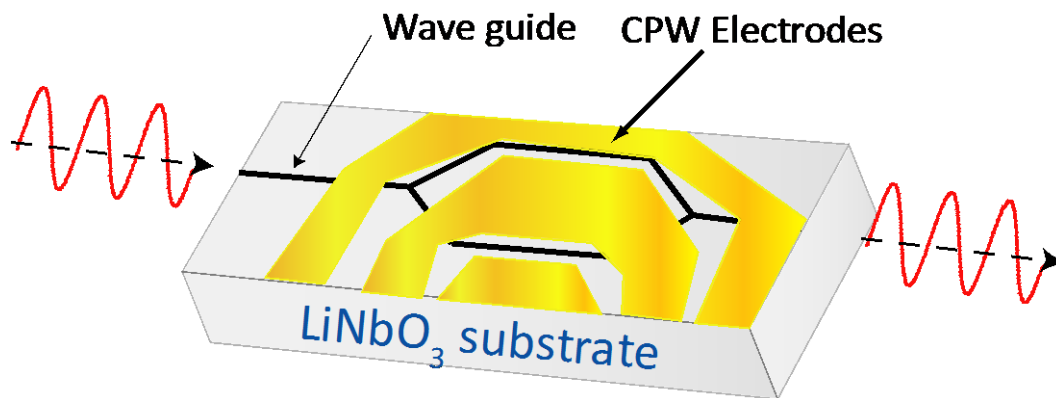
1.3.4 Strontium barium niobate

Strontium barium niobate ($(\text{Sr}_x\text{Ba}_{1-x})\text{Nb}_2\text{O}_6$, SBN) single crystal and thin film exhibit a large EO effect ($r_c = 1350 \times 10^{-12}$ m/V) in $x = 0.75$ ⁷⁶⁻⁸². The EO coefficient of SBN is larger than that of PLZT, however no devices were developed using SBN because it indicate strong hysteresis in birefringence between before and after applying electric field⁸³.

Thus, all materials introduced in this paper did not achieve requirements for alternative EO material to LN single crystal therefore the alternative EO material has not been developed yet.

1.4 Relaxation of driving efficiency in EO modulator

The coplanar waveguide (CPW) electrode is commonly used as a traveling-wave electrode for LN optical modulators because it provides good connection to an external coaxial line⁸⁴⁻⁸⁷. In a modulator with a traveling-wave electrode, the modulation bandwidth is limited by the difference between the velocity of the optical wave and that of a microwave, the characteristic impedance of the electrode, and the propagation loss of the electrode. To date, obtaining this velocity matching condition is treated as one of the aims of structure design. A conventional LN modulator consists of LN substrate, a buffer layer of silicon oxide, and a CPW gold-plated electrode. Fig. 1.4 shows a top view and a cross section of a Mach-Zehnder type optical modulator with CPW electrode.



(a)

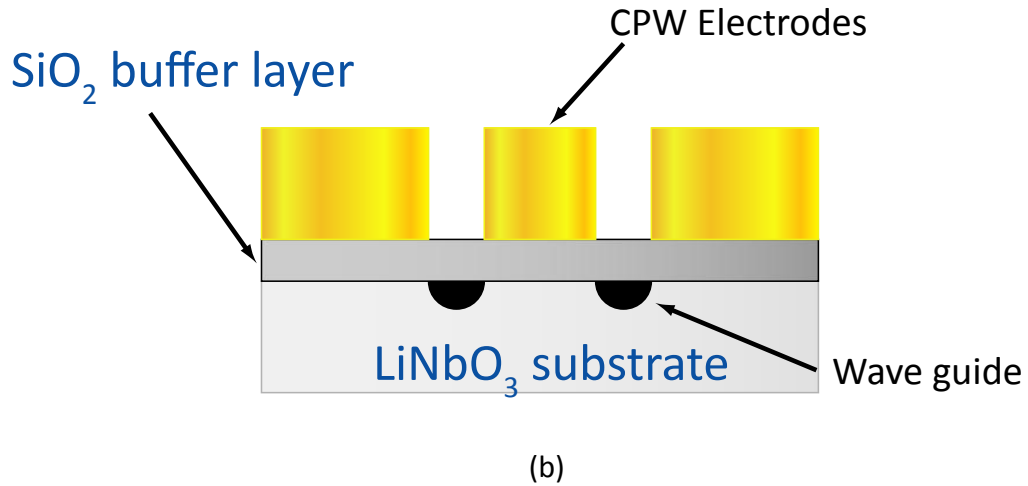


Fig. 1.4 Top view (a) and cross section (b) of the ridged Mach-Zehnder optical modulator.

A titanium-diffused waveguide is formed in LN substrate. The substrate is coated with a buffer layer of silicon oxide. A CPW gold electrode is formed on the buffer layer. For the velocity matched modulator, half wave voltage is 3 to 5.5 V²⁸⁻³² and a driving efficiency remains constant with varying the frequency of applied electric field up to 70GHz as shown in Fig. 1.5. Driving efficiency is determined by EO coefficient therefore the EO coefficient of LN single crystals remain constant with varying frequency of electric field. However, this modulator required a modulator length $l = 3$ cm. It is the minimum length due to lack of EO coefficient in LN single crystal.

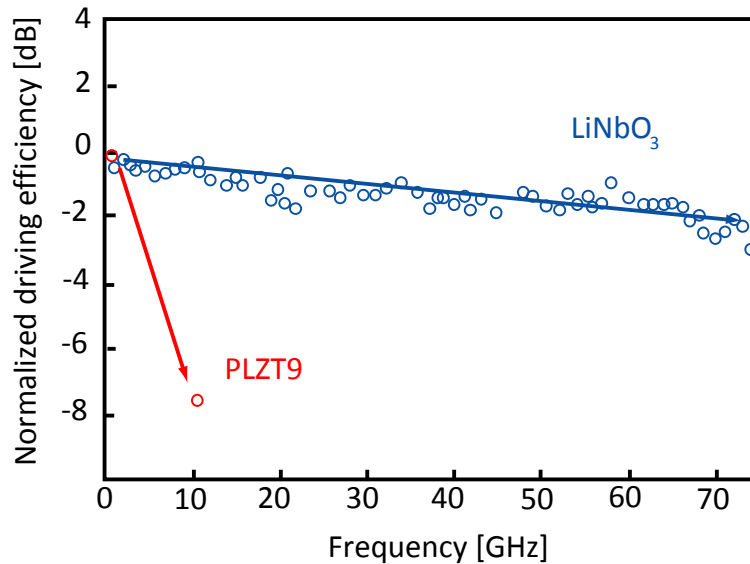


Fig. 1.5 Frequency dependence of driving efficiency in EO modulators using LN single crystal and PLZT9 ceramic normalized to driving efficiency at low frequency.

PLZT transparent ceramics that show higher EO properties than LN single crystals were also employed to EO modulators. Especially, a modulator length and half wave voltage of PLZT9 modulator were 10 mm and $11V^{88}$ in 10 GHz driving. They need higher half wave voltage but overwhelming miniaturization was achieved because of their high EO coefficients. However EO coefficient of PLZT9 shows relaxation with varying a frequency of applied electric field⁸⁹. The driving efficiency of PLZT9 at 10GHz was 8dB lower than that at low frequency as shown in Fig. 1.5. PLZT9 shows relaxation though the driving principle is EO effect that is the same to LN.

Thus, it is indispensable to consider the relaxation of EO coefficient to developed material. We cannot apply the high EO coefficient at low frequency as

alternative EO material to LN single crystal if it shows large relaxation in driving frequency

1.5 Pioneer work for origin of EO effect

As mentioned above, the alternative EO materials to LN single crystal had not been developed yet. And EO materials show different frequency dependence respectively of EO coefficient. To develop the alternative material for EO modulators, a material search like a try-and-error is not effective, but a development based on a principle derived from the origin of EO effect is indispensable.

Pioneering work analyzing to the origin of EO effect in dielectrics was reported by several workers⁹⁰⁻⁹⁴. M. Didomenico and S. Wemple proposed that the EO coefficient normalized a number of oxygen octahedral (BO_6) in unit cell are all same in materials with oxygen octahedral structure despite the species of B site ions is different^{90,91}. This result is derived from phenomenological analysis for oxygen octahedral. Therefore all cubic dielectrics show the same EO coefficient. The differences of EO coefficients are caused by the differences of polarization and other parameters induced by anisotropic crystal structures. They concluded that the materials with high EO coefficient must be with high permittivity and spontaneous polarization. However, the analysis cannot be applied to the cubic relaxor materials and the ferroelectrics with diffuse phase transition (DPT ferroelectrics). They indicated relatively high EO coefficient

although they do not show high dielectric permittivity. In relaxor and DPT materials, it is believed that the fluctuations of dipole moments in polar nano-regions (PNRs) derive dipole polarization and it contributes to permittivity up to GHz region in the paraelectric symmetry⁹⁵⁻¹⁰². The PNRs are in paraelectric phase of relaxor materials and DPT ferroelectrics but they do not show anisotropy without electric field. The PNRs contribute to dielectric polarization with applied electric field therefore the relaxor materials and DPT ferroelectrics indicate high permittivity though their crystal structure is cubic. The change of polarization may induce the change of refractive index due to lattice distortion. This is why the relaxor materials and DPT ferroelectrics show exception from the analysis in Ref 90, 91. The change of polarization caused by PNRs was not considered in previous work undertaken by M. Didomenico and S. Wemple. Therefore another principle that can be applied to relaxor materials is necessary.

Moreover, influence of strain to EO effect is not negligible. M. Zgonik and G. Pauliat reported that the analysis for influence of strain due to piezoelectric displacement and proposed the novel equation including a contribution of strain^{92,93}. They separated influence of strain from EO effect from experimental result and concluded strain induced not only the change of light path length but also variation of birefringence. However, this equation did not consider the frequency dependence therefore it cannot be applied in high frequency. In order

to discuss about frequency dependence, formularization of new equation is indispensable.

In this way, we noted three problems: (i) previous work did not consider the relaxation in frequency dependence of EO coefficient, (ii) the relaxor materials show relatively high EO coefficient, and (iii) the influence of strain was not considered in previous works.

1.6 Objectives and organization of thesis

From the literature survey and the background described in 1.1 to 1.5, objectives of this study are as follows,

- 1) Elucidation to the origin of electro-optic effect
- 2) Development of a novel electro-optic crystal through the results in this research

In this study, we determined the origin of EO effect phenomenologically through solving problems (i) to (iii) described above. In order to accomplish the objective, this thesis was organized and undertaken thorough chapter 1 to 7 as follows,

In chapter 1, "Introduction"; from a literature survey, the background, the present problems and objective were described.

In chapter 2, "Electro-optic effect and piezoelectric resonance"; the novel equation for EO-effect around piezoelectric resonance frequency was formularized to figure out the influence of strain to EO effect that is problem (iii).

This novel equation explained the whole influences of strain to EO effect and it was firstly invented. Influences of strain to EO effect were quantified and the most susceptible influence was discussed.

In chapter 3, “Electric field dependence of birefringence and dielectric permittivity”; the electric field dependence of dielectric permittivity (dielectric tunability) and birefringence (electro-optic effect) of barium strontium titanate ($\text{Ba}_{1-x}\text{Sr}_x\text{TiO}_3$, BST) thin films were measured and the relation of polarization and birefringence variation with varying the electric field was discussed to figure out why the relaxor materials indicated the exceptions in previous work. This chapter solved the problem (ii).

In chapter 4, “Relaxation and frequency dependence of electro-optic coefficient”; the frequency dependence of dielectric permittivity in lanthanum added lead zirconate titanate ($\text{Pb}_{1-x}\text{La}_x\text{Zr}_{1-y}\text{Ti}_y\text{O}_3$, PLZT) ceramics was measured and discussed to figure out a relation between the relaxation of dielectric permittivity and EO coefficient in frequency dependence. An equation for EO effect including an influence of dielectric permittivity was derived and it elucidated the parameter determined the frequency dependence and relaxation of EO coefficient. This chapter solved the problem (i).

In chapter 5, “Variation of birefringence due to lattice distortion and polarization”; summarizing the results from chapter 2 to 4, the origin of EO effect was discussed in order to find out what parameter determines the EO coefficient. A novel equation for EO effect that can be applied to relaxor materials and including an influence of lattice distortion was derived. It elucidated the conditions to develop the EO materials with high EO coefficients.

In chapter 6, “Electro-optic effect of Bi-based relaxor”; EO property of lead-free Bi-based relaxor single crystal $67\text{Bi}_{0.5}\text{Na}_{0.5}\text{TiO}_3 - 33\text{Bi}_{0.5}\text{K}_{0.5}\text{TiO}_3$ (67BNT33BKT) was demonstrated. 67BNT33BKT single crystals satisfy all conditions derived from chapter 2 to 5 for new EO materials with high EO properties. The EO Property of 67BNT33BKT was discussed with a comparison of that of conventional EO materials.

In chapter 7, “Summary”; results obtained in this study were all simply summarized.

References

- [1]R. Newnham, Properties of materials: Anisotropy, Symmetry, Structure, (Oxford Univ. Pr.,Oxford, 2005)
- [2]T. Ogawa, Fundamentals on crystal technology, (Shokabo, Tokyo, 1998)
- [3] K. Nakamura, J. Miyazu, M. Sasaura, K. Fujiura, Appl. Phys. Lett. 89, 131115 (2006)
- [4]T. Imai, S. Yagi, S. Toyoda, M. Sasaura, NTT Tech. Journal, 24 (2009)
- [5]K. Noguchi, O. Mitomi, H. Miyazawa, J. Lightwave Tech. 16, 615 (1998)
- [6]D. Dolfi, M. Nazarathy, R. Jungerman, Elec. Lett. 24, 528 (1988)
- [7]K. Tokuhashi, K. Ashizawa, D. Ishii, T. Arakawa, N. Yamanaka, K. Wakayama, Trans. of High Performance Switching and Routing, 978 (2009)
- [8]L. Levinson, Elec. Ceram., (Marcel dekker, Newyork, 1988)
- [9]A. Kumada, K. Kitta, K. Kato, T. Komata, Proc. of Ferroelectric mat. and Appl. 2, 205 (1977)
- [10]K. Murano, Ceramic Trans. of 14 Electro-optics and nonlinear opt. mat., 283 (1990)
- [11]K. Uchino, K. Tokiwa, J. Giniewicz, Y. Murai, K. Ohmura, Ceramic Trans. of 14 Electro-optics and nonlinear opt. mat., 297 (1990)
- [12]K. Uchino, Ceram. international 21, 309 (1995)
- [13]M. Lines, A. Glass, Principles and applications of ferroelectrics and related materials, (Clarendon press, Oxford, 1977)
- [14]I. Kaminov, Trans. Microwave Theory and Techniques 23, 57 (1975)
- [15]F. Chen, J. Geusic, S. Kurtz, J. Skinner, S. Wemple, J. Appl. Phys 37, 388 (1966)
- [16]J. Lotspeich, Spectrum 5, 45 (1968)

- [17]Q. Chen, Y. Chiu, D. Lambeth, T. Schlesinger, D. Stancil, J. Lightwave Tech. 12, 1401 (1994)
- [18]J. Hsing, C. Cheng, M. Kawas, D. Lambeth, T. Schlesinger, D. Stancil, Photonics Tech. Lett. 8, 1486 (1996)
- [19]Y. Chiu, R. Burton, D. Stancil, T. Schlesinger, J. Lightwave Tech. 13, 2049 (1995)
- [20]M. Ye, B. Wang, S. Sato, Appl. Opt. 43, 6407 (2004)
- [21]T. Tatebayashi, T. Yamamoto, H. Sato, Appl. Opt., 30, 5049 (1991)
- [22]S. Toyoda, K. Fujiura, M. Sasaura, K. Enbutsu, A. Tate, M. Shimokozono, H. ushimi, T. Imai, K. Manabe, T. Matsuura, T. Kirihara Japanese J. Appl. Phys. 43, 5862 (2004)
- [23]G. Jin, Y. Zou, V. Fuflyigin, S. Liu, Y. Lu, J. Zhao, M. Cronin-Golomb, J. Lightwave Tech. 18, 807 (2000)
- [24]A. Wagner, S. Brueck, A. Wu, Ferroelectrics 116, 195 (1991)
- [25]R. Thapliya, S. Nakamura, J. Lightwave Tech. 21, 1820 (2003)
- [26]F. Liu, Q. Ye, F. Pang, J. Geng, R. Qu, Z. Fang, J. Opt. Sec. Am. B 23, 709 (2006)
- [27]T. Lin, A. Ersen, J. Wang, S. Dasgupta, S. Esener, S. Lee, Appl. Opt., 29, 1595 (1990)
- [28]P. Kaminow, V. Ramaswamy, V. Schmidt, H. Turner, Appl. Phys. Lett. 24, 622 (1974)
- [29]M. Abouellell, F. Leonberger, J. Am. Ceram. Soc.72, 1311 (1989)
- [30]K. Higuma, S. Oikawa, Y. Hashimoto, H. Nagata, M. Izutsu, Elec. lett. 37, 515 (2001)
- [31]Y. Shi, C. Zhang, J. Bechtel, L. Dalton, B. Robinson, W. Steier, Sci. 288, 119 (2000)

- [32]E. Wooten, K. Kissa, A. Yan, E. Murphy, D. Lafaw, P. Hallemeier, D. Maack, D. Attanasio, D. Fritz, G. McBrien, D. Bossi, J. Selected topics in quantum electronics 6, 69 (2000)
- [33]A. Yariv, Opt. elec. in modern communications, (Oxford Univ. Pr., Oxford, 1997)
- [34]A. Suematsu, K. Kobayashi, Photonics, (Ohmsha, Tokyo, 2007)
- [35]P. Cho, V. Grigoryan, Y. Godin, A. Salamon, Y. Achiam, Photonics Tech. Lett. 15, 473 (2003)
- [36]H. Yamazaki, T. Yamada, T. Goh, Y. Sakamaki, A. Kaneko, Proc. in Opt. communication, 1 (2009)
- [37]K. Chah, M. Aillerie, M. D. Fontana, G. Malovichko, Opt. Communications 176, 261 (2000)
- [38]J.D. Zook, D. Chen, G.N. Otto, Appl. Phys. Lett. 11,159 (1967)
- [39]E.H. Turner, Appl. Phys. Lett. 8, 303 (1966)
- [40]R. S. Weis, T. K. Gaylord, Appl. Phys. A 37, 191 (1985)
- [41]G. Zhou, M. Gu, Appl. Phys. Lett. 87, 241107 (2005)
- [42]A. Dhar, A. Mansingh, J. Appl. Phys. 68, 5804 (1990)
- [43]Z. Jiangou, Z. Shipin, X. Dingquan, W. Xiu, X. Guanfeng, J. Phys.: Condens. Matter 4, 2977 (1992)
- [44]G. Haertling, Ferroelectrics 75, 25 (1987)
- [45]S. Miga, K. Wojcik, Ferroelectrics 100, 167 (1989)
- [46]Q. Jiang, L. Cross, J. Mat. Sci., 28, 4536 (1993)
- [47]R. Sabat, P. Rochon, Ferroelectrics 386, 105 (2009)
- [48]M. Dambekalne, M. Antonova, M. Livinsh, B. Garbarz-Glos, W. Smiga, A.

- Sternberg, J. Euro. Ceramic Soc., 36, 2963 (2006)
- [49]K. Kitaoka, J. Am. Ceram. Soc. 81, 1189 (1998)
- [50]S. Kamba, V. Bovtun, J. Petzelt, I. Rychetsky, R. Mizaras, A. Brilingas, J. Banys, J. Grigas, M. Kosec, J. Phys.: Condens. Matter 12, 497 (2000)
- [51]Y. Honda, S. Yokoyama, H. Funakubo, K. Saito, Mat. Sci. and Eng. B 120, 161 (2005)
- [52]H. Jiang, Y. Zou, Q. Chen, K. Li, R. Zhang, Y. Wang, Optoelectronic Devices and Integration 5644, 380 (2005)
- [53]C Kirkby, Ferroelectrics 37, 567 (1981)
- [54]P. D. Thacher, J. Appl. Phys. 41, 4790 (1970)
- [55]G. Haertling, Ferroelectrics 75, 25 (1987)
- [56]T.Fujii, T.Suzuki, Y.Fujimori, T.Nakamura, M.Moriwake, H.Takasu, Jpn. J. Appl. Phys. 45, 7520 (2006)
- [57]D.Y. Wang, C. L. Mak, K. H. Wong, H. L. W. Chan, C. L. Choy, Ceram. International 30, 1745 (2004)
- [58]J. Li, F. Duewer, C. Gao, H. Chang, X. Xiang, Appl. Phys. Lett. 76, 769 (2000)
- [59]D. Kim, S. Moon, E. Kim, S. Lee, J. Choi, H. Kim, Appl. Phys. Lett. 82, 1455 (2003)
- [60]D. Wang, J. Wang, H. Chan, C. Choy, Integrated Ferroelectrics 88, 12 (2007)
- [61]J. Qiu, Q. Jiang, J. Appl. Phys. 102, 074101 (2007)
- [62]D. Wang, S. Li, H. Chang, C. Choy, Appl. Phys. Lett. 96, 061905 (2010)
- [63]C. Vijayaraghavan, T. Goel, R. Mendiratta, Trans. on Dielectrics and Electrical Insulation 6, 69 (1999)
- [64]W. Zhang, Y. Huang, M. Zhang, Appl. Surf. Sci. 158, 185 (2000)

- [65]H. Choi, Y. Park, J. Dougherty, N. Jang, C. Park, J. Mat. Sci. 35, 1475 (2000)
- [66]K. Nakamura, J. Miyazu, M. Sasaura, K. Fujiura, Appl. Phys. Lett. 89, 131115 (2006)
- [67]K. Fujiura, K. Abe, ITE Tech. Rep. 33, 7 (2009)
- [68]S. Toyoda, K. Fujiura, M. Sasaura, K. Enbutsu, A. Tate, M. Shimokozono, H. Ushimi, T. Imai, K. Manabe, T. Matsuura, T. Kirihara Japanese J. Appl. Phys. 43, 5862 (2004)
- [69]J. Raalte, J. Opt. Soc. Am. 57, 671 (1967)
- [70]A. Gentile, F. Andres, Mat. Res. Bull. 2, 853 (1967)
- [71]X. Wang, J. Wang, Y. Yu, H. Zhang, R. Boughton, J. Crys. Growth 293, 398 (2006)
- [72]M. Zhang, H. Li, J. Zhang, D. Wang, T. Huang, M. Yu, S. Xu, M. Wang, Am. Ceram. Soc. Bull. 80, 57 (2001)
- [73]S. Yagi, NTT Techn. Journal, 12 (2009)
- [74]K. Naganuma, J. Miyazu, S. Yagi, NTT Tech. Journal, 16 (2009)
- [75]Y. Sasaki, NTT Tech. Journal, 20 (2009)
- [76]K. Megumi, H. Kozuka, M. Kobayashi, Y. Furuhata, Appl. Phys. Lett. 12, 631 (1977)
- [77]S. Sakamoto, T. Yazaki, Appl. Phys. Lett. 22, 429 (1973)
- [78]R. Neurgaonkar, J. Oliver, W. Cory, Ferroelectrics 160, 265 (1994)
- [79]P. Tayebati, D. Trivedi, M. Tabat, Appl. Phys. Lett. 69, 1023 (1996)
- [80]D. Trivedi, P. Tayebati, M. Tabat, Appl. Phys. Lett. 68, 3227 (1996)
- [81]O. Kwon, O. Eknayan, H. Taylor, R. Neurgaonkar, Elec. Lett. 35, 219 (1999)
- [82]L. Zhu, J. Zhao, F. Wang, P. Norris, G. Fogarty, B. Steiner, P. Lu, B. Kear, S. Kang,

- B. Gallois, M. Sinclair, D. Dimos, M. Cronin-Golomb, *Appl. Phys. Lett.* 67, 1836 (1995)
- [83] H. Hatano, S. Tanaka, T. Yamaji, Y. Itoh, H. Matsushita, *Pioneer R&D* 11, 73 (2009)
- [84] S. Zhang, Y. Chiu, P. Abraham, J. Bowers, *Phot. Tech. Lett.* 11, 191 (1999)
- [85] C. Lim, A. Nirmalathas, D. Novak, R. Waterhouse, *J. Lightwave Tech.* 21, 3308 (2003)
- [86] G. Gopalakrishnan, W. Burns, R. McElhanon, C. Bulmer, A. Greenblatt, *J. Lightwave Tech.* 12, 1807 (1994)
- [87] R. Alferness, S. Korotky, E. Marcatili, *J. Quantum Elec.* QE-20, 301 (1984)
- [88] H. Hara, S. Masuda, A. Seki, K. Shiota, *Proc. of Jpn Soc. Appl. Phys.* 05, 120 (2011)
- [89] K. Tokuhashi, K. Ashizawa, D. Ishii, T. Arakawa, N. Yamanaka, K. Wakayama, *Trans. of High Performance Switching and Routing*, 978 (2009)
- [90] M. Didomenico, S. Wemple, *J. Appl. Phys.* 40, 720 (1969)
- [91] S. H. Wemple, M. Didomenico, *J. Appl. Phys.* 40 735 (1969)
- [92] M. Zgonik, P. Bernasconi, M. Duelli, R. Schlessler, P. Gunter, *Phys. Rev.* 50, 1942 (1991)
- [93] G. Pauliat, P. Mathey, G. Roosen, *J. Opt. Soc. Am. B* 8, 1942 (1991)
- [94] S. Shandarov, *Appl. Phys. A* 55, 91 (1992)
- [95] A. Glazounov and A. Tagantsev, *Phys. Rev. Lett.* 85, 2192 (2000)
- [96] G. Smolensky, *J. Phys. Soc. Jpn.* 28, 26 (1970)
- [97] A. Levstik, Z. Kutnjak, C. Filipi and R. Pirc, *Phys. Rev. B* 57, 11204 (1998)
- [98] A. Glazounov and A. Tagantsev, *Appl. Phys. Lett.* 73, 856 (1998)

- [99] R. Sommer, N. Yushin, and J. Klink, Phys.Rev. B 48, 13230 (1993)
- [100] D. Viehland, S. Jang, L. Cross, and M. Wuttig, J. Appl. Phys. 68, 2916 (1990)
- [101] B. Vugmeister and H. Rabitz, Phys. Rev. B 57, 7581 (1998)
- [102] R. Pirc and R. Blinc, Phys. Rev. B 60, 13470 (1999)
- [103] J. Geusic, H. Levinstein, J. Rubin, S. Singh, L. Uitert, Appl. Phys. Lett. 11, 269 (1967)
- [104] S. Singh, D. Draegert, J. Geusic, Phys. Rev. 2, 1 (1970) B
- [105] F. Wang, Phys. Rev. B 59, 9733 (1999)
- [106] T. Sliker, S. Burlage, J. Appl. Phys. 34, 1837 (1963)
- [107] J. Ott, T. Sliker, J. Opt. Soc. of America 54, 1442 (1964)
- [108] A. Cabanes, J. Castillo, F. Lopez, Materials Electro-optic Inorganic (Taylor & Francis, New York, 2007)

Chapter 2

Electro-optic Effect and Piezoelectric Resonance

2.1 Introduction

2.1.1 Influence of piezoelectric effect to EO effect

For designing high-speed EO devices, it is necessary to take into account the effect of piezoelectric resonance as long as ferroelectric oxides are employed as EO crystals. The EO coefficients depend on the mechanical constraints imposed on the crystal. If the crystal is free (unclamped), the stress in the crystal is zero, if the crystal is rigidly held (clamped), the strain in the crystal is zero. In the free condition, the EO coefficient value measured will also include a contribution from the strain in the crystal through the converse piezoelectric effect. This electrically induced strain then causes a change in the crystal's refractive index through the photo-elastic effect and the change of light path length¹⁻³.

Thus, to an observer who applies the electric field and is measuring the change in refractive index, this contribution of strain is inseparable from the unclamped EO effect. The relationship between the clamped EO coefficient and the unclamped EO coefficient can be written

$$r_{ij}^T = r_{ij}^S + p_{ik} d_{jk} \quad (2.1)$$

where r_{ij}^T is the value measured at constant stress (free crystal), r_{ij}^S is the value measured at constant strain, p_{ik} is the photo-elastic coefficient, and d_{jk}

is the piezoelectric coefficient. A measurement made with a static applied electric field corresponds to the unclamped case. A measurement made with a high frequency electric field corresponds to the clamped condition and only the clamped EO effect will be measured⁴. This is the pioneering work for EO effect considering the contribution of piezoelectric effect undertaken by R. S. Weis and co-workers⁵. And some reports proposed expanding formulae of EO coefficient from Eq. (2.1) assuming that the EO effect is the result of the change of light path length and/or photo-elastic effect due to piezoelectric effect¹⁻³. They determined the origin of EO effect phenomenologically through analyzing and separating in influence of strain in this way.

However, these formulae could not explain the change of EO coefficients around piezoelectric resonance: P. Günter reported that the EO coefficient of KNbO_3 single crystal indicated maximum and minimum in the frequency dependence, though the theoretical formula of piezoelectric displacement gives only maximum at resonance frequency⁶. These contradictions indicate that previous formulae of EO effect should be modified to explain experimental results for realizing more accurate understanding of EO effect.

The lithium niobate (LiNbO_3 , LN) single crystals have been used for EO modulators, realizing high-speed (over 10 Gbps) and wide-band optical modulations⁷⁻¹¹. This LN single crystal was employed as a sample for this study because of low frequency dependence of EO effect.

2.1.2 Objective

In this chapter, we aimed to analyze the EO effect of an LN single crystal in order to determine the influence of strain focusing on the behavior of EO coefficients around piezoelectric resonance frequency. We formularized the exact formula including the influence of strain to EO effect. It helped to elucidate the origin of EO effect.

2.2 Experimental procedure

2.2.1 Measurement system for EO effect

A schematic illustration and photograph of the measurement system is shown in Fig. 2.1. The EO coefficient of a rectangular LN single crystal (NEL crystal) with sample size of $3.9 \times 0.54 \times 0.40 \text{ mm}^3$ was measured as a function of frequency and strength of external electric field using Senarmont method with semi-conductive laser (Amonics Ltd, ALS-I5-B-FA, wavelength: $1.55 \text{ }\mu\text{m}$). Piezoelectric resonance of fundamental 31-mode of this crystal plate was observed at 758.9 kHz. A polarizer and an analyzer were respectively placed before and after the sample crystal. Between the polarizer and analyzer, a compensator was inserted to compensate the initial birefringence of the LN single crystal. The output light intensity was measured by a photodiode (Electro-optics Technology, ET-3010). The intensity of transmittance light was measured with keeping the extinction position of the polarizer and analyzer as a function of voltage (0–20V). The sample was held at the vibration nodes with two needles to prevent from clamping of piezoelectric vibration at resonance frequency as shown in Fig. 2.1.

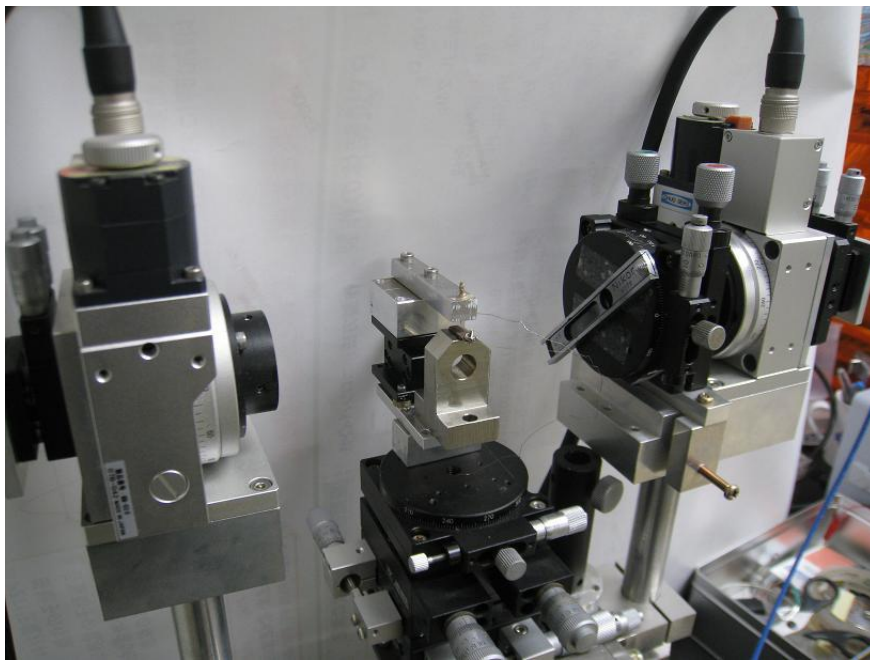
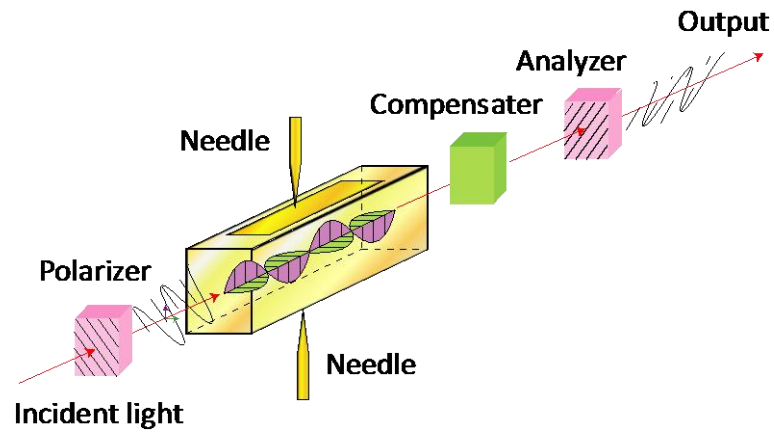


Fig. 2.1. Schematic illustration and photograph of measurement system for EO-effect

2.2.2 Measurement of piezoelectric effect around piezoelectric resonance frequency

The piezoelectric displacement and its phase lags to the applied electric field were measured using laser doppler vibrometer (NEOARK corp., MLD-301A) connected to a lock-in amplifier (NF corp., LI5640) as shown in Fig. 2.2. The driving voltage was 20V (peak to peak) in the resonance frequency range at 757 - 762 kHz.

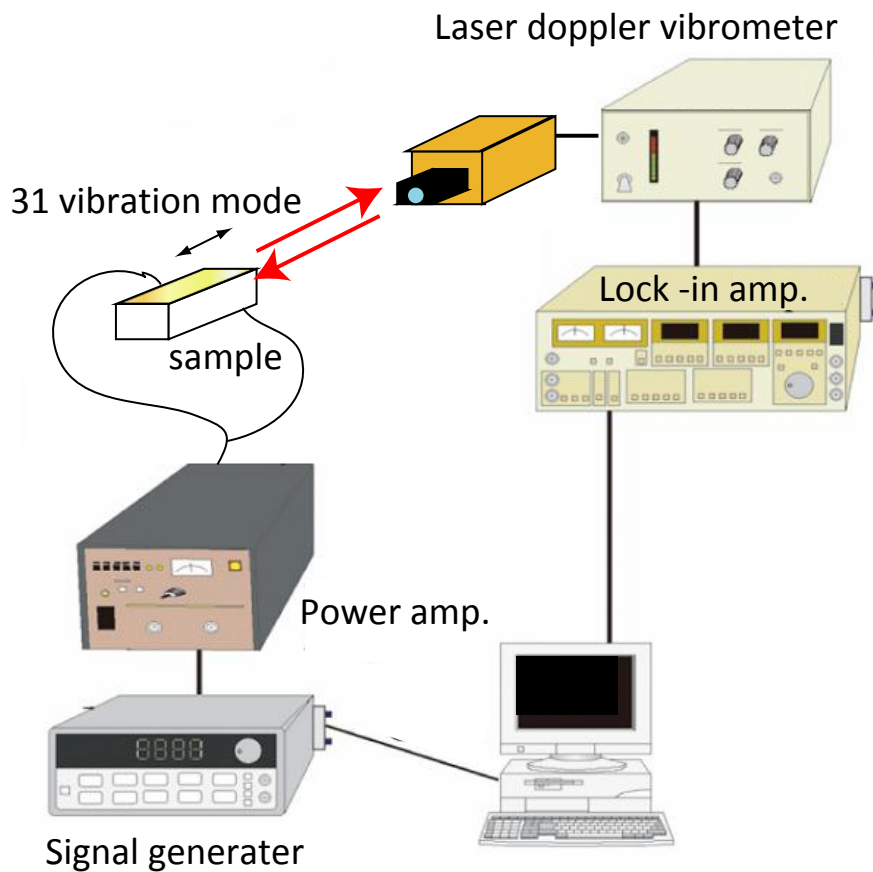


Fig. 2.2. Schematic illustration of measurement system for piezoelectric displacement

2.2.3 Evaluation of EO coefficient

From transmitted light intensity (I) normalized to the reference light intensity (I_0) (I / I_0) vs. electric field curves, the EO coefficient was evaluated as described below: A linear polarizing light does not change its polarizing state after passing through an optically isotropic medium, giving rise to $I / I_0 = 0$ at the extinction position. Therefore, I / I_0 measured at the extinction position includes the information on the degree of birefringence of the sample. The retardation R could be calculated using the following equation,

$$R = \tan^{-1} \left(\frac{2\sqrt{\frac{I}{I_0}}}{1 - \frac{I}{I_0}} \sin \varphi \right) \quad (2.2)$$

where φ is the analyzer angle⁴. From the definition of retardation, it can be also represented by,

$$R = \frac{2\pi l \Delta n}{\lambda} \quad (2.3)$$

where l is the light pass length, λ is the wavelength and Δn is the initial birefringence. From Eqs. (2.2) and (2.3), we obtained the following relation:

$$\Delta n = \frac{\lambda}{2\pi l} \tan^{-1} \left(\frac{2\sqrt{\frac{I}{I_0}}}{1 - \frac{I}{I_0}} \sin \varphi \right) \quad (2.4)$$

The EO effect is electrically induced birefringence and normally consists of the Pockels effect and Kerr effect. The Pockels effect gives a linear change of birefringence with electric field. The retardation R' due to the Pockels effect is represented by

$$R' = \frac{\pi n_e^3 r_c E l}{\lambda} \quad (2.5)$$

where n_e is the extraordinary refractive index, E is the electric field intensity and r_c is called as the Pockels coefficient defined by,

$$r_c = r_{33} - \left(\frac{n_o}{n_e}\right)^3 r_{13} \quad (2.6),$$

where n_o is the ordinary refractive index, r_{33} and r_{13} are the longitudinal and transverse Pockels coefficients, respectively. If the electric field induced birefringence is defined as $\delta(\Delta n)$, Δn in Eq. (2.3) should be written as $\delta(\Delta n)$. Inserting R in Eq. (2.3) into R' in Eq. (5), $\delta(\Delta n)$ can be represented by

$$\delta(\Delta n) = \frac{n_e^3 r_c}{2} E. \quad (2.7)$$

The electric field dependence of birefringence was fitted to Eq. (2.7) to evaluate Pockels coefficient r_c .

2.3 Results and discussion

2.3.1 Evaluation of EO coefficient in LN single crystal

Figure 2.3 shows electric field (DC) dependence of transmitted light intensity (I) normalized to the reference light intensity (I_0). Similar curves were obtained in AC-field dependences. From this result, the electric field dependence of birefringence was calculated by Eq. (2.4) as shown in Fig. 2.4. The Pockels effect is dominantly determined the EO effect of the LN single crystal because the electric field dependence of birefringence shows liner behavior. The *Electric field* dependence of birefringence in Fig. 2.4 was fitted to Eq. (2.7) to evaluate Pockels coefficient r_c . The Pockels coefficient was determined as 16.2×10^{-12} m/V which was almost consistent with some literature values¹²⁻¹⁴.

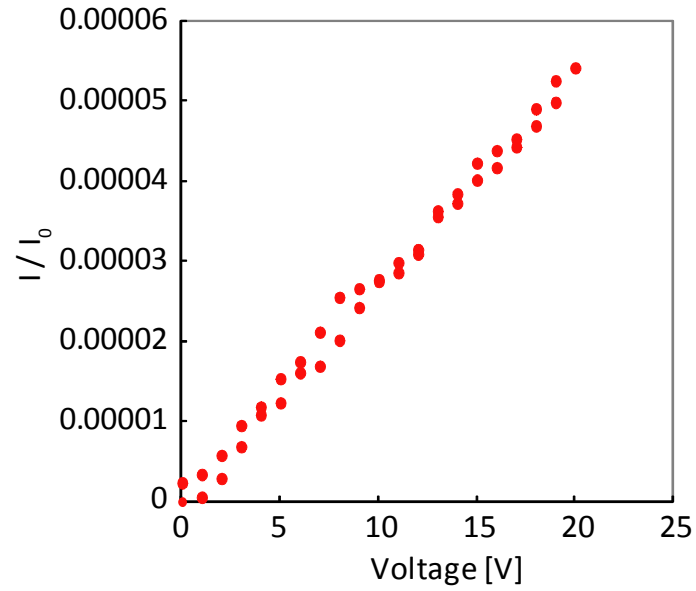


Fig. 2.3. Electric field dependence of the intensity of transmitted light (I) normalized to the intensity of incident light (I_0)

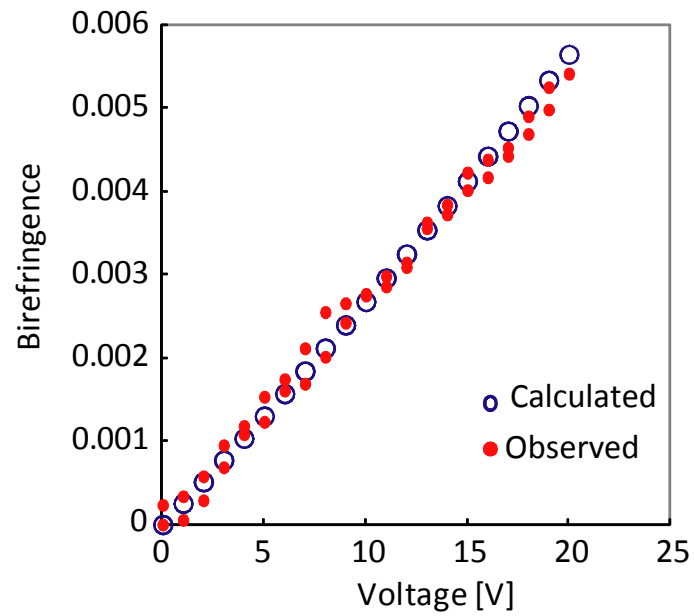


Fig. 2.4. Electric field dependence of observed and calculated birefringence.

2.3.2 Contribution to EO effect due to piezoelectric effect

The EO effect is defined as the electric field dependence of birefringence. However, the change of birefringence caused by piezoelectric displacement must be considered in addition to electric field dependence of birefringence when the piezoelectric crystals are employed as mentioned in 2.1.1. The light path length is generally considered as constant when the birefringence is calculated by retardation. In piezoelectric crystals, the light path length is elongated caused by piezoelectric effect depending on the electric field. This elongation gives rise to the change of retardation with increasing of electric field. However, this retardation due to piezoelectric displacement must be discriminated from the retardation due to EO effect. Therefore, the Pockels coefficient calculated by Eq. (2.7) should be defined as apparent Pockels coefficient because it does not consider the contribution of piezoelectric displacement. And the piezoelectric displacement gives rise to photo-elastic effect whose contribution is also included in apparent Pockels coefficient. Thus the apparent EO effect of piezoelectric crystals is expressed by summing up three effects: the retardation change caused by (i) application of electric field, (ii) change of light path length, (iii) photo-elastic effect. Further, the piezoelectric displacement shows lag from electric field when the alternative electric field is applied to piezoelectric crystals.

2.3.3 Frequency dependence of EO coefficient

Figure 2.5 shows the frequency dependence of EO (Pockels) coefficient r_c of an LN single crystal. It was confirmed that the EO coefficient showed a

maximum (758.9 kHz) and a minimum (760 kHz) around the piezoelectric resonance frequency as indicated by P. Günter⁶.

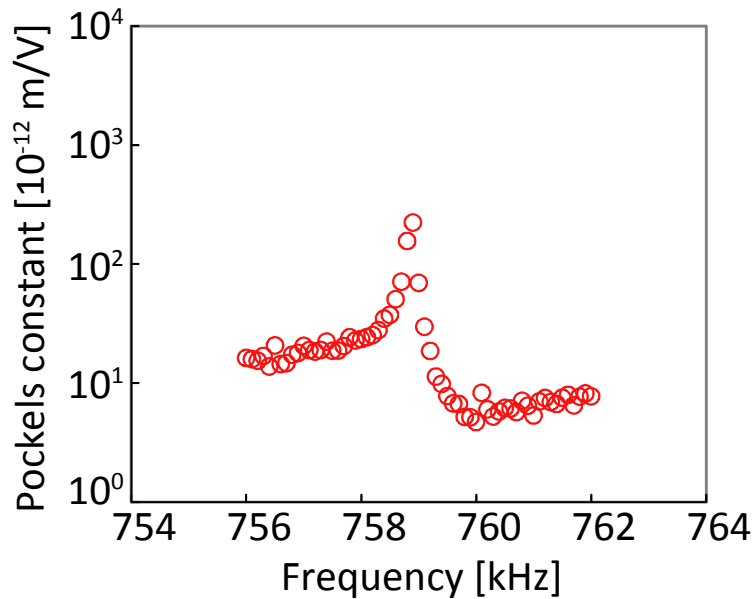


Fig. 2.5. The frequency dependence of observed EO coefficient.

The piezoelectric displacement shows relaxation at piezoelectric resonance frequency. As mentioned above, at frequencies far over the piezoelectric resonance, the piezoelectric displacement is negligible therefore the Pockels coefficient observed at this frequency is defined clamped (constant-stress, strain-free) Pockels coefficient. On the other hands, at frequencies far below the piezoelectric resonance, the Pockels coefficient observed at this frequency is defined unclamped (constant-strain, stress-free) Pockels coefficient because the displacement is observed caused by piezoelectric effect. This definition is as same as the definition for dielectric permittivity at

piezoelectric resonance frequency¹⁵.

In this paper, the Pockels coefficient measured at 756 kHz (16.2×10^{-12} m/V) was defined as unclamped Pockels coefficient r_c^T , and the Pockels coefficient measured at 762 kHz (7.7×10^{-12} m/V) was defined as clamped Pockels coefficient r_c^S .

The retardation induced by unclamped Pockels effect is calculated by summing three effects: (i), (ii), and (iii), because the unclamped Pockels effect includes the contribution of piezoelectric effect. On the other hand, the retardation induced by clamped Pockels effect is calculated by an effect (i), because the clamped Pockels effect does not include the contribution of piezoelectric effect, i.e. the retardation change caused by application of electric field (effect (i)) is same to the retardation due to clamped Pockels effect. Afterward, the effect (i) is redefined as the retardation change caused by the clamped Pockels effect.

2.3.4 Analysis on EO effect around piezoelectric resonance

2.3.4.1 Retardation caused by the clamped Pockels effect

As the first analysis of EO effect, the retardation due to clamped Pockels effect R_c is defined as

$$R_c = \frac{\pi n_e^3 r_c^S E l}{\lambda} \quad (2.8)$$

where r_c^S is clamped Pockels coefficient. This retardation calculated by Eq. (2.8) is regarded as the retardation caused by effect (i).

2.3.4.2 Retardation caused by the change of light path length

For the analysis of the effect (ii), we calculated the retardation R_L due to the change of light path length resulted from piezoelectric strain. The retardation caused by the change of light path length R_L can be represented by modifying Eq. (2.3) as

$$R_L = \frac{2\pi\Delta n}{\lambda} \Delta l \quad (2.9)$$

where Δl is the change of light path length. Δn in Eq. (2.9) is initial birefringence that does not change by applying electric field. Using Eqs. (2.8) and (2.9), the Pockels coefficient considering the contribution of light path length r'_c is given by

$$r'_c = \frac{\lambda}{\pi n_e^3 E l} (R_c + R_L) = \frac{\lambda}{\pi n_e^3 E l} \left(\frac{\pi n_e^3 r_c^S}{\lambda} E l + \frac{2\pi\Delta n}{\lambda} \Delta l \right). \quad (2.10)$$

In Fig. 2.6 compared frequency dependence of apparent Pockels coefficient calculated by Eq. (2.10) with that observed, indicating that both results did not agreed at all. The Pockels coefficients estimated from the change of optical path length caused by the piezoelectric strain was too small to explain the result of measurement.

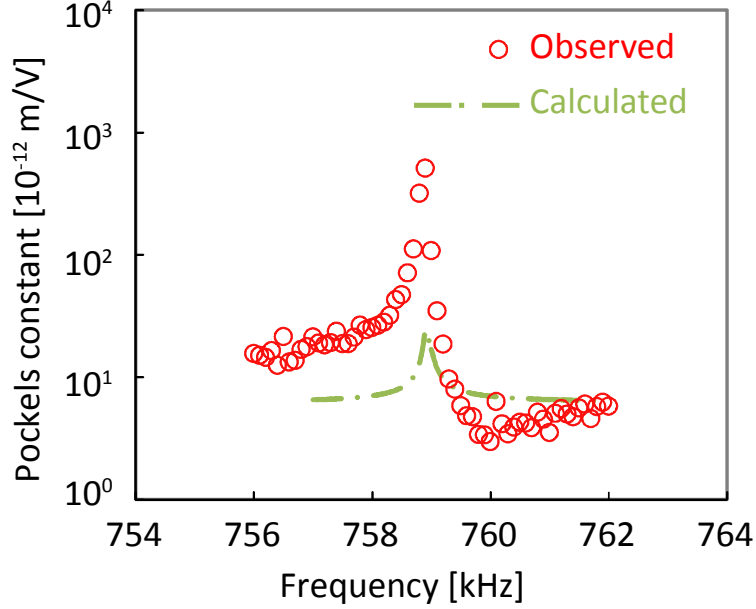


Fig. 2.6 The frequency dependence of observed EO coefficient and calculated EO coefficient by Eq. (2.9). Eq (2.9) is formularized from the retardation due to the clamped Pockels effect and the change of light path length.

2.3.4.3 Retardation caused by the photo-elastic effect

The piezoelectric effect should induce the distortion of crystal lattices, which gives rise to the change of refractive index through the deformation of electronic clouds in the crystal lattices. The change of refractive index thus produced in the crystal is called as the photo-elastic effect¹⁶. For the analysis of the effect (iii), the contribution of photo elastic effect to the EO effect was considered. The retardation due to the photo-elastic effect R_{ph} is described by following relation^{17,18}.

$$R_{ph} = \frac{\pi n_e^3 l}{\lambda} \sum_{i,j,k,l} p_{ijkl} S_{kl} \quad (2.11)$$

where p_{ijkl} are photo-elastic coefficients and S_{kl} are elastic strain. The retardation in the above equation can be expanded as

$$R_{ph} = \frac{\pi n_e^3 l}{\lambda} \{ S_{11}(p_{11} + p_{31}) + S_{22}(p_{12} + p_{32}) + S_{33}(p_{13} + p_{33}) \} \quad (2.12)$$

where the transverse and longitudinal coefficients should contribute to the retardation in a opposite way. The following equation was obtained by adding the contribution of photo elastic effect to Eq. (2.9),

$$r_c'' = \frac{\lambda}{\pi n_e^3 E l} (R_c + R_L + R_{ph}) = \frac{\lambda}{\pi n_e^3 E l} \left(\frac{\pi n_e^3 r_c^S}{\lambda} E l + \frac{2\pi \Delta n}{\lambda} \Delta l + \frac{\pi n_e^3 l}{\lambda} \sum_{i,j,k,l} p_{ijkl} S_{kl} \right) \quad (2.13)$$

where r_c'' is the Pockels coefficient considering the contribution of light path length and photo-elastic effect. Figure 2.7 shows frequency dependence of apparent EO coefficient calculated from Eq. (2.13) where photo-elastic coefficients were taken from literature⁵ as shown in Table 2.1.

Table 2.1 Photo-elastic coefficients at constant electric field.

P_{11}	P_{33}	P_{44}	P_{12}	P_{13}	P_{14}	P_{31}	P_{41}
0.036	0.066	—	0.072	0.135	—	0.178	0.155
0.025	0.068	—	0.079	0.132	0.1	0.168	0.158
0.034	0.060	0.30	0.072	0.139	0.066	0.178	0.154
—	0.069	0.152	0.088	0.126	0.080	0.176	0.134
0.045	0.076	0.019	0.096	0.149	0.055	0.138	—
-0.026	0.071	0.146	0.090	0.133	-0.075	0.179	-0.151
-0.02	0.07	0.12	0.08	0.13	-0.08	0.17	-0.15

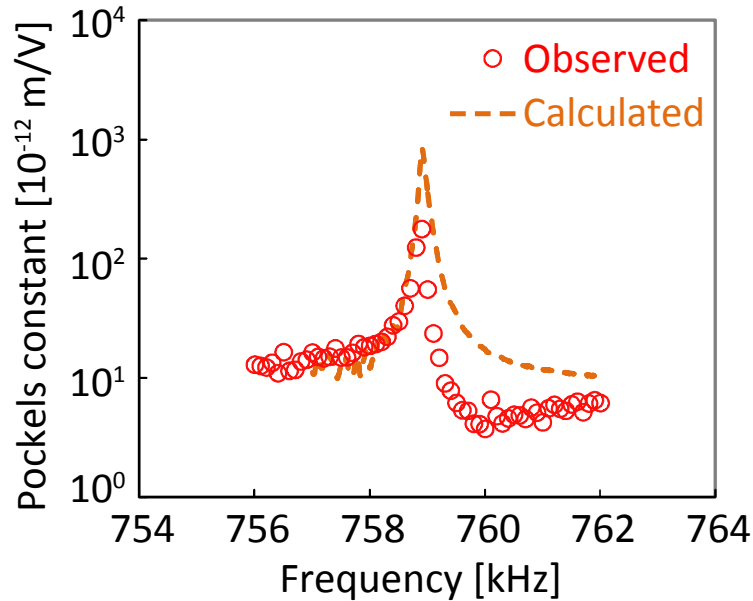


Fig. 2.7 The frequency dependence of observed EO coefficient and calculated EO coefficient by Eq. (2.12). Eq (2.12) is formulated from the retardation due to the clamped Pockels effect, the photo-elastic effect, and the change of light path length.

A marked improvement was obtained from Fig. 2.6, indicating that the retardation due to the photo elastic effect (effect (iii)) was much higher than that of the change of light path length (effect (ii)) and clamped Pockels effect (effect (i)). However, notable discrepancy was observed at 757 kHz where experimentally determined EO coefficient showed a minimum. Figure 2.8 shows the piezoelectric displacement as well as the phase-lags between electric field and piezoelectric displacement as a function of frequency. The piezoelectric displacement shows only maximum at 758.9 kHz which is consistent with the formula of piezoelectric strain¹⁹. It is therefore reasonable that the apparent EO

coefficient estimated from the change of optical path length and photo elastic effect showed only maximum at resonance frequency.

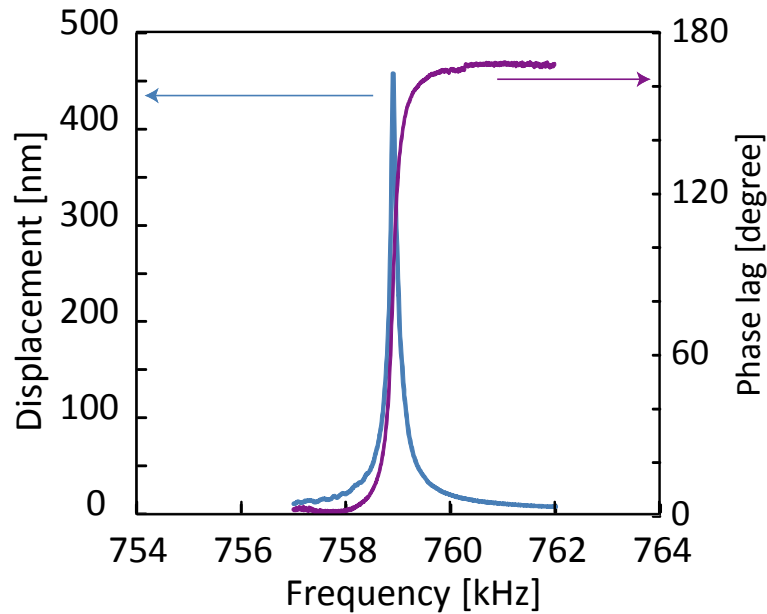


Fig. 2.8. Piezoelectric displacement field and phase lag between electric field and piezoelectric displacement of LN single crystal as a function of frequency of applying electric field.

2.3.4.4 Contribution to EO effect due to the phase lag

To explain the minimum in the frequency dependence of apparent EO coefficient observed in Fig. 2.5, we have considered a phase lag between electric field and piezoelectric displacement. The phase lag is negligible at frequencies far below the piezoelectric resonance. It steeply increases near the resonance frequency from zero to π through $\pi / 2$ at the resonance frequency as shown in Fig. 2.8. The phase lag of piezoelectric displacement should be incorporated into

Eq. (2.13).

If the alternative electric field applied to EO crystals, the retardation is replaced as

$$\begin{aligned} R &= R_c \sin \omega t + (R_L + R_{ph}) \sin(\omega t - \delta) = R_c \sin \omega t + R_p \sin(\omega t - \delta) \\ &= (R_c + R_p \cos \delta) \sin \omega t - R_p \sin \delta \cos \omega t \end{aligned} \quad (2.14)$$

where ω is frequency of applying electric field, δ is the phase lag between piezoelectric displacement and electric field shown in Fig. 2.8. $R_p = R_L + R_{ph}$ is the retardation caused by piezoelectric displacement.

The retardation R in the above equation can be calculated as

$$R = \sqrt{(R_c + R_p \cos \delta)^2 + (R_p \sin \delta)^2} \sin(\omega t + \alpha) \quad (2.15)$$

$$\alpha = \cos^{-1} \frac{R_c + R_p \cos \delta}{\sqrt{(R_c + R_p \cos \delta)^2 + (R_p \sin \delta)^2}} = \sin^{-1} \frac{-R_p \sin \delta}{\sqrt{(R_c + R_p \cos \delta)^2 + (R_p \sin \delta)^2}} .$$

The amplitude of retardation $|R|$ is given by

$$|R| = \sqrt{(R_c + R_p \cos \delta)^2 + (R_p \sin \delta)^2} . \quad (2.16)$$

The retardation in Eq.(12) ($R_c + R_L + R_{ph}$) should be substituted to the amplitude of combined retardation $|R|$. Thus Eq. (13) is replaced as

$$\begin{aligned} r_c''' &= \frac{\lambda}{\pi n_e^3 E l} |R| = \frac{\lambda}{\pi n_e^3 E l} \sqrt{(R_c + R_p \cos \delta)^2 + (R_p \sin \delta)^2} \\ &= \frac{\lambda}{\pi n_e^3 E l} \sqrt{\left(\frac{\pi n_e^3 r_c^s E l}{\lambda} + \left(\frac{2\pi \Delta n}{\lambda} \Delta l + \frac{\pi n_e^3 l}{\lambda} \sum_{i,j,k,l} \rho_{ijkl} S_{kl} \right) \cos \delta \right)^2 + \left(\frac{2\pi \Delta n}{\lambda} \Delta l + \frac{\pi n_e^3 l}{\lambda} \sum_{i,j,k,l} \rho_{ijkl} S_{kl} \sin \delta \right)^2} \end{aligned} \quad (2.17)$$

where r_c''' is the Pockels coefficient considering the contribution of light path length and photo-elastic effect and phase lag. Figure 2.9 show calculated result by Eq. (2.17) and observed values. Good fitting indicated that the minimum in behavior of apparent Pockels coefficient.

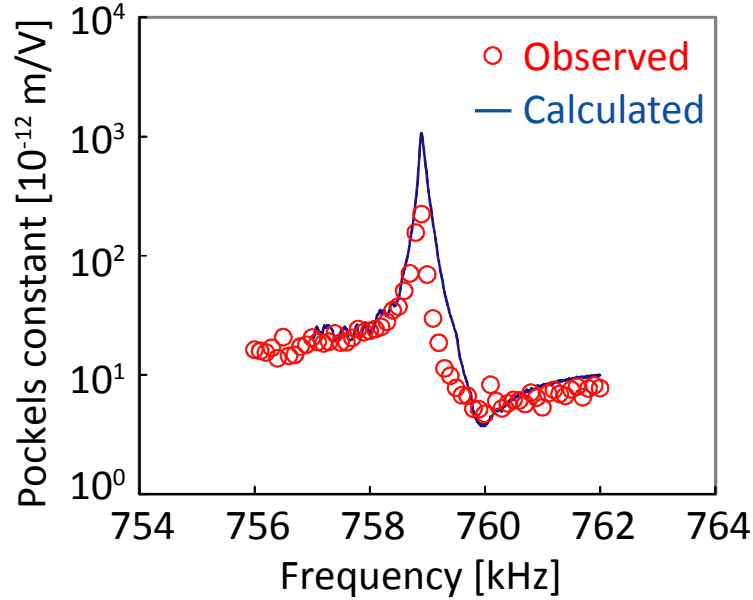


Fig. 2.9. The frequency dependence of observed EO coefficient and calculated EO coefficient by Eq. (2.17). Eq (2.17) is formularized from the retardation due to the clamped Pockels effect, the photo-elastic effect, and the change of light path length. And Eq. (2.17) is considering the phase lag between R_p and R_c .

The minimum in behavior of apparent Pockels coefficient did not be explained in previous works. This behavior can be explained as described following. If the phase lag is negligible, the retardation is calculated as sum of R_p and R_c as shown in Fig. 2.10 (a). If the phase lag is equal to π , the retardation is calculated as difference between R_p and R_c as shown in Fig. 2.10 (b). As mentioned above, the retardation due to piezoelectric effect R_p is much higher than the retardation due to clamped EO effect R_c . Therefore the sum of R_p and R_c is as same as the difference between R_p and R_c at piezoelectric resonance frequency. This is why the apparent Pockels coefficient does not change steeply

through the piezoelectric resonance frequency. At frequencies far over piezoelectric resonance, the retardation due to piezoelectric effect is decreasing with decreasing of piezoelectric displacement. With decreasing piezoelectric displacement, the retardation due to piezoelectric becomes equal to the retardation due to clamped Pockels effect at the frequency as shown in Fig. 2.11. At this frequency, the retardation shows the minimum therefore the apparent Pockels coefficient shows the minimum. This is why the frequency dependent of apparent EO coefficient shows the minimum at frequency far over piezoelectric resonance.

The piezoelectric displacement contributes to EO effect as the change of light path length and photo-elastic effect. Among them, photo-elastic effect that is birefringence induction due to strain mainly contributes to EO effect. On the contrary, the influence of the change of light path length is negligible. Hereafter, we consider the influence of strain to EO effect is photo-elastic effect dominantly. Therefore we conclude that the photo-elastic coefficient must be considered as parameter for material search in order to solve the problem (iii).

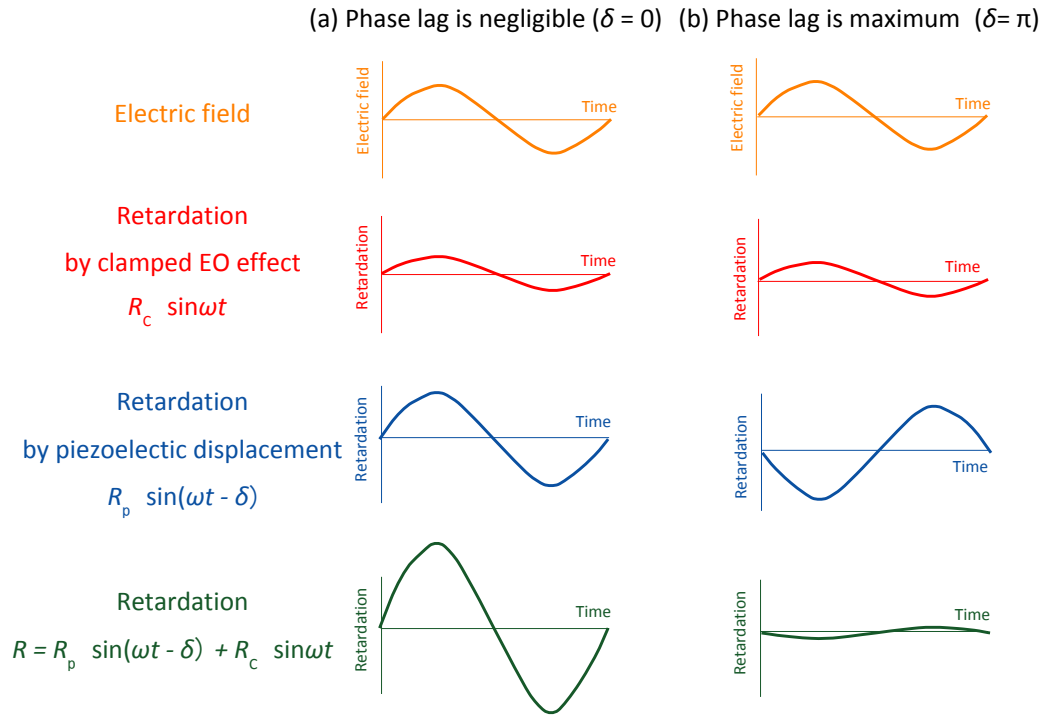


Fig. 2.10. Physical image of the retardation changed by piezoelectric effect and clamped EO effect around resonance frequency. (a) Phase lag is negligible ($\delta = 0$), (b) phase lag is maximum ($\delta = \pi$)

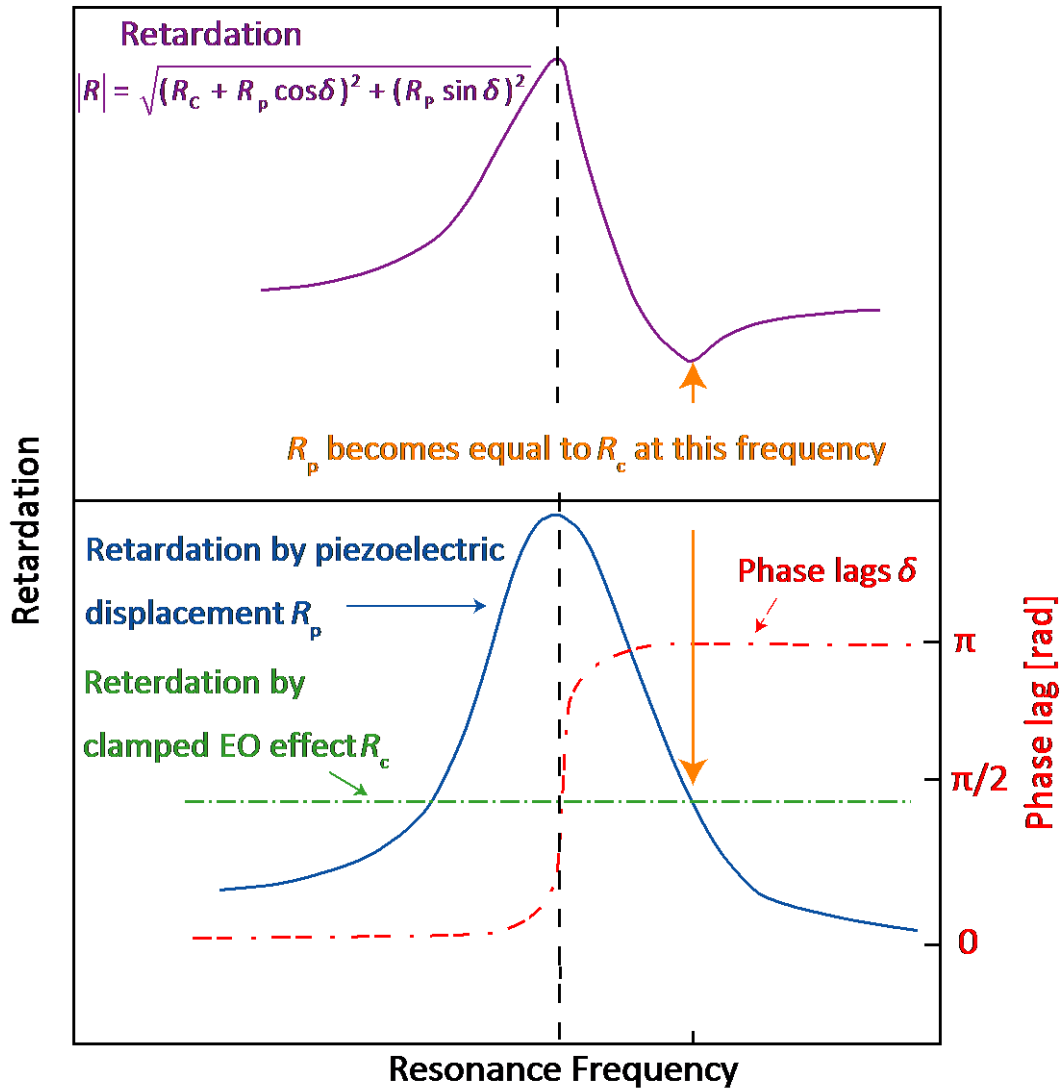


Fig. 2.11. Relation among the retardation by piezoelectric displacement, the retardation by clamped EO effect, and phase lag.

2.4 Summary of chapter 2

In this chapter, the apparent EO coefficient around resonance frequency was

measured to analyze the contribution of piezoelectric displacement and formularize an equation. The frequency dependence of apparent EO coefficient around resonance frequency shows the maximum and minimum. The maximum was observed at piezoelectric resonance frequency, the minimum was observed at frequency far over resonance frequency. We conclude that the unclamped EO coefficient is due to retardation from (i) clamped Pockels effect, (ii) change of light path length, (iii) photo-elastic effect. The minimum is caused by phase lag between piezoelectric displacement and applying electric field. It is notable that the photo-elastic effect that is birefringence induction due to strain mainly contributed to EO effect in these effects. Therefore we concluded that the influence of strain to EO effect is photo-elastic effect.

References

- [1] M. Zgonik, P. Bernasconi, M. Duelli, R. Schlessler, P. Gunter, Phys. Rev. 50, 1942 (1991)
- [2] G. Pauliat, P. Mathey, G. Roosen, J. Opt. Soc. Am. B 8, 1942 (1991)
- [3] S. Shandarov, Appl. Phys. A 55, 91 (1992)
- [4] T. Ogawa, Fundamentals on crystal technology, (Shokabo, Tokyo, 1998)
- [5] R. S. Weis, T. K. Gaylord, Appl. Phys. A 37, 191 (1985)
- [6] P. Gunter, Opt. Communications 11, 285 (1974)
- [7] L. N. Binh, J. Crystal Growth 288, 180 (2006) LN
- [8] E. L. Wooten, K. M. Kissa, A. Y. Yan, E. J. Murphy, D. A. Lafaw, P. F. Hallemeier, D. Maack, D. V. Attanasio, D. J. Fritz, G. J. McBrien, D. E. Bossi, J. Selected topics in quantum electronics 6, 69 (2000)
- [9] K. Noguchi, H. Miyazawa, O. Mitomi, Elec. Lett. 30, 949 (1994)
- [10] K. Noguchi, O. Mitomi, H. Miyazawa, J. Lightwave Tech. 16, 615 (1998)
- [11] D. W. Dolf, M. Nazarathy, R. L. Ungerman, Elec. Lett. 28, 528 (1988)
- [12] K. Chah, M. Aillerie, M. D. Fontana, G. Malovichko, Opt. Communications 176, 261 (2000)
- [13] J.D. Zook, D. Chen, G.N. Otto, Appl. Phys. Lett. 11,159 (1967)
- [14] E.H. Turner, Appl. Phys. Lett. 8, 303 (1966)
- [15] T. Ikeda, *Fundamental of Piezoelectric Materials*, (Ohmsha, Tokyo, 1984)

- [16] H. Hueller, *Rhps. Rev.* 47, 947 (1935)
- [17] M. Zgonik, R. Schlessler, I. Biaggio, E. Voit, J. Tscherry, P. Gunter, *J. Appl. Phys.* 74, 1287 (1993)
- [18] H. Sasaki, K. Tsubouchi, N. Chubachi, N. Mikoshiba, *J. Appl. Phys.* 47, 2046 (1976)
- [19] K. Uchino, J. R. Giniewicz, *MicroMechatronics*, (CRC, New York, 2003)

Chapter 3

Electric field dependence of birefringence and dielectric permittivity

3.1 Introduction

3.1.1 Dielectric tunability and electro-optic effect

As mentioned in chapter 2, the photo-elastic effect is an unmissable factor to analyze the EO effect. We estimated that the polarization that induced the lattice distortion gave rise to the photo-elastic effect. The variation of birefringence caused by polarization is supposed as origin of EO effect. To elucidate the influence of polarization to EO effect, it is necessary to understand the microscopic mechanism determining the performance of EO effect in ferroelectric materials. The polarization is proportional to the dielectric permittivity in the electrical region. Further the dielectric permittivity was varied with application of the electric field in some relaxor materials¹⁻⁷ that is called (dielectric) tunability. The EO effect is regarded as the tunability of refractive

index with varying of external electric fields because the refractive index is dielectric permittivity at high frequency. Therefore, we can expect the tunability of refractive index (EO effect) shows a similar behavior to the tunability of permittivity measured at low frequencies. We estimated that the problem (ii): “the relaxor materials show relatively high EO coefficient” is caused by the tunability.

However, it is possible to consider in another way, *i.e.*, the polarization mechanism at low frequencies involves electronic, ionic and dipole polarizations but that at optical frequencies is only due to the electronic polarization, which may give different behaviors in the tunability of low frequency permittivity and refractive index. Dielectric tunability of barium strontium titanate ($\text{Ba}_{1-x}\text{Sr}_x\text{TiO}_3$, BST) thin films have been studied for realizing tunable capacitors and tunable filters operating at microwave frequencies⁸⁻¹⁴. On the other hand, some reports showed that BST thin films exhibited relatively high EO effects¹⁵⁻²¹ though EO coefficients reported in literatures were not consistent with each other. We believe that BST thin films are a suitable sample for understanding the relationship between the low frequency dielectric tunability and EO effect. However, a lack of experimental data on simultaneous measurements of dielectric tunability and EO effect restricted further understanding of the relation and the microscopic mechanism of EO effect.

3.1.2 Objective

In this chapter, we measured the electric field dependence of birefringence and dielectric permittivity in BST thin films to confirm that the polarization variation contribute to EO effect. High quality BST epitaxial films were used for a sample of the measurements to elucidate the relation between the dielectric tunability and the EO effect, and why the relaxor materials show relatively high EO coefficient in order to solve the problem (ii).

3.2 Experimental procedure

3.2.1 Sample preparation

Epitaxial BST thin films were deposited on (001) STO single crystal substrates using RF-magnetron sputtering method (SMM3-R, RST Co. Ltd.) at substrate temperature of 600°C and at RF power of 30 W. The sputtering gas was a mixture of 80 % Ar and 20 % O₂. The gas pressure during the depositions was 30 mTorr.

3.2.2 Characterization of BST thin film

The crystallinity of the films was verified by x-ray diffraction (XRD) and reflection high-energy electron diffraction (RHEED) analyses. The film thickness

was determined by a surface profiler (Dektak, Veeco). Polarizations (P) vs. electric field (E) curves of the films are measured using a ferroelectric tester (Radiant, RT6000). For the measurements of the EO-effect of the films, planer electrodes with a dimension of $2.8 \times 1.4 \text{ mm}^2$ separated by $20 \text{ }\mu\text{m}$ spacing were formed on the film surfaces using lithography technique. Figure 3.1 shows an illustration of a sample with a planer electrode which was aligned parallel to the cubic axis of STO substrates that was defined as the $[100]$ direction.

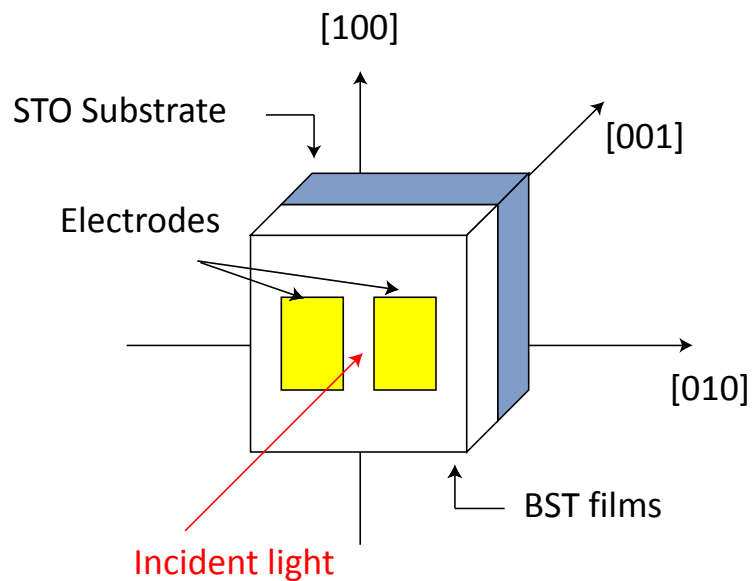


Fig. 3.1. Geometric relation of planer electrode with the crystal axes of STO substrate.

3.2.3 Formation of micro-sized planer electrodes

Designed planer electrodes were formed on the BST thin films. Lift-off method, an electric circuit formation technique, was used to form the designed electrode pattern on the surface of sample. The procedure of this method is shown in Fig. 3.2. At first, photo resist solution (OFPR-800, Tokyo Ohka) was coated on the surface of sample. A spin coater (1H-D7, MIKASA) performed the coating operation under the conditions of 2500 rpm rotation speed and 25 second long. Then, the resist coated sample was put in an electric oven and heat treatment was performed in 90°C for 10 minutes for the purpose of evaporation of organic solvent. The adhesive force of resist could also be strengthened by heat treatment. Coated resist was then exposed using a mask alignment with ultrahigh pressure mercury lamp (MA-10, MIKASA) for 10 sec. After the exposure, the development was performed by sinking the sample into alkali developer (NMD-3, Tokyo Ohka) for 1minute, then the water washing was done. Post developing bake was done in electric oven at 120°C for 10 minutes. Gold layer with 60 nm thickness was deposited on the surface of sample by the DC sputtering. Finally, the sputtered sample was dipped in exfoliation agent. In this process, unexposed resist dissolved in exfoliation agent, and then the Au film deposited on these areas was lift-off.

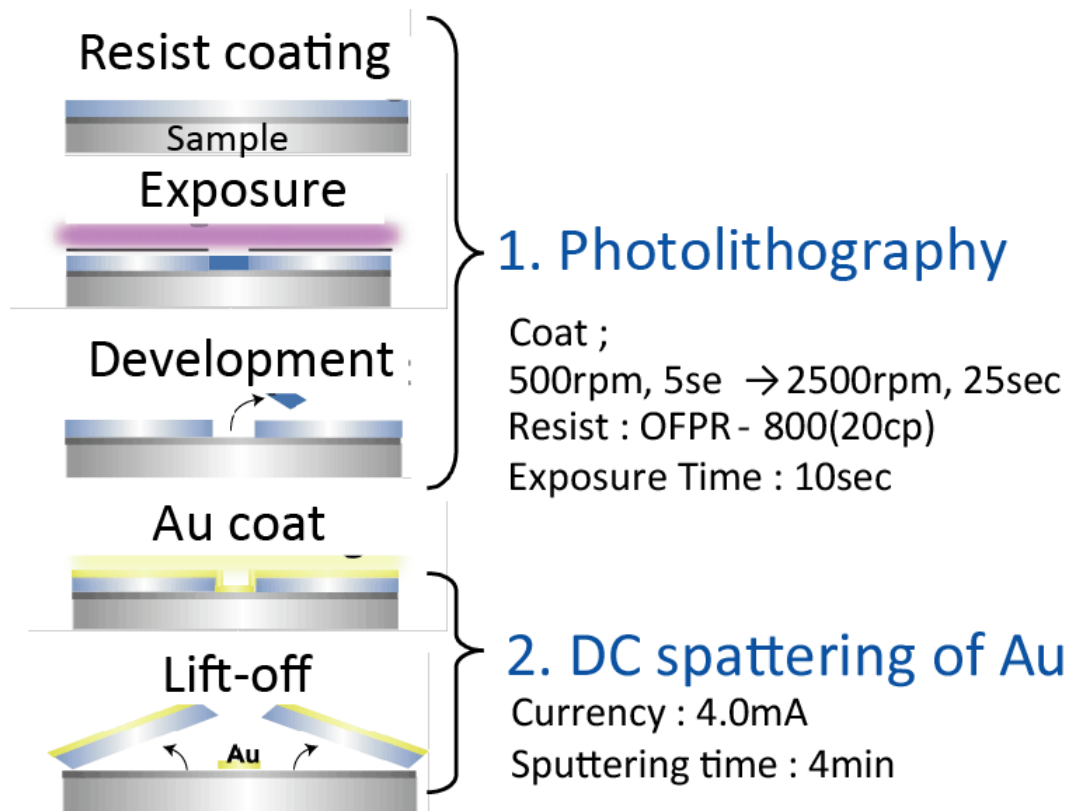


Fig. 3.2. Procedure for the lift-off method.

3.2.4 Measurement of dielectric tunability

Dielectric tunability of the BST films was determined from electric field dependence of the permittivity. Figure 3.3 shows a schematic illustration of measurement system for dielectric tunability. A frequency response analyzer (5060, NF corporation) was used to measure electric current, voltage and a phase difference between them. Electric signals applied to the sample were generated by superimposing dc voltages (0 – 200 V) to ac signals (10 kHz, 10 V_{p-p})

in amplitude) with a hand-made bias-tee coupler. Here, the complex voltage measured at clip 1 as shown in Fig. 3.3 is defined as V_1^* , the complex voltage measured at clip 2 is defined as V_2^* , the phase difference between them is defined as δ , and the complex current flowing in the pure resistance in Fig. 3.3 is defined I^* , these parameters are estimated as

$$V_2^* = V_2 \exp(i\omega t) \quad (1)$$

$$V_1^* = V_1 \exp\{i(\omega t + \delta)\} \quad (2)$$

$$I^* = \frac{V_1^*}{R_{pure}} \quad (3)$$

$$(Z_{SAM}^* + R_{pure})I^* = V_2^* \quad (4)$$

where Z_{SAM}^* is complex impedance of sample, R_{pure} is terminal resistance of pure resistance $R_{pure} = 500 \Omega$, V_1 and V_2 is amplitude of V_1^* and V_2^* , and ω is frequency of applied electric field. The complex impedance of sample Z_{SAM}^* is calculated by substituting Eq (2), (3) to (4) as .

$$Z_{SAM}^* = R_{pure} \left[\frac{V_2}{V_1} \exp\{i(-\delta)\} - 1 \right] \quad (5)$$

Here, the complex admittance of sample Y_{SAM}^* is derived from Eq. (5) as

$$Y_{SAM}^* = \frac{1}{Z_{SAM}^*} = \frac{1}{R_{pure} \left[\frac{V_2}{V_1} \exp\{i(-\delta)\} - 1 \right]} \quad (6)$$

On the other hand, the complex admittance of sample Y_{SAM}^* and the capacitance of sample C_{SAM}^* have relation described as

$$Y_{SAM}^* = G_{SAM} + iB_{SAM} = i\omega C_{SAM}^* = i\omega(C' - iC'') = C' + i\omega C'' \quad (7)$$

where G_{SAM}^* is conductance of sample, B_{SAM}^* is susceptance of sample, C' is real part of complex capacitance, and C'' is imaginary part of complex capacitance²². Therefore, the real part of capacitance C' can be calculated by the susceptance of sample B_{SAM}^* . Since the dielectric properties were measured with planer electrodes as shown in Fig. 3.3, the permittivity was not easily evaluated by capacitance. To solve this problem, an electromagnetic field analysis (MW STUDIO, AET Inc) was employed. In the analysis, the sample permittivity was evaluated to obtain the best fitting between the complex admittances calculated and measured. The electric field dependence of dielectric permittivity was obtained from this analysis with varying electric field.

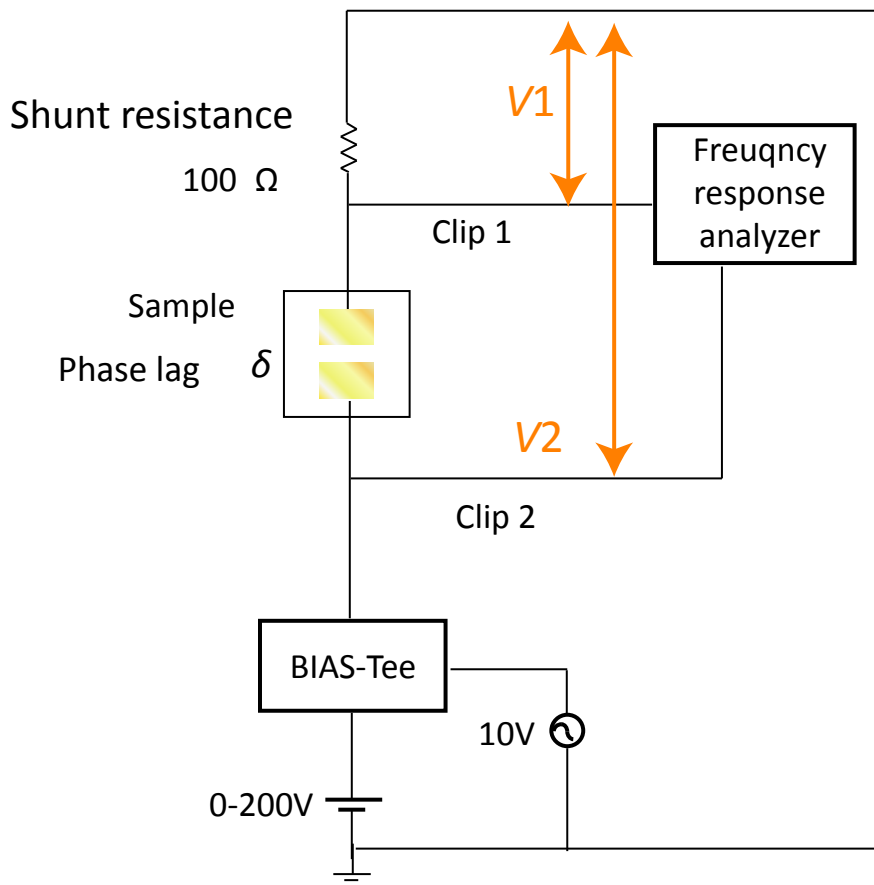
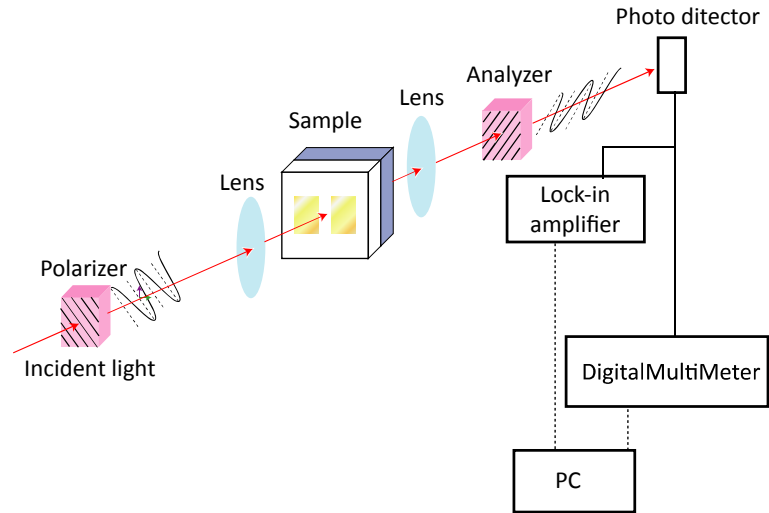


Fig. 3.3. Schematic illustration of measuring system for dielectric tunability

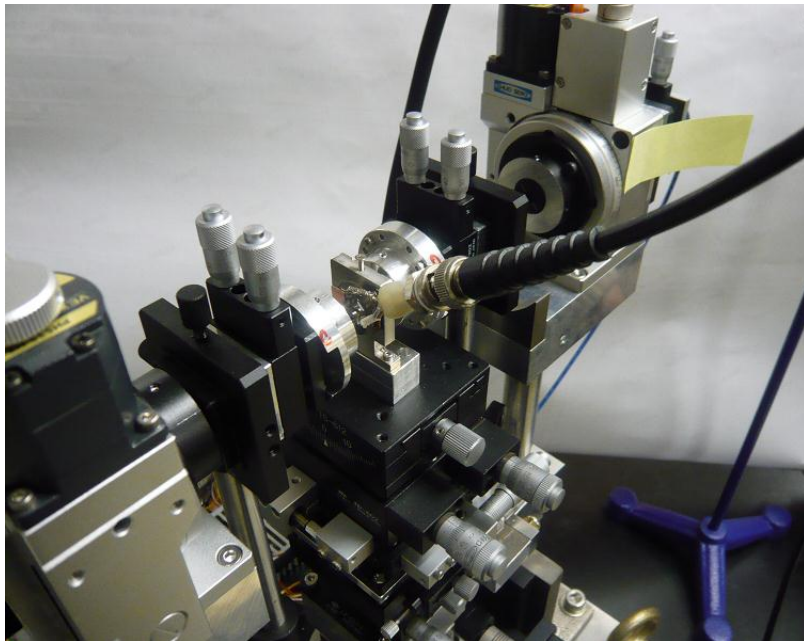
3.2.5 Measurement system for EO-effect

A schematic illustration and a photograph of the system developed for the measurements of the EO-effect as a function of electric field are shown in Fig. 3.4.

The films surface was set with the direction perpendicular to the incident light passing through the 20 μm spacing between electrodes. A polarizer and an analyzer were respectively placed before and after the sample. A lens was placed between the samples and the polarizer to focus the incident light beam on the electrode spacing. The intensity of transmittance light was measured with keeping the extinction position of the polarizer and analyzer as a function of voltage (0 - 200 V) between the two electrodes. The electric field applied to samples with the planer electrode was estimated from the simulation using a finite element method (ANSYS, ANSYSver9.0). In the transmission geometry, the birefringence of substrates cannot be separated from that of films. Therefore, we first measured the birefringence induced by the EO-effect of STO substrates and confirmed that the birefringence of the substrates was negligible in comparison with that of films. Other constitution is the same to the measurement system in chapter 2.



(a)



(b)

Fig. 3.4. (a) Schematic illustration and (b) a photograph of measuring system for EO-effect and dielectric tunability

3.2.6 Evaluation of EO effect

The electric field dependence of birefringence due to EO effect was evaluated by the same method described in chapter 2. Note that the EO effect of BST thin film indicates non-linear behavior that is Kerr effect. The birefringence shift in a quadratic EO effect (Kerr effect) is given by

$$\delta\Delta n = \frac{1}{2} n^3 R_c E^2 \quad (8)$$

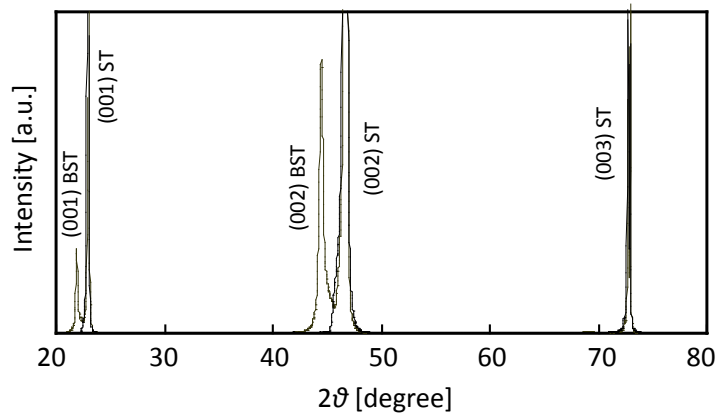
where R_c is the quadratic EO coefficient (Kerr coefficient)²³. The electric field dependence of birefringence was fitted to Eq. (6) to evaluate Kerr coefficient R_c .

3.3 Results and Discussion

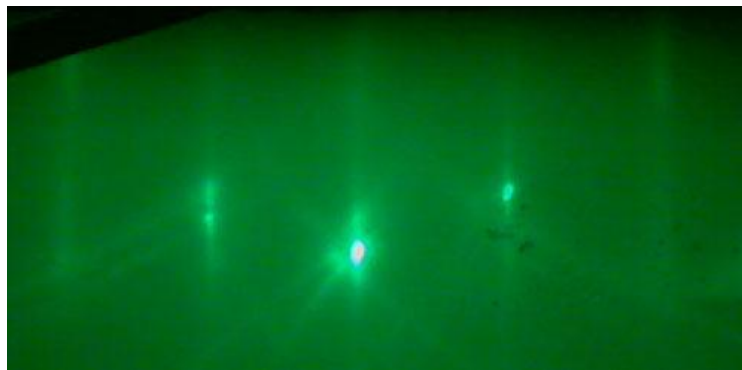
3.3.1 Epitaxy and lattice distortion of BST film

Figure 3.5 (a) shows an XRD profile and Fig. 3.5 (b) shows an RHEED pattern of the BST films. Only 00l and 002 diffraction peaks are observed in the XRD profile and diffraction spots are observed in the RHEED pattern, indicating that the films were grown epitaxially on STO substrates. From the 002 diffraction angle of the films, the c-parameter was determined to be about 0.395 nm which was larger than that of BST bulk ceramics, 0.407 nm with cubic symmetry²⁴. This results indicated that the BST films epitaxially grown on STO substrates had a strained lattice with a large lattice parameter along the thickness direction²⁵. A

spontaneous polarization should be induced in the BST films due to the lattice distortion²⁶.



(a)

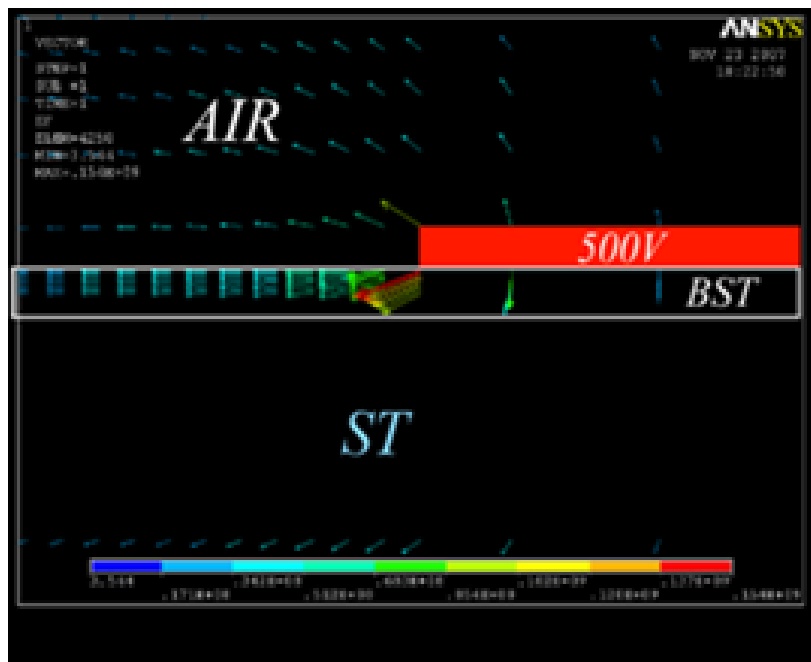


(b)

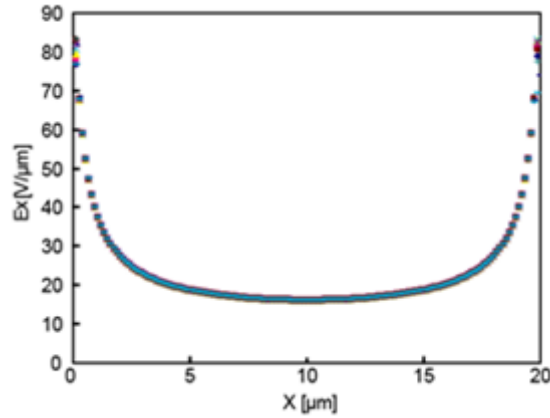
Fig. 3.5. (a) XRD profile and (b) RHEED pattern of epitaxial BST thin film.

3.3.2 Electric property of BST film

Figure 3.6 (a), (b) shows the result of electrical field analysis using finite element method. The transverse axis in Fig. 3.6 (b) indicates a position between the planer electrodes' gap. From Fig. 3.6 (b), steep change of electric field was observed at the edge of the planer electrodes' gap, and the smooth field was observed at the center of planer electrodes. Averaging this distribution, the accurate electric field on the BST film was calculated.



(a)



(b)

Fig. 3.6. (a) The result of electrical field analysis using finite element method. (b) The electric field distribution between the planer electrodes on BST thin film.

Figure 3.7 shows a polarization P vs. electric field E curve of a BST film measured with the electrode shown in Fig. 3.1, where the polarization (P) was simply calculated as the charge divided by the electrode area. A slim hysteresis loop seen in the P vs. E curve indicated that the switching of spontaneous polarization by the application of electric field was negligible. It should be stressed that the electric field applied using planer electrode was parallel to the film surface²⁵.

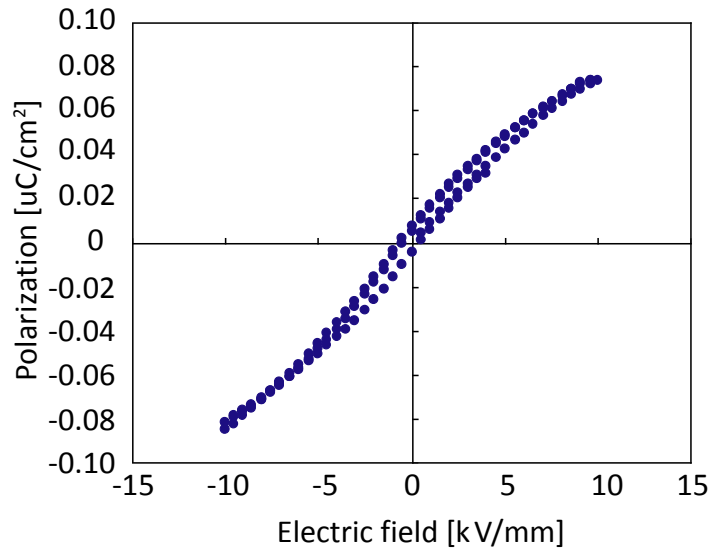


Fig. 3.7. Polarization vs. electric field curve of BST thin film.

3.3.3 Dielectric tunability of BST thin film

Figure 3.8 shows electric field dependence of capacitance in the BST film and STO substrate measured at 10 kHz. The capacitance of BST film decreases with increasing electric field though that of STO substrate is independent of the electric field, indicating that the electric field dependence of permittivity is entirely derived from the BST film. Figure 3.9 shows electric field dependence of dielectric permittivity of BST film. The permittivity of BST films was evaluated using electromagnetic field analysis as mentioned above. We found that the change of dielectric permittivity (dielectric tunability) was 53.1 % by application of electric field from 0 to 10 kV/mm. XRD analysis indicated that lattice

distortions were induced to the BST films to elongate the c-axis perpendicular to the film plane. The electric field was applied in the film plane between two planer electrodes. Nonlinear dependence without hysteresis in Fig. 3.9 may imply that polarization switching was not remained after removing electric field.

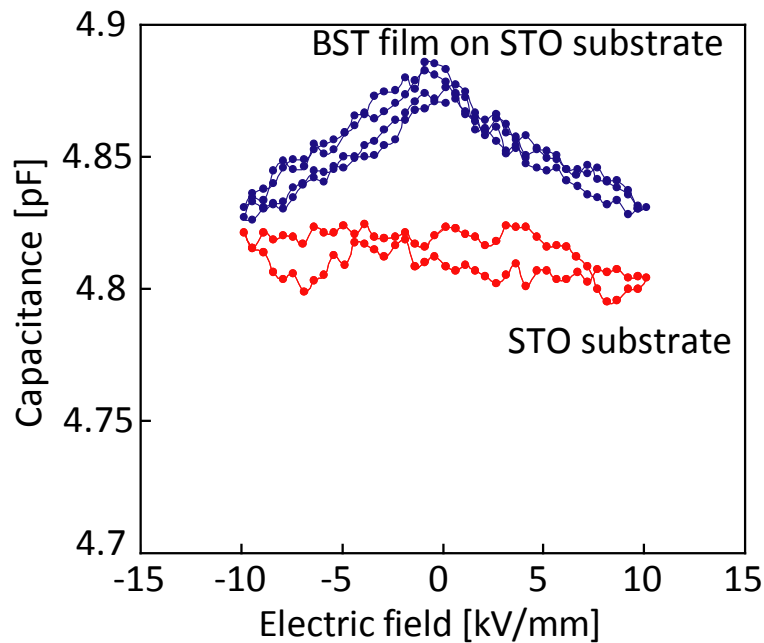


Fig. 3.8. Electric field dependence of capacitance in BST film on STO substrate and STO substrate.

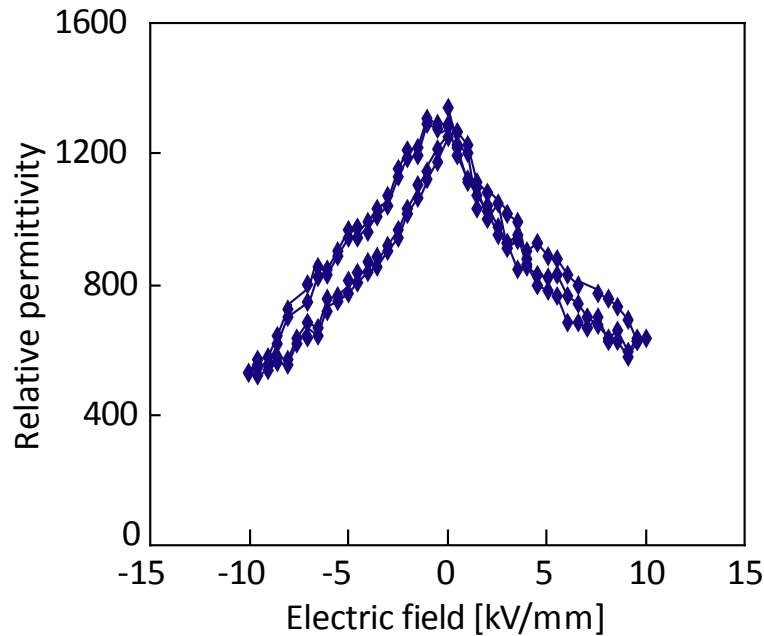


Fig. 3.9. Electric field dependence of relative permittivity in BST film calculated by electromagnetic field analysis.

3.3.4 Polarizing direction dependence of EO effect

Before the measurements of EO effect of the BST films, the EO effect of STO substrate was evaluated because it cannot be separated from the EO effect of films in the transmission geometry used in this study. Figure 3.10 shows the electric field dependence of birefringence in STO substrate. The initial birefringence is about 6.0×10^{-6} that is four times lower than that of BST. And the change of birefringence is also too small compared with that of BST thin film.

This result revealed that STO substrates showed the Kerr effect but it is negligible in comparison with that of BST thin films.

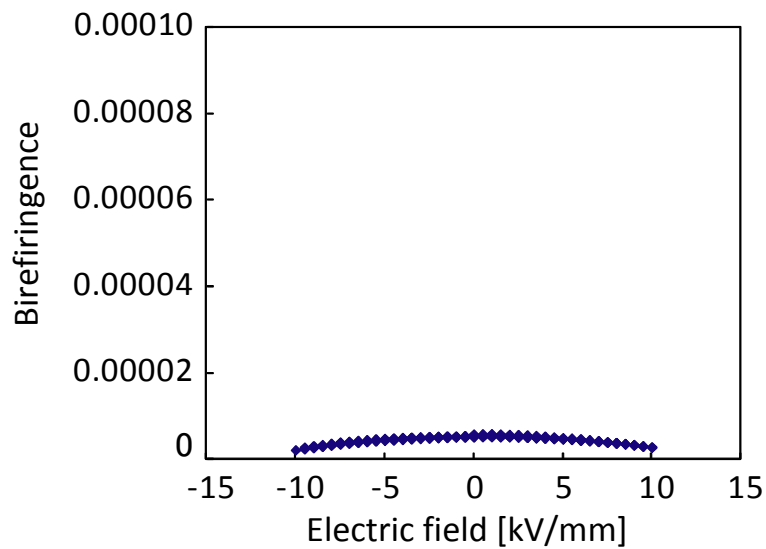


Fig. 3.10. Electric field dependence of the birefringence (Δn) in STO substrate.

Figure 3.11 shows the electric field dependence of the intensity of transmitted light (I) normalized to the intensity of incident light (I_0) measured for a BST film of 154 nm thick. Theta ϑ in the Fig. 3.11 is the angle between the polarizing direction of the incident light and the direction of electric field applied on the electrode spacing. As mentioned before, the transmitted light intensity was measured at the extinction position of the polarizer and analyzer at various electric fields. It should be recalled that a linear polarizing light does not change its polarizing state after passing through an optically isotropic medium, which

gives $I/I_0 = 0$ at the extinction position. Therefore, the I/I_0 measured at the extinction position shows the degree of birefringence of the sample. The I/I_0 measured at $\vartheta = 0$ and 90° was almost negligible, which means that the birefringence was not observed even under the electric field. On the other hand, it was found that the I/I_0 had considerable values at $\vartheta = 45^\circ$ even without electric field ($E = 0$), indicating that the BST film prepared in this study had in-plane optical anisotropy. The as-deposited film showed a relatively low I/I_0 value, but it increased after several cycles of electric field before the measurement, which was shown by an arrow in the Fig. 3.11.

Form the I/I_0 data shown in Fig. 3.11, the birefringence Δn of the film was evaluated. The birefringence of the BST film is shown in Fig. 3.12 as a function of electric field. The arrow in the figure shows the change of birefringence of the as-deposited film after several cycles of electric field.

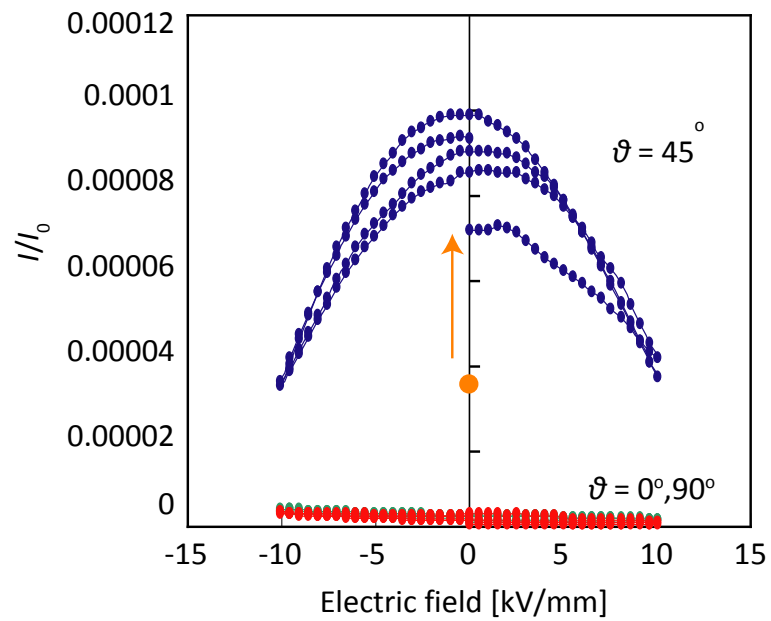


Fig. 3.11. Electric field dependence of the intensity of transmitted light (I) normalized to the intensity of incident light (I_0) in BST thin film. The arrow in the figure shows the change of intensity of the as-deposited film after several cycles of electric field.

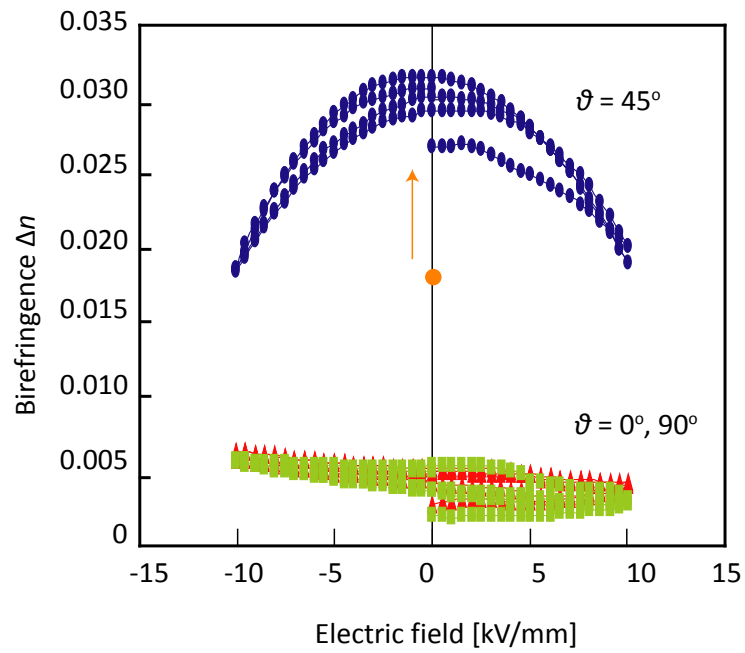


Fig. 3.12. Electric field dependence of the birefringence (Δn) in BST thin film. The arrow in the figure shows the change of birefringence of the as-deposited film after several cycles of electric field.

The birefringence observed at $E = 0$ will be discussed at first. The birefringence observed at $\vartheta = 45^\circ$ indicates that the film is an optically anisotropic medium. Nearly zero birefringence at $\vartheta = 0$ and 90° means that the optical axis of the BST film is in the [100] or [010] directions in Fig. 3.1, because birefringence should not be observed when the polarizing direction of incident light is parallel to the optical axis. If the optical axis is parallel to the [100] or [010] directions, maximum birefringence should be observed at $\vartheta = 45^\circ$, which is consistent with the experimental results obtained in this study. The anisotropy of the film is attributable to the existence of lattices with the c -axis aligned in the film plane. In the transmission geometry shown in Fig. 3.4, the film would behave as an optically isotropic medium if the c -axes of all lattices aligned along the film thickness. In the as-deposited film, most of lattices have the c -axis along the film thickness as shown in Fig. 3.13 (a) but some lattices have the c -axis along the [100] or [010] direction with different probabilities. This gives rise to the small birefringence observed in the as-deposited film. By applying electric field along the [100] direction before the measurement, the c -axis of some lattices rotates from the [001] to [100] direction to increase the birefringence, which was shown by the arrow in Fig. 3.12. It should be noted that the portion of lattices with the c -axis in the film plane is quite small even after the application of electric field because the birefringence (Δn) observed was in the order of 10^{-3} .

The change of birefringence induced by electric field (EO-effect) will be discussed in the followings. The EO-effect was not observed at $\vartheta = 0$ and 90° because the change of refractive index by the electric field cannot be detected as the change of birefringence when the polarizing direction of the incident light is along the optical axis as shown in Fig. 3.13 (b). On the other hands, the EO-effect was observed at $\vartheta = 45^\circ$ because the change of refractive index along the light axis by the electric field affected to the change of birefringence when the polarizing direction of incident light is aligned at 45° to planer electrode as shown in Fig. 3.13 (c). This result indicates that the optical axis of the BST film is not changed by the electric field applied in the measurement. In the case of $\vartheta = 45^\circ$, the change of birefringence with electric field does not show a clear hysteresis as shown in Fig. 3.12, indicating that the c -axes aligned in the [100] direction were not switched by the electric field. This result is consistent with the slim P vs. E hysteresis curve shown in Fig. 3.7.

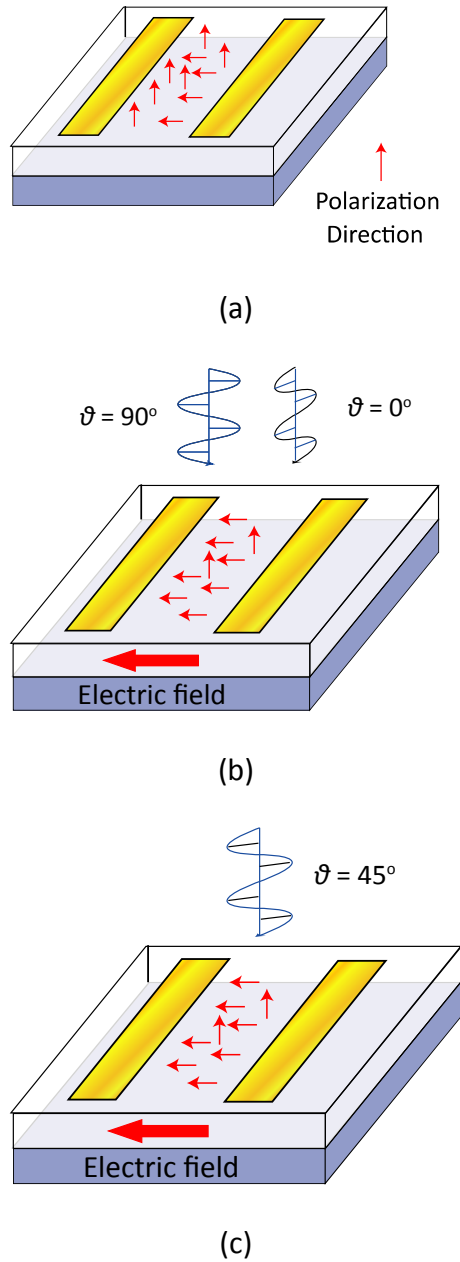


Fig. 3.13. Orientation of BST lattices, direction of electric field and polarizing direction of incident light (θ) in the EO-measurement. (a) as-deposited films measured at $\theta = 45^\circ$, (b) films after several cycles of electric field measured at $\theta = 0$ and 90° and (c) films after several cycles of electric field measured at $\theta = 45^\circ$.

As mentioned above, the birefringence of BST film is caused by the lattice distortions to elongate the c -axis and the application of electric field to the as-deposited film increased the birefringence with the switching of c -axis from the film thickness direction to the electric field direction. On the other hand, the EO-effect is dominantly determined by the Kerr effect to reduce the birefringence but the switching of c -axis was hardly observed after several cycles of electric field.

3.3.5 Comparison of electric field dependence of birefringence and dielectric permittivity

The electric field dependence of birefringence measured at $\vartheta = 45^\circ$ in Fig. 3.12 was nearly parabolic, showing that the Kerr effect is dominantly determined the EO-effect of the BST film. The Kerr coefficient calculated from the change of birefringence at $\vartheta = 45^\circ$ was $3.44 \times 10^{-17} \text{ m}^2/\text{V}^2$ which was almost consistent with the literature values^{15,16}. The birefringence induced by applying 200 V of bias voltage (10 kV/mm) is 0.018, giving rise to the $\delta(\Delta n) / n = 0.6 \%$, where $n = 2.038$ was refractive index at wavelength of $1.55 \text{ }\mu\text{m}$ ²⁷. This denominator must be the refractive index because a birefringence is the remainder between crystal orientations' refractive indices. The birefringence does not show direct contribution from electric polarization. On the other hand, we believe difference

between the birefringence and the refractive index changes due to EO-effect is little because the birefringence change is mainly contributed by a change of refractive index in the crystal orientation where electric field was applied.

The dielectric tunability and EO effect of the BST film evaluated in this study were 53.1 % and 0.6 % from 0 to 10 kV/mm, respectively. This result gives us an important conclusion that a material exhibiting a high dielectric tunability does not always exhibit a high EO effect although the lattice distortion induced variation of birefringence.

Dielectric permittivity of oxide ferroelectric is mainly determined by the ionic and dipole polarizations, where the ionic polarization is due to phonon effects while the dipole polarization is due to domain contributions as well as dipole fluctuations in polar nano-regions (PNRs) in relaxor materials²⁸. The dielectric tunability can be regarded as a nonlinear dielectric response to electric fields. The dipole polarization dominates the dielectric tunability. On the other hand, refractive index is determined by the electronic polarizations and EO effect can be regarded as a nonlinear response of electric polarization to external electric fields. Nonlinear response appearing in the expansion series of susceptibility with respect to electric fields normally increases with linear susceptibility, which means that the nonlinear response giving rise to EO effect increases with refractive index. Therefore the tunability is only one factor to

realize a high EO effect. It is known that high electron density materials containing heavy ions exhibit high refractive index²⁹⁻³².

This speculation explains the experimental facts that dielectric tunability of lanthanum added lead zirconate-titanate ($\text{Pb}_{1-x}\text{La}_x\text{Zr}_{1-y}\text{Ti}_y\text{O}_3$, PLZT) is comparable to that of BST but EO effect of PLZT is much higher than that of BST³³⁻³⁶ because PLZT contains heavy ions such as lead and lanthanum, and also that the dielectric tunability and EO effect of potassium tantalate (KTaO_3 , KTO) are almost the same as BST³⁷ because molar weights of the two materials are comparable. It should be recalled that the EO effect of bismuth silicate ($\text{Bi}_{12}\text{SiO}_{20}$, BSO) is much lower than that of PLZT though it contains a heavy ion of bismuth³⁸⁻⁴⁰.

This implies that the heavy ions are only one factor to realize a high EO effect. The other important factor is the variation of polarization (tunability) due to application of electric field. EO effect is defined in another way as electrically induced changes of birefringence. PNRs are clusters with anisotropic nature caused by thermally fluctuating spontaneous polarizations. Reorientations of these spontaneous polarizations by electric fields should produce very high optical anisotropy in relaxors, which is actually the origin of high EO effect of relaxor.

3.4 Summary of chapter 3

BST epitaxial films were grown on STO single crystal substrates using RF-sputtering method and planer electrodes were formed on the film surfaces using lithography technique. The BST films had strained lattices to elongate the *c*-axis perpendicular to the film surface. Small birefringence observed in the as-deposited film was enhanced by the application of in-plane electric field before the measurement, which was interpreted by the switching of *c*-axis of some lattices from the [001] to [100] directions. We concluded that this birefringence was induced by lattice distortion. The birefringence caused by these lattices had the optical axis along the [001] direction.

The Kerr coefficient of the BST film was determined to be $3.44 \times 10^{-17} \text{ m}^2/\text{V}^2$. The tunability of dielectric permittivity by applying electric field from 0 to 10 kV/mm was 53.1 %, while the tunability of birefringence (EO effect) was only 0.6 %. This result indicated that the materials with high tunability didn't always exhibit a high EO effect though the reorientation of polarization induced the variation of birefringence.

By considering the results obtained in this study with literature data, we concluded that the variation of the polarization by applying of electric field (tunability) in relaxor materials was not a sufficient condition to obtain high EO effect but high electric polarization is important to obtain the materials with

high EO effect, which means that a material exhibiting high EO effect will be obtained in relaxors containing heavy ions such as PLZT and BST as shown in problem (ii).

References

- [1] X. Tang, K. Chew, H. Chan, *Acta Materialia* 52, 5177 (2004)
- [2] K. Chen, C. Yang, W. Tzou, C. Huang, D. Chou, *Ferroelectrics* 384, 166 (2009)
- [3] J. Cheng, J. Wang, T. Dechakupt, S. Mckinstry, *Appl. Phys. Lett.* 87, 232905 (2005)
- [4] W. Ren, S. Mckinstry, C. Randall, T. Shrout, *J. Appl. Phys.* 89, 767 (2001)
- [5] J. Park, J. Lu, S. Stemmer, R. York, *J. Appl. Phys.* 97, 084110 (2005)
- [6] S. Liu, Y. Lin, J. Weaver, W. Donner, X. Chen, C. Chen, J. Jiang, E. Meletis, A. Bhalla, *Appl. Phys. Lett.* 85, 3202 (2004)
- [7] X. Chou, J. Zhai, X. Yao, *Appl. Phys. Lett.* 91, 122908 (2007)
- [8] A. Tombak, J-P. Maria, F. Ayguavives, Z. Jin G. T. Stauf, A. I. Kingon A. Mortazawi, *Microwave and Wireless Component Lett.* 12, 3 (2002)
- [9] E. G. Erker, A. S. Nagra, Y. Liu, P. Periaswamy, T. R. Taylor, J. Speck, R. A. York, *Microwave and Wireless Component Lett.* 10, 10 (2000)
- [10] A. Tombak, J-P. Maria, F. Ayguavives, Z. Jin G. T. Stauf, A. I. Kingon A. Mortazawi, *Trans. on Microwave Theory and Techniques* 51, 462 (2003)
- [11] J. Im, O. Auciello, P. K. Baumann, S. K. Streiffer, D. Y. Kaufman, A. R. Krauss, *Appl. Phys. Lett.* 76, 625 (2000)
- [12] J. Im, O. Auciello, S. K. Streiffer, *Thin Solid Films* 413, 243 (2002)
- [13] H. D. Wu, Z. Zhang F. Barnes, M. Jackson, A. Kain, J. D. Cuchiaro, *Trans. on*

Appl. Superconductivity 4, 156 (1994)

[14] B. Su, J. E. Holmes, C. Meggs, T. W. Button, J. Eur. Ceram. Soc. 23, 2699 (2003)

[15] J. Li, F. Duewer, C. Gao, H. Chang, and X. -D. Xiang, Am. Inst. Phys. 76(6), 769 (2000)

[16] D.Y. Wang, C. L. Mak, K. H. Wong, H. L. W. Chan, C. L. Choy, Ceram. International 30, 1745 (2004)

[17] J. Li, F. Duewer, C. Gao, H. Chang, X. Xiang, Appl. Phys. Lett. 76, 769 (2000)

[18] D. Kim, S. Moon, E. Kim, S. Lee, J. Choi, H. Kim, Appl. Phys. Lett. 82, 1455 (2003)

[19] D. Wang, J. Wang, H. Chan, C. Choy, Integrated Ferroelectrics 88, 12 (2007)

[20] J. Qiu, Q. Jiang, J. Appl. Phys. 102, 074101 (2007)

[21] D. Wang, S. Li, H. Chang, C. Choy, Appl. Phys. Lett. 96, 061905 (2010)

[22] K. Nagata, Electromagnetics, (Asakura, Tokyo, 1981)

[23] T. Ogawa, *Fundamentals on crystal technology*, (Shokabo, Tokyo, 1998)

[24] M. McQuarrie. J. Am. Chem. Soc. 38, 444 (1955)

[25] Z. Ye, *Handbook of advanced dielectric, piezoelectric and ferroelectric materials*, first ed., (CRC, New York, 2008)

[26] Y. Lin, Jang-Sik Lee, H. Wang, Y.Li, S.R.Foltyn, Q.X.Jia, Appl. Phys. Lett. 85, 5007 (2004)

- [27] F. Tcheliabou, H.S. Ryu, C.K. Hong, W.S. Park, S.Baik, *Thin Solid Films* 305, 30 (1997)
- [28] T. Tsurumi, J.Li, T.Hoshina, H.Kakemoto, M.Nakata, J.Akedo, *Appl. Phys. Lett.* 91, 182905 (2007)
- [29] K. Nashimoto, N. Tanaka, M. Labuda, D. Ritums, J. Dawley, M. Raj, D. Kudzauma, T. Vo, *Trans. of Broadband networks*, 195 (2005)
- [30] Y. Bing, R. Guo, A. Bhalla, *Ferroelectrics* 242, 1 (2000)
- [31] W. Tsang, K. Chan, C. Mak, K. Wong, *Appl. Phys. Lett.* 83, 1599 (2003)
- [32] D. Mchenry, J. Giniewicz, T. Shrout, S. Jang, A. Bhalla, *Ferroelectrics* 102, 161 (1990)
- [33] P. D. Thacher, *J. Appl. Phys.* 41, 4790 (1970)
- [34] G. Haertling, *Ferroelectrics* 75, 25 (1987)
- [35] C. Kirkby, *Ferroelectrics* 37, 567 (1981)
- [36] T.Fujii, T.Suzuki, Y.Fujimori, T.Nakamura, M.Moriwake, H.Takasu, *Jpn. J. Appl. Phys.* 45, 7520 (2006)
- [37] Chen Ang, A.S.Bhalla, L.E.Cross, *Phys Review* 64, 184104 (2001)
- [38] M. Henry, S. Mallick, D. Rouede. *J. Appl. Phys.* 59, 2650 (1986)
- [39] K.Nomura, H.Ogawa, *J. Appl. Phys.* 70, 3234 (1991)
- [40] I. Vasconcelos. M. Pimenta. A. Sombra, *J. Mat. Science* 36, 587 (2001)

Chapter 4

Relaxation and frequency dependence of electro-optic coefficient

4.1 Introduction

4.1.1 Relaxation of dielectric permittivity and driving efficiency in EO modulators

The dielectric permittivity in dielectrics exhibits relaxation with varying frequency of the external electric field. Figure 4.1 shows the schematic diagram of the dielectric dispersion in a wide frequency range in the oxide materials¹⁻³. Gradual depression of permittivity is observed with increasing applying frequency of the external electric field. Dielectric function can be described as the sum of four polarizations, namely the interfacial, dipole, ionic, and electronic polarizations, as shown in Fig. 4.1. In chapter 3, we concluded that the polarization induced birefringence. Therefore, it is estimated that the frequency dependence of EO effect show the relaxation with increasing applying frequency of the external electric field corresponding with the relaxation in dielectric dispersion.

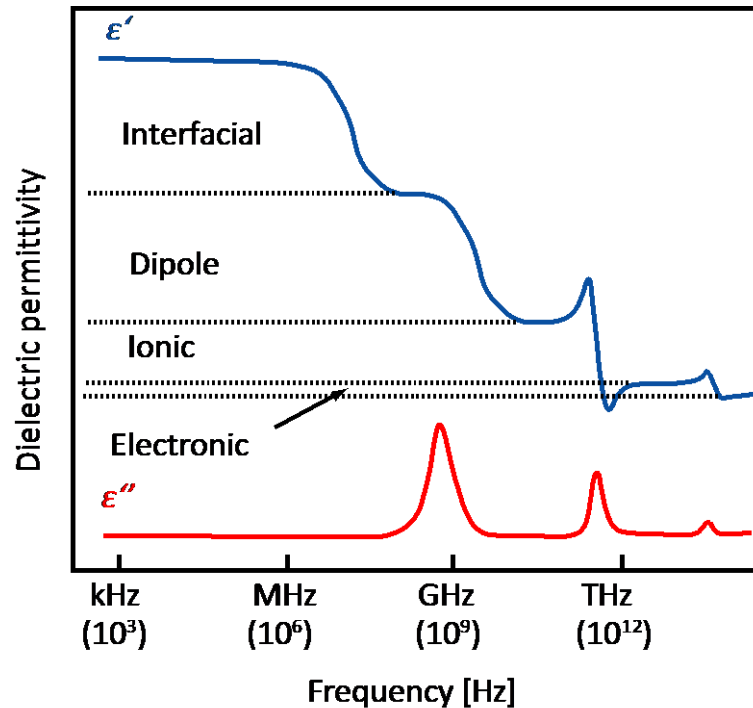


Fig. 4.1 Schematic diagram of dielectric dispersion in oxide ferroelectrics

Lanthanum added lead zirconate titanate ($(\text{Pb}_{0.91}\text{La}_{0.09}\text{Zr}_{0.65}\text{Ti}_{0.35}\text{O}_3, \text{PLZT9})$ and lithium niobate ($\text{LiNbO}_3, \text{LN}$) are major EO materials employed in EO modulators⁴⁻¹³. As mentioned in chapter 1, the driving efficiency of EO modulator using PLZT9 indicate a relaxation of modulation efficiency in high speed driving up to 10GHz, though that of EO modulator using LN single crystal does not show relaxation until 10 GHz as shown in Fig. 1.5¹⁴⁻¹⁶. PLZT9 shows high dielectric permittivity, and it indicates gradual depression of permittivity with increasing applying frequency of the external electric field. On the other hands, LN shows low permittivity, and flat dielectric dispersion at any frequencies¹⁷⁻²⁰. It is noted that the EO coefficient determine the

modulation efficiency in EO modulator, and the polarization is determined by dielectric permittivity. Therefore this result consisted with the estimation as described below. However the analysis to formularize this relation between EO coefficient and dielectric permittivity was not reported therefore the contribution of dielectric permittivity to EO effect is still ambiguous.

4.1.2 Objective

In this chapter, we measured the dielectric dispersion of PLZT9 and LN optical modulator to elucidate the relation between the EO coefficient and dielectric permittivity in high speed driving. We aimed to formularize the contribution of dielectric permittivity to EO effect from analysis of this relation.

4.2 Experimental procedure

4.2.1 Measurement of dielectric permittivity at low frequency

The driving efficiency of each modulators were already measured as shown in Fig. 1.5. Therefore in this chapter, we measured the frequency dependence of dielectric permittivity up to GHz region. The transparent PLZT9 (Furuuchi Chemical Corp.) ceramics and LN single crystal (NEL crystal) was employed as samples. The dielectric permittivity if these samples in low frequencies, namely kHz region, were measured by the conventional impedance method. Top and bottom planer electrodes

were formed on the surfaces by DC gold sputtering. The impedance was measured using impedance analyzer (4294A, Agilent Tech.) up to 1 MHz and was converted to dielectric permittivity.

4.2.2 Methodology of micro-sized planar electrodes method

In the electric region, namely low frequencies to GHz, several methods have been proposed to determine the complex permittivity. Typical methods are displayed in the Fig. 4.2. Plate condenser method that is the conventional impedance method done in 4.2.1 enables the direct measurement of permittivity continuously as a function of frequency, $\omega = 1/\sqrt{LC}$, suppose the equivalent circuit is a parallel resonant LCR circuit²¹. Since capacitance of dielectric specimen mostly determines the ω_0 , we cannot measure the impedance of the pure sample due to an impedance resonance occurring in MHz to GHz region if the permittivity of the samples are above hundreds.

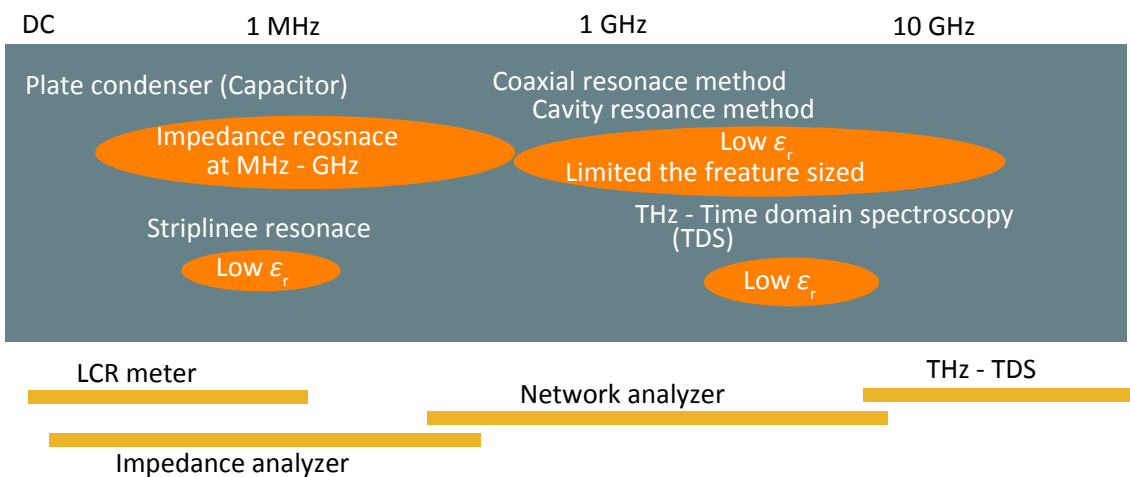


Fig. 4.2 Typical methods of measurement of permittivity in microwave region.

We've already proposed the novel dielectric measurement technique in high frequencies, "Micro-sized planar electrodes method"^{22,23}. In this method, micro-sized planar metal electrodes with the source and ground ports are formed on the dielectric specimen surface using photolithography technique. When AC field is applied between the source and ground ports of electrodes, curved electric fields are generated in dielectrics as shown in Fig. 4.3.

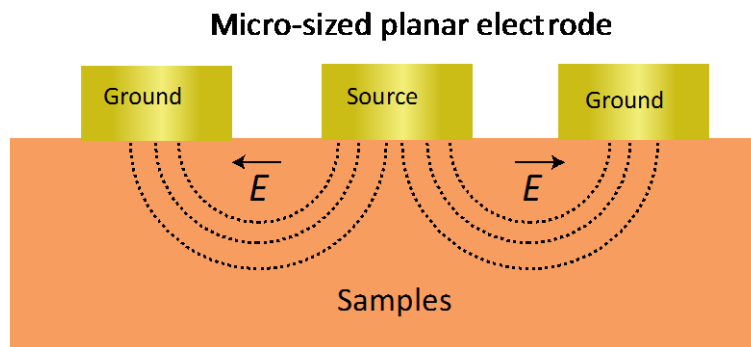


Fig. 4.3 Generated field inside the dielectrics in the micro-sized planar electrodes method.

The admittance between the source and ground ports is measured with an impedance analyzer (4991A, Agilent Tech.) and the dielectric permittivity was determined with the help of electromagnetic field simulation (Sonnet ver. 11, Sonnet Software Inc.).

Capacitance in sample flat electrodes plates model (C_s) can be given by $C_s = \epsilon \frac{S}{d}$.

Where ϵ is permittivity of sample, S is surface area, and d is distance between electrodes. We can decrease S by one of hundreds to thousands scale, instead of

decreasing d . Capacitance of micro-sized planar electrodes can be decreased into the scale of one of hundreds, compared to that of flat electrodes. As a result, we can measure dielectric permittivity continuously as a function of frequency up to GHz without impedance resonance.

4.2.3 Designing of micro-sized planar electrodes

Besides the decreasing the capacitance of sample, we also have to consider the impedance matching. Since the characteristic impedance (Z_0) of output circuit^{24,25}, namely Z_0 of an impedance analyzer, is 50 Ω , we need to move the impedance of a measured circuit close to 50 Ω at measuring frequencies. Measurement accuracy of sample impedance E_{total} can be described as the following,

$$E_{total} = E_a + E_b \quad (4.1)$$

where E_a is accuracy derived from power supply of impedance analyzer and E_b is accuracy due to sample impedance²⁶, namely,

$$E_b = \pm \left(\frac{Z_s}{|Z_x|} + Y_0 |Z_x| \right) \quad (4.2)$$

where Z_s , Y_0 are stray impedance and stray admittance, respectively. We can obtain accurate output impedance, adjusting the sample impedance $|Z_x|$ into 50 Ω at target frequency. Micro-sized planar electrodes were designed and their impedances were calculated using the electromagnetic field simulation (Sonnet-em ver. 11). The sonnet-em solves the Maxwell equation of the planar problems by the moments

method as shown in Fig. 4.4.

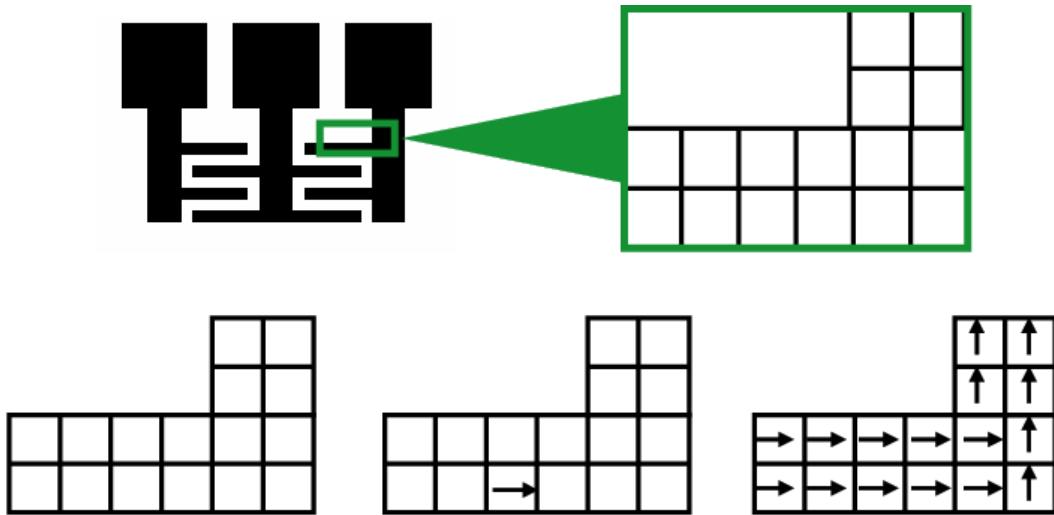
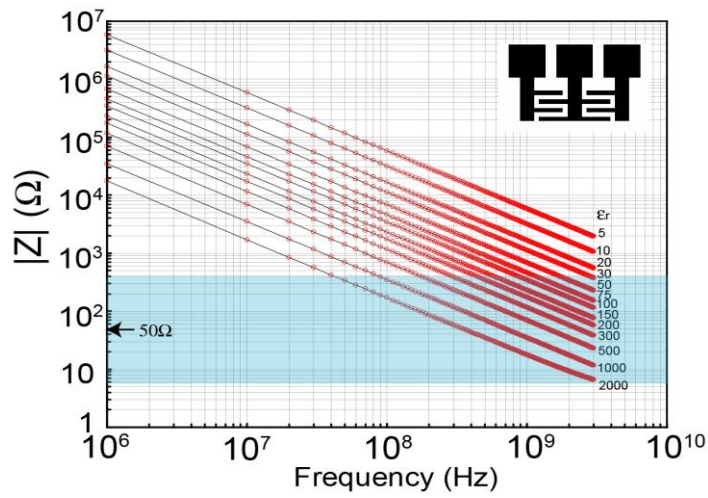
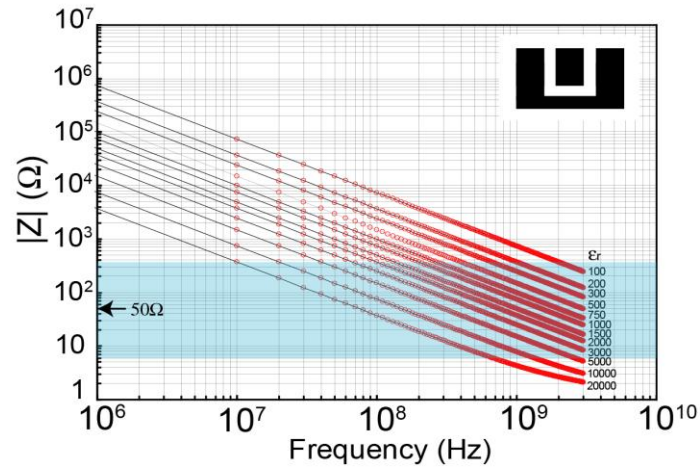
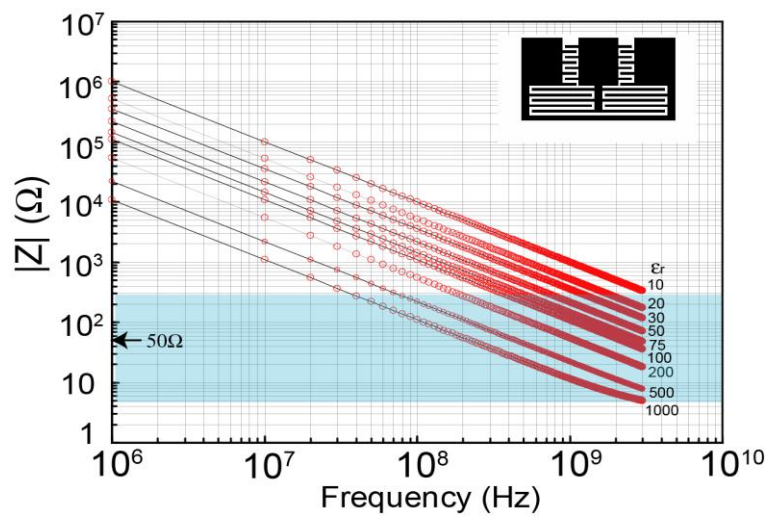


Fig. 4.4 Calculation procedure by the moment method.

Figure 4.5 (a) - (c) are the calculated impedance $|Z_x|$ as a function of frequency for different ϵ_r using electromagnetic field simulation for different electrodes which has different numbers of inter digital fingers (pattern 1 - 3). Semi-transparent band shows the area of $E_{\text{total}} < \pm 5\%$. Figures of designed planar electrodes and their top-view photographs are shown in Table 4.1. We can determine the dielectric permittivity of samples with $\epsilon_r = 50 - 7000$ using these electrodes.

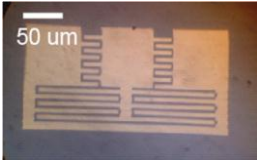
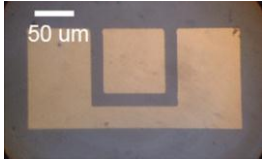






(c)

Fig. 4.5 Calculated impedance $|Z_x|$ as a function of frequency using electromagnetic field simulation (a) pattern 1, (b) pattern 2, and (c) pattern 3

Table 4.1 Features of designed planar electrodes and their top-view photographs

Photograph		
Electrode type		
Pattern	1	2
Permittivity of sample	20 - 500	1000 - 20000
Measurement frequency	up to 3 GHz	up to 3 GHz
Electrode size [um]	267 x 123	280 x 125
Gap width [um]	2.6	20

4.3 Result and discussion

4.3.1 Determination for dielectric permittivity up to GHz

The complex admittance of formed electrodes was measured at 1 MHz – 3 GHz with an impedance analyzer (E4991A, Agilent Tech.). Although the equivalent circuit cannot be assumed due to the distributed constant circuit, the capacitive complex admittance Y^* , of the total circuit can be described by

$$Y^* = j\omega C^* = G + jB \quad (4.3)$$

where the C^* denotes the capacitance of the total circuit, G is conductance, and B is susceptance²⁷. Suppose the total capacitance of the circuit is constant, we can obtain the liner relationship between the frequency and susceptance B . Before the measurement of the sample, open short and 50Ω load calibrations were performed using an impedance standard substrate kit (Impedance Standard Substrates, Cascade Microtech). Figure 4.6 shows the schematic diagram of the measurement system of micro-sized planar electrodes method.

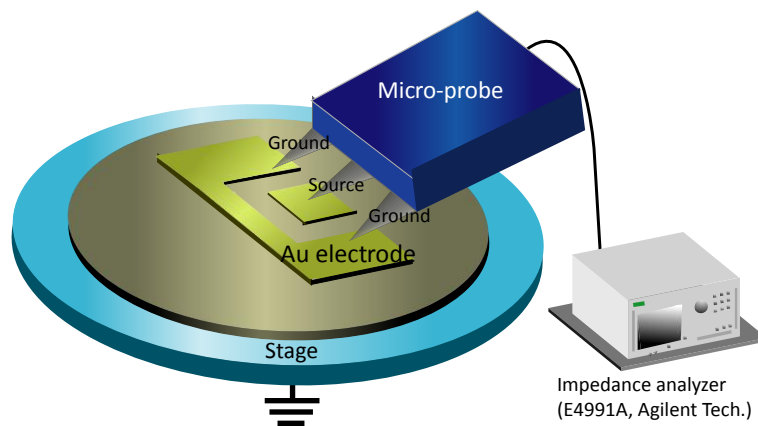


Fig. 4.6 Schematic diagram of the measurement system of micro-sized planar electrodes method.

Figure 4.7 and 4.8 show susceptance B measured for the electrode on LN single crystal and PLZT9 ceramics as a function of frequency in the frequency range up to 3GHz (showed by open circles). The result of simulation at $\epsilon_r = 58$ by using electrodes pattern 1 was also indicated in Fig. 4.7 as solid line. Good fitting between experiment and simulation indicates that the measuring method developed this study is reliable.

Dielectric permittivity of LN single crystal was determined by the try-and-error method at each frequency, with taking different permittivities corresponds to that calculated. Permittivity of LN single crystal was almost constant with the value of $\epsilon_r = 50$ up to 3GHz. In the case of PLZT9, although the susceptance B corresponded to the calculation of $\epsilon_r = 3650$ at low frequency, B value corresponded to the calculation $\epsilon_r = 1350$ near the 3 GHz by using electrodes pattern 2 as shown in Fig. 4.8. This result indicates the permittivity depression in GHz region in PLZT9 ceramics. The dielectric permittivity of PLZT9 was also determined by fitting measured susceptance into that calculated using try-and-error method at each frequency.

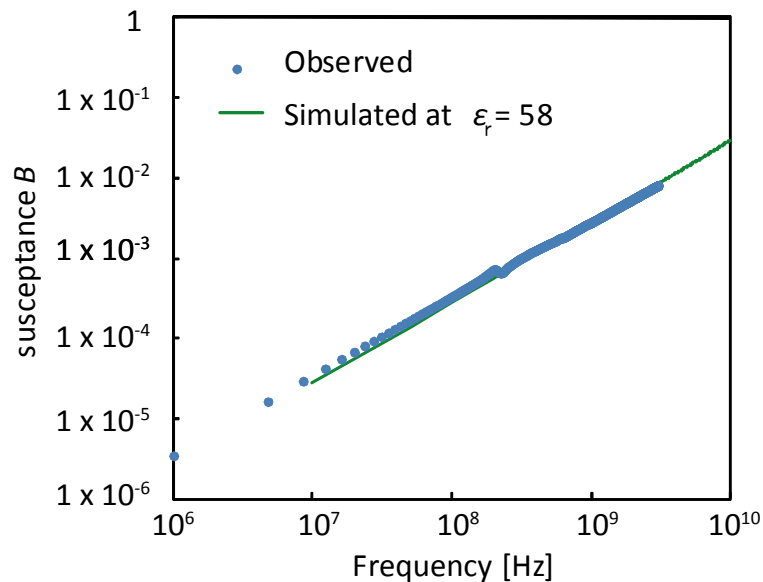


Fig. 4.7 Observed susceptance (circles) and calculated result (solid lines) of the planar electrodes at $\epsilon_r = 58$ as a function of frequency up to 3 GHz

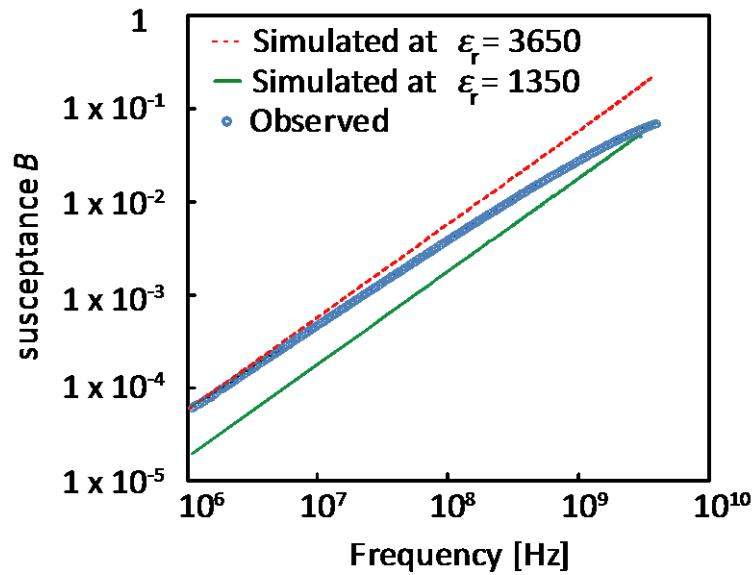


Fig. 4.8 Observed susceptance (circles) and calculated result of the planar electrodes at $\epsilon_r = 3650$ (dashed lines) and 1350 (solid lines) as a function of frequency up to 3 GHz

Figure 4.9 and 4.10 show the dielectric dispersion of LN single crystal and PLZT9 ceramics. The dielectric permittivity of LN was almost independent from frequency up to 3GHz as shown in Fig. 4.9. On the other hand, the dielectric dispersion of PLZT9 shows large relaxation up to 3GHz as shown in Fig. 4.10. These results were almost consistent with tendency from some literatures²⁸⁻³⁰.

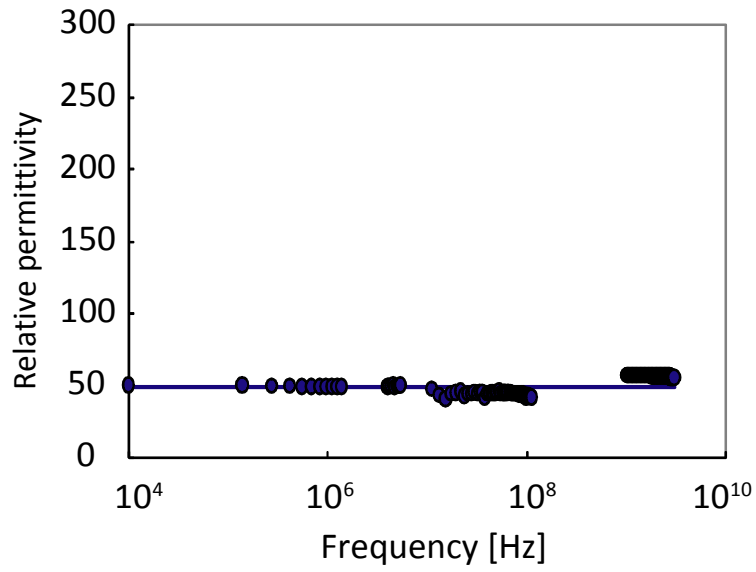


Fig. 4.9 Dielectric dispersion of LN single crystal up to 3GHz.

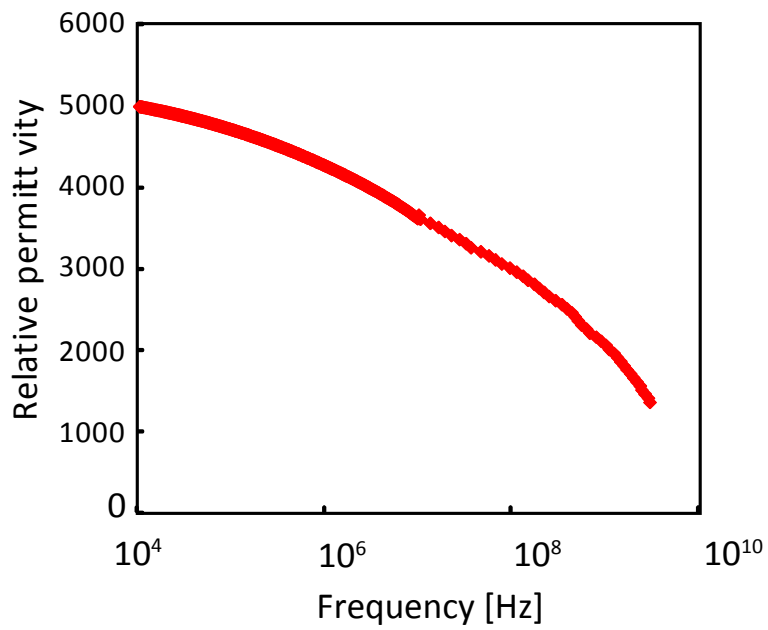


Fig. 4.10 Dielectric dispersion of PLZT9 ceramic up to 3GHz.

4.3.2 Expansion of equation for EO effect

As mentioned in chapter 2 and 3, the linear and quadratic EO effect is expressed as

$$\Delta\left(1/n_{ij}^2\right)=r_{ijk}E_k + R_{ijkl}E_kE_l \quad (4.4)$$

where r_{ijk} is the Pockels coefficient, R_{ijkl} is Kerr coefficient, n is refractive index, and E is electric field³¹. Generally, the EO effect is expressed that the change of refractive indices as a function of electric field. For example if the electric field E_3 is applied, the Eq. (4.4) is expressed as

$$\Delta\left(1/n_{ij}^2\right)=r_{ij3}E_3 + R_{ij33}E_3^2 \quad (4.5)$$

However, in dielectrics, we employed the polarization instead of electric field. The change of polarization with applying electric field induces the lattice distortion. This lattice distortion gives rise to the change of refractive index caused by the change of electron polarization as shown in Fig. 4.11. Therefore, in dielectrics, we have to consider two contributions to the change of refractive index: the contribution of applying electric field, and the contribution of lattice distortion due to the change of polarization.

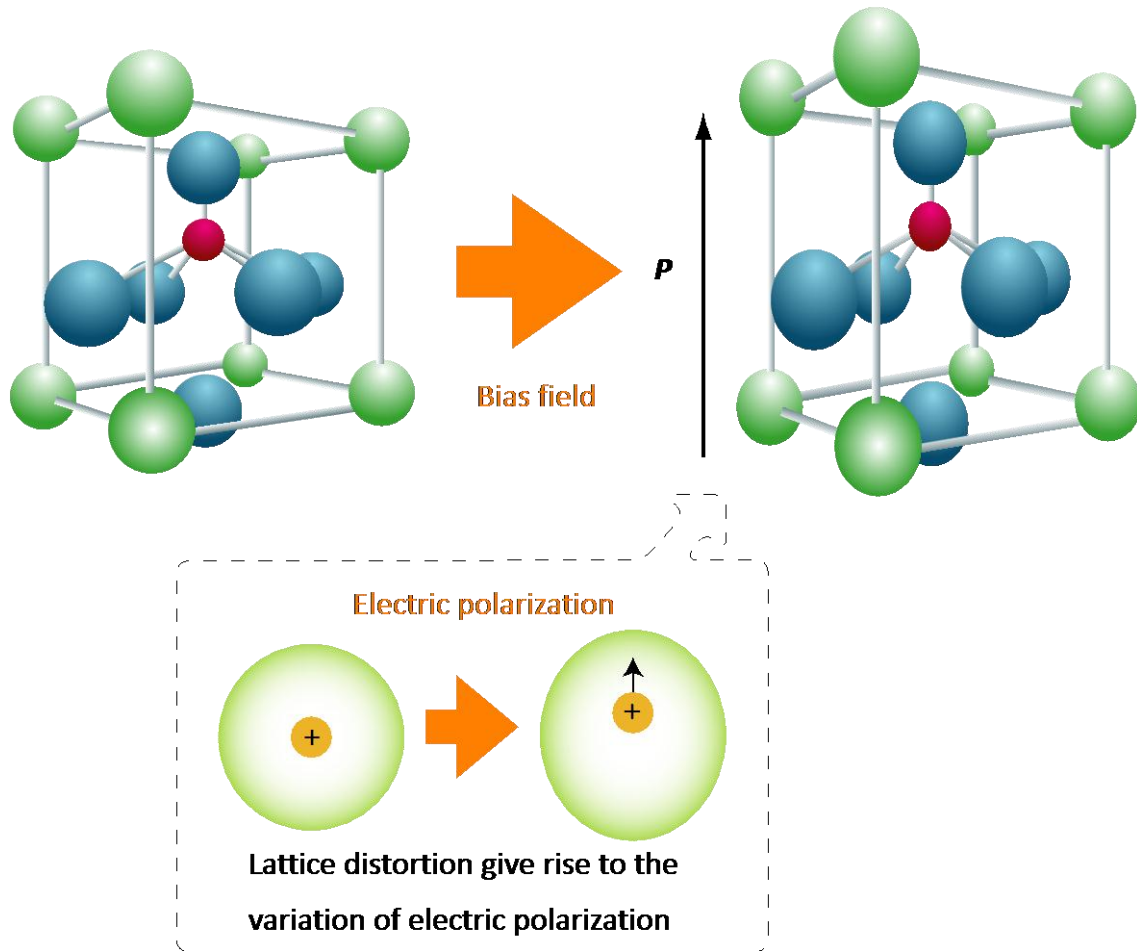


Fig. 4.11 The change of electric polarization due to lattice distortion that gives rise to the change of refractive index in dielectric materials.

Thus, the polarization is better variable number than electric field to express the EO effect. Here, the equation for EO effect is redefined as

$$\Delta\left(1/n_{ij}^2\right)=g_{ijkl}P_kP_l \quad (4.6)$$

where g_{ijkl} is the EO coefficient as defined EO coefficient proportional to polarization^{32,33}, and P_k and P_l are the polarization expresses as $\mathbf{P}(P_1, P_2, P_3 + P_s)$.

Chapter 4 Relaxation and frequency dependence of electro-optic coefficient

After that, we called this EO coefficient as “EO coefficient g ” to distinguish by the conventional EO coefficient. The P_s is the spontaneous polarization ($P_s \gg P_3$). For example, the polarization is described as following equation if the external electric field E_3 is applied.

$$P_3 = \epsilon_0 (\epsilon_r - 1)E_3 \quad (4.7)$$

where ϵ_0 is permittivity of free space, and ϵ_r is relative permittivity. The Eq. (4.6) was expanded as described following equation with substituting the polarization P in Eq. (4.7) into Eq. (4.6).

$$\begin{aligned} \Delta(1/n_{ij}^2) &= g_{ij33} P_s^2 + 2g_{ij33} P_3 P_s + g_{ij33} P_3^2 \\ &= g_{ij33} P_s^2 + 2g_{ij33} \epsilon_0 (\epsilon_r - 1) P_s E_3 + g_{ij33} (\epsilon_0 (\epsilon_r - 1))^2 E_3^2 \end{aligned} \quad (4.8)$$

In this equation, the first term in Eq. (4.8) is initial birefringence that is independent from the electric field. The second term in Eq. (4.8) is Pockels effect that is proportional to the electric field. The third term in Eq. (4.8) is Kerr effect that is proportional to the square of electric field. From the comparison of Eq. (4.5) and (5.8), the Pockels and Kerr coefficient is described as

$$r_{ij3} = 2g_{ij33} \epsilon_0 (\epsilon_r - 1) P_s \quad (4.9)$$

$$R_{ij33} = g_{ij33} \epsilon_0^2 (\epsilon_r - 1)^2 \quad (4.10)$$

The Pockels and Kerr coefficients are products of EO coefficient g , dielectric permittivity, and spontaneous polarization. Therefore the material with high permittivity, and spontaneous polarization. Therefore the material with high permittivity show high EO coefficient because it show high Polarization and

spontaneous polarization. Moreover, the Pockels effect is the EO effect caused by the product of spontaneous polarization and polarization induced by external electric field. This is why the Pockels effect only observed in anisotropic crystals. It is similar relations in the case of piezoelectric effect and electrostrictive effect³⁴.

4.3.3 Calculation of driving efficiency due to EO effect

As mentioned above in 5.1, the driving efficiency as shown in Fig. 1.5 is derived from EO effect dominantly. If the expanded equation Eq. (4.8) is reliable, the Pockels and Kerr coefficient are functions of dielectric permittivity. The frequency dependence of driving efficiency due to EO effect in LN single crystal and PLZT9 ceramics were calculated with substituting the frequency dependence of dielectric permittivity as shown in Fig. 4.9 and 4.10. Figure 4.12 show the calculated and observed results of frequency dependence of driving efficiency in LN single crystal and PLZT9 ceramic. Good agreement between the calculated and observed results indicated that the expanded equation in this chapter is reliable. From this result, we estimated that the EO coefficient g remains constant with varying the frequency of applied electric field, because if the EO coefficient g indicates relaxation corresponding to dielectric permittivity, the EO coefficient should show larger decreasing than the calculated result from Eq. (4.10). Therefore the relaxation of driving efficiency is determined by that of dielectric permittivity due to polarization P and spontaneous polarization P_s .

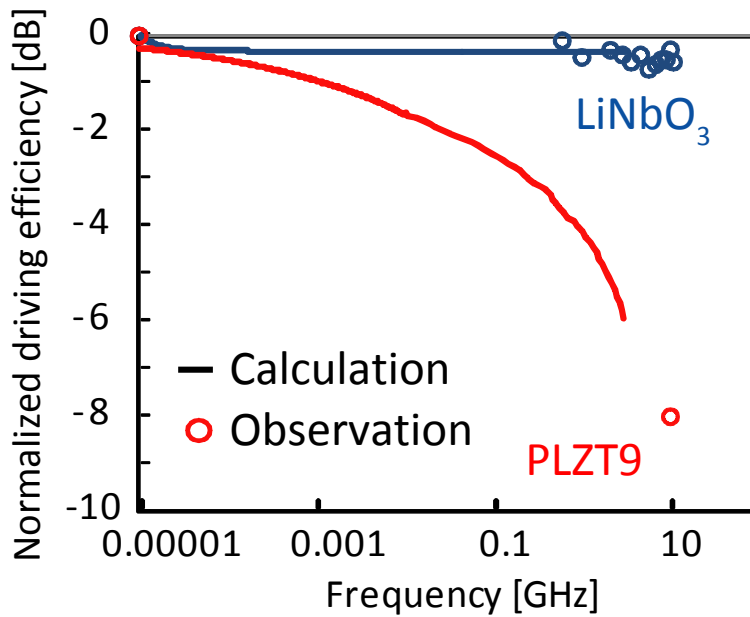


Fig. 4.12 Calculated result (open circle) and observed result (solid line) of frequency dependence of Normalized driving efficiency in LN single crystal and PLZT9 ceramic.

The Kerr coefficient in Eq. (4.10) includes the square of dielectric permittivity. Therefore the Kerr effect is more susceptible than the Pockels effect to the relaxation of dielectric permittivity. In the case of the EO modulator employed LN single crystal, it indicated the Pockels effect as driving principle and the dielectric permittivity of LN single crystal is independent from frequency up to GHz. On the contrary, the EO modulator employed PLZT9 ceramic employed the Kerr effect as driving principle and the frequency dependence of dielectric permittivity show large relaxation until GHz region. Thus the PLZT9 ceramic show large relaxation though the driving principle is EO effect that is the same driving principle in LN single crystal. Therefore we conclude that the EO coefficient g must be employed as parameter for material search in order to

except the influence of frequency dependence and solve the problem (i).

The material with high permittivity show large relaxation in frequency dependence of dielectric permittivity^{35,36}. On the other hand, the materials with high permittivity estimated to show high EO coefficient in this chapter because they show high polarization and spontaneous polarization. As a result, the materials with high permittivity cannot keep high EO coefficient in high speed driving because of their large relaxation of dielectric permittivity that give rise to large relaxation of EO coefficients. In order to develop the EO devices with good frequency dependence, we should employ the materials with low permittivity.

4.4 Summary of chapter 4

In this chapter, the dielectric dispersion of PLZT9 and LN optical modulator were measured by using micro-sized planar electrodes method. We demonstrated the expanded equation for EO effect including the contribution of dielectric permittivity. From the comparison of calculated and observed results in the EO coefficient and dielectric permittivity at high speed driving, we conclude this expanded equation is reliable. The expanded equation indicated the correlation between dielectric permittivity and EO coefficient. We conclude that the relaxation of driving efficiency due to EO effect is mainly cause by the relaxation of dielectric permittivity.

References

- [1] A. Jonscher, *Dielectric relaxation in solids*, (Chelsea Dielectrics, London, 1983)
- [2] C. Bucci and P. Bordewijk, *Theory of electric polarization*, vol. II. (1978).
- [3] A. Jonscher, *J. Phys. D: Appl. Phys.* 32, R57 (1999).
- [4] G. Jin, Y. Zou, V. Fuflyigin, S. Liu, Y. Lu, J. Zhao, M. Cronin-Golomb, *J. Lightwave Tech.* 18, 807 (2000)
- [5] A. Wagner, S. Brueck, A. Wu, *Ferroelectrics* 116, 195 (1991)
- [6] R. Thapliya, S. Nakamura, *J. Lightwave Tech.* 21, 1820 (2003)
- [7] F. Liu, Q. Ye, F. Pang, J. Geng, R. Qu, Z. Fang, *J. Opt. Soc. Am. B* 23, 709 (2006)
- [8] T. Lin, A. Ersen, J. Wang, S. Dasgupta, S. Esener, S. Lee, *Appl. Optics*, 29, 1595 (1990)
- [9] P. Kaminow, V. Ramaswamy, V. Schmidt, H. Turner, *Appl. Phys. Lett.* 24, 622 (1974)
- [10] M. Abouellell, F. Leonberger, *J. Am. Ceram. Soc.* 72, 1311 (1989)
- [11] K. Higuma, S. Oikawa, Y. Hashimoto, H. Nagata, M. Izutsu, *Elect. Lett.* 37, 515 (2001)
- [12] Y. Shi, C. Zhang, J. Bechtel, L. Dalton, B. Robinson, W. Steier, *Science* 288, 119 (2000)
- [13] E. Wooten, K. Kissa, A. Yan, E. Murphy, D. Lafaw, P. Hallemeier, D. Maack, D. Attanasio, D. Fritz, G. McBrien, D. Bossi, *J. Selected topics in quantum electronics* 6, 69 (2000)
- [14] K. Noguchi, O. Mitomi, H. Miyazawa, *J. Lightwave Tech.* 16, 615 (1998)
- [15] D. Dolfi, M. Nazarathy, R. Jungerman, *Elect. Lett.* 24, 528 (1988)

- [16] K. Tokuhashi, K. Ashizawa, D. Ishii, T. Arakawa, N. Yamanaka, K. Wakayama, *Trans. of High Performance Switching and Routing*, 978 (2009)
- [17] C Kirkby, *Ferroelectrics* 37, 567 (1981)
- [18] P. D. Thacher, *J. Appl. Phys.* 41, 4790 (1970)
- [19] G. Haertling, *Ferroelectrics* 75, 25 (1987)
- [20] T.Fujii, T.Suzuki, Y.Fujimori, T.Nakamura, M.Moriwake, H.Takasu, *Jpn. J. Appl. Phys.* 45, 7520 (2006)
- [21] Y. Inuishi, T. Nakajima, K. Kawabe, M. Ieda, *Phenomenology in dielectrics*, (Denki-gakkai, Tokyo, 1973)
- [22] T. Harigai, T. Teranishi, S. Nam, H. Kakemoto, S. Wada and T. Tsurumi, *Key Eng. Mat.* 269, 215 (2004)
- [23] T. Harigai, D. Tanaka, S. Nam, H. Kakemoto, S. Wada, K. Saito and T. Tsurumi, *Jpn. J. Appl. Phys.* 43, 6530 (2004)
- [24] H. Pues, A. Capelle, *IEEE Trans. Antennas Propaga.* 37, 1345 (1989)
- [25] M. Amirhosseini, *Progress In Electromagnetics Research* 66, 15 (2006)
- [26] In “Instruction manual of Agilent E4991A RF impedance/material analyzer” , Agilent technology. Co., Ltd.
- [27] K. Nagata, *Electromagnetics*, (Asakura, Tokyo, 1981)
- [28] S. Kamba, V. Bovtun, J. Petzelt, I. Rychetsky, R. Mizaras, A. Brilingas, J. Banys, J. Grigas, M. Kosec, *J. Phys.: Condens. Matter* 12, 497 (2000)
- [29] W. Robertson, G. Arjavalingam, G. Kopcsay, *Elect. lett.* 27, 175 (1991)

Chapter 4 Relaxation and frequency dependence of electro-optic coefficient

- [30] M. Valente, C. Silva, A. Sombra, M. Graca, J. Non-Crystalline Solids, 356, 800 (2010)
- [31] T. Ogawa, *Fundamentals on crystal technology*, (Shokabo, Tokyo, 1998)
- [32] M. Didomenico, S. Wemple, J. Appl. Phys. 40, 720 (1969)
- [33] S. H. Wemple, M. Didomenico, J. Appl. Phys. 40 735 (1969)
- [34] T. Ikeda, *Base of Piezoelectric Materials*, (Ohmsha, Tokyo, 1984)
- [35] T. Teranishi, T. Hoshina, H. Takeda, T. Tsurumi, J. Appl. Phys. 105, 114102 (2009)
- [36] T. Teranishi, T. Hoshina, H. Takeda, T. Tsurumi, *Trans. on Ultrasonics, Ferroelectrics, and Frequency Control* 57, 2118 (2010)

Chapter 5

Variation of birefringence due to lattice distortion and polarization

5.1 Introduction

5.1.1 EO coefficient g in dielectrics

In chapter 4, we concluded that the EO coefficient was determined by the product of EO coefficient g , dielectric permittivity, and spontaneous polarization. Further, frequency dependence of EO effect was determined by the dielectric permittivity and spontaneous polarization. Thus, EO coefficient g remains constant with varying the frequency of applied electric field. In this chapter, we focused on the EO coefficient g as the key parameter to develop the materials with high EO coefficient. If the material with high EO coefficient g is developed, it would remain constant in EO coefficient at high frequency.

Pioneering work analyzing to the EO coefficient g in dielectrics was undertaken by M. Didomenico and S. Wample^{1,2} as described in chapter 1. They indicated that EO coefficient normalized a number of oxygen octahedral (BO_6) in unit cell are all same in

materials with oxygen octahedral structure despite the species of B site ions is different. Therefore, all cubic dielectrics show the same EO coefficient g . The differences of EO coefficients are caused by the differences of polarization and other parameters induced by anisotropic crystal structures. For example, they indicated the EO coefficient g_{11} normalized a number of oxygen octahedral (BO_6) in unit cell always shows almost $0.17 \text{ m}^4/\text{C}^2$ in cubic dielectrics. The conventional EO crystals: LiNbO_3 ³⁻⁶, LiTaO_3 ⁷⁻⁹, $\text{KTa}_{0.65}\text{Nb}_{0.35}\text{O}_3$ ¹⁰⁻¹² and $\text{Ba}_2\text{NaNb}_5\text{O}_{15}$ ¹³⁻¹⁵ show EO coefficient g_{11} among 0.14 to $0.17 \text{ m}^4/\text{C}^2$ as shown in Table 5.1, this result indicated that the analysis undertaken by M. Didomenico and S. Wample is reliable. However, the analysis cannot be applied to the cubic relaxor materials and the ferroelectrics with diffuse phase transition (DPT ferroelectrics), namely lanthanum added lead zirconate titanate ($\text{Pb}_{0.91}\text{La}_{0.09}\text{Zr}_{0.65}\text{Ti}_{0.35}\text{O}_3$, PLZT9)¹⁶⁻²⁰ and barium strontium titanate ($\text{Ba}_{0.5}\text{Sr}_{0.5}\text{TiO}_3$, BST)²¹⁻²³. PLZT9 and BST show EO coefficient $g_{11} = 0.47 \text{ m}^4/\text{C}^2$ and $0.22 \text{ m}^4/\text{C}^2$ though their crystal structure are cubic. We estimated this exception is due to the dipole moments in polar nano-regions (PNRs).

Table 5.1 The EO coefficient g_{11} normalized a number of oxygen octahedral (BO_6) in unit cell of conventional EO crystals.

Material	g_{11}	Ref.
LiNbO_3	0.16	3-6
LiTaO_3	0.17	7-9
$\text{KTa}_{0.65}\text{Nb}_{0.35}\text{O}_3$	0.14	10-12
$\text{Ba}_2\text{NaNb}_5\text{O}_{15}$	0.17	13-15
$\text{Ba}_{0.5}\text{Sr}_{0.5}\text{TiO}_3$	0.22	21-23
$\text{Pb}_{0.89}\text{La}_{0.09}\text{Zr}_{0.65}\text{Ti}_{0.35}\text{O}_3$	0.47	16-20

In relaxor and DPT materials, it is believed that the fluctuations of dipole moment in PNRs derive dipole polarization and it contributes to permittivity up to GHz region in the paraelectric symmetry²⁴⁻³¹. The PNRs are in paraelectric phase of relaxor materials and DPT ferroelectrics but they do not show anisotropy without electric field. The PNRs contribute to dielectric polarization with applied electric field therefore the relaxor materials and DPT ferroelectrics indicate high permittivity though their crystal structure is cubic. As mentioned in chapter 4, the change of polarization induces the change of refractive index due to lattice distortion. This is why the relaxor materials and DPT ferroelectrics show exception from the analysis in Ref 1 and 2. The change of polarization caused by PNRs was not considered in previous work undertaken by M. Didomenico and S. Wample.

On the other hands, we estimated the differences of EO coefficient g between PLZT and BST is caused by differences of ions in crystal lattice. As mentioned in chapter

3, we proposed that the materials including heavy ions should show high EO coefficient because of their high refractive indices. Therefore, if the speculation in chapter 3 is reliable, the weight of ions in EO materials should have concerning with the EO coefficient g . However the analysis to formularize this relation between the weight of ions in crystal lattice and EO coefficient g was not reported therefore the contribution of weight of ions to EO effect is still ambiguous.

In this chapter, we discussed about the case of isotropic EO materials because the isotropic EO materials PLZT9 and BST indicate the exception from analysis in Ref 1 and 2, and the liner EO effect (Pockels effect) is caused by EO effect proportional to polarization therefore the result from analysis of quadratic EO effect (Kerr effect) can be applied to the case of liner EO effect. The transparent PLZT10 ceramic was employed as samples in this study. It is more isotropic than PLZT9 therefore the Kerr effect is more dominant in EO effect of PLZT10 and it also show high EO coefficient g^{32-35} . We believe that transparent PLZT10 ceramic is a suitable sample analysis in this chapter.

5.1.2 Objective

In this chapter, we elucidate the relation among the variation of polarization, lattice distortion and birefringence. We aimed to elucidate the origin of the EO effect and derive the principle for development of material with high EO property by summarizing the results in chapter 2 to 4.

5.2 Experimental procedure

5.2.1 Measurement of EO effect

The EO coefficient of a rectangular transparent PLZT10 ceramics (Furuuchi Chemical Corp.) with sample size of 4.0 x 1.0 x 0.9 mm³ was measured with varying the strength of external electric field using the same measurement system described in chapter 2. The top and bottom gold planer electrodes were formed on the 4.0 x 0.9 mm² surfaces by DC gold sputtering. We employed the Senarmont method to measure the EO effect with semi-conductive laser (Wavelength: 1.55 μ m). The birefringence of samples were calculated by Eq. (2.4) with transmitted light intensity (I) normalized to the reference light intensity (I_0) (I / I_0) that is the same evaluation described in chapter 2. The incident light was induced in 4.0 x 1.0 mm² face. Applied voltage was -500 to 500 V that corresponds to the electric field of -5 to 5 kV/cm.

5.2.2 Measurement of electrostrictive effect

The electrostrictive displacement of PLZT10 ceramics were measured using mechanical strain gage with varying the strength of external electric field (0 to 6 kV/cm) as shown in Fig. 5.1. The electrostrictive coefficient was calculated by

$$S = QE^2 \quad (5.1)$$

where S is strain, Q is electrostrictive coefficient, and E is electric field. The electric field dependence of strain was fitted to Eq. (5.1) to evaluate electrostrictive coefficient.

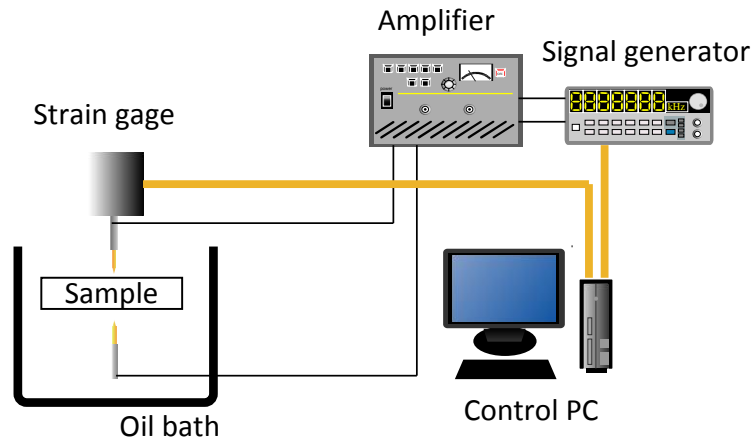


Fig. 5.1 Measurement system for electrostrictive displacement

5.2.3 Measurement of Polarization

Polarizations (P) vs. electric field (E) curves of the PLZT10 ceramics are measured using a ferroelectric tester (Radiant, RT6000). Applied voltage was -500 to 500 V that corresponds to the electric field of -6 to 6 kV/cm.

5.3 result and discussion

5.3.1 Expectation for the origin of EO effect

As mentioned in chapter 4, the contribution of lattice distortion due to the change of polarization must be considered in EO effect. This lattice distortion gives rise to the change of electric polarization that corresponds to the change of refractive indices.

On the other hand, as mentioned in chapter 3, refractive index is purely

determined by the electric polarizations and EO effect can be regarded as a nonlinear response of electric polarization to external electric fields. Nonlinear response appearing in the expansion series of susceptibility normally increases with linear susceptibility, which means that the nonlinear response giving rise to EO effect increases with refractive index.

Thus, we can estimate the mechanism of EO effect described as following two steps: (i) the electric field applying gives rise to the change of polarization, the polarization change induces the lattice distortion, (ii) this lattice distortion gives rise to change of electric polarization. Furthermore, the susceptibility of electric polarization with respect to lattice distortion increases with refractive index.

5.3.2 Expansion of equation for EO coefficient g

The lattice distortion caused by polarization described as step (i) is calculated by the coupled equation defined as

$$S_{ij} = s_{ijkl}^D T_{kl} + d_{ijkl} D_{kl} + Q_{ijkl} D_{kl}^2 \quad (5.3)$$

where S_{ij} is the strain as lattice distortion, s_{ijkl}^D is elastic compliance, T_{kl} is stress, d_{ijkl} is piezoelectric coefficient, D_{kl} is electric displacement, and Q_{ijkl} is electrostrictive coefficient. As described above, we focused on the case of isotropic EO materials, so the piezoelectric coefficients are negligible. And the stress is free because we discussed about strain inducing case, therefore $T = 0$ and $D_{kl} = P_{kl}$.

Next, we focused on the change of refractive index caused by lattice distortion

described as step (ii) below. The refractive index change due to strain is called the photo-elastic effect as discussed in chapter 2. The relation between the change of birefringence and strain is expressed as

$$\Delta\left(\frac{1}{n_{ij}^2}\right) = p_{ijkl} S_{kl} \quad (5.2)$$

where p_{ijkl} is the photo-elastic coefficient^{36, 37}. The photo-elastic effect is usually observed when the large strain was applied such as piezoelectric displacement at piezoelectric resonance as shown in chapter 2. In this analysis, we supposed that the photo-elastic effect can be applied in micro strain, namely lattice distortion, therefore the lattice distortion due to polarization should indicate photo-elastic effect.

As a result, the coupled equation is represented by modifying Eq. (5.3) as

$$S_{ij} = Q_{ijkl} P_k P_l \quad (5.4)$$

Using Eq. (5.3) and (5.4), the change of birefringence due to polarization is given by

$$\Delta\left(\frac{1}{n_{ij}^2}\right) = p_{ijkl} Q_{klmn} P_n P_m \quad (5.5)$$

Eq. (5.5) is represented as

$$\Delta n_{ij} = -1/2 n^3 p_{ijkl} Q_{klmn} P_n P_m \quad (5.6)$$

From the comparison of Eq. (5.5) and (4.6) in chapter 4, the EO coefficient g is described as

$$p_{ijkl} Q_{klmn} = g_{ijnm} \quad (5.7)$$

Therefore, the EO coefficient g is equal to the product of the photo-elastic and

electrostrictive coefficient. From this equation, we can estimate that the material with high photo-elastic coefficient and electrostrictive coefficient show high EO coefficient because they would show high EO coefficient g .

5.3.3 Verification for expanded equation

5.3.3.1 Clausius-Mossotti relation and photo-elastic coefficient

The photo-elastic coefficient indicates a proportionate relation to dielectric permittivity at high frequency (ϵ_∞). The relation between the photo-elastic coefficients and dielectric permittivity can be derived from the Clausius-Mossotti relation as described following: The Clausius-Mossotti relation is described as

$$\frac{\epsilon_\infty - 1}{\epsilon_\infty + 2} = \frac{4\pi\alpha_\infty}{3V} \quad (5.8)$$

where ϵ_∞ is dielectric permittivity at high frequency, α_∞ is the polarizability, and V is the volume per ion pair, respectively³⁷⁻⁴¹. Differentiation of Eq. (5.8) with respect to volume yields

$$\frac{V}{\epsilon_\infty} \frac{d\epsilon_\infty}{dV} = - \frac{(\epsilon_\infty - 1)(\epsilon_\infty + 2)}{3\epsilon_\infty} \quad (5.9)$$

Equation (5.9) was employed by Burstein and co-workers⁴² to analyze the photo-elastic data for several alkali halides and MgO. In deriving Eq. (5.9), it was assumed that the polarizability remains constant when the crystal is compressed. However, this assumption is not consistent with experimental data on the pressure dependence of

dielectric constant⁴³. If one considers the variation of polarizability with changing volume, Eq. (5.9) modified as follows

$$\frac{V}{\epsilon_{\infty}} \frac{d\epsilon_{\infty}}{dV} = -\frac{(\epsilon_{\infty} - 1)(\epsilon_{\infty} + 2)}{3\epsilon_{\infty}} (1 - \lambda) \quad (5.10)$$

where λ is strain polarizability parameter defined as

$$\lambda = \frac{V}{\alpha_{\infty}} \frac{d\alpha_{\infty}}{dV} = \frac{R}{3\alpha_{\infty}} \frac{d\alpha_{\infty}}{dR} \quad (5.11)$$

where R is the inter-ionic separation. On the other hand, the photo-elastic coefficient indicates the relation as follows

$$dn = -1/2n^3 p_{11} S_3 \quad (5.12)$$

where S_3 is the strain³⁸. Note that we estimated $S_3 \gg S_1, S_2$, so influence of S_1, S_2 were omitted. The volume variation is described as following

$$dV/V = \frac{xy\Delta z}{xy(z + \Delta z)} = S_3. \quad (5.13)$$

From Eq. (5.12) and (5.13), the refractive index with changing volume was described as

$$\frac{dn}{dV} = \frac{-n^3 p_{11}}{2V}. \quad (5.14)$$

From Eq. (5.14), the variation of polarizability with changing volume is calculated as

$$\frac{V}{\epsilon_{\infty}} \frac{d\epsilon_{\infty}}{dV} = -\epsilon_{\infty} p_{11}. \quad (5.15)$$

Noted that the dielectric permittivity at high frequency is square of refractive index described as $n^2 = \epsilon_{\infty}$. Comparing Eq. (5.10) and (5.15), the relation of photo-elastic coefficients is given by

$$-\frac{(\epsilon_{\infty} - 1)(\epsilon_{\infty} + 2)}{3\epsilon_{\infty}}(1 - \lambda) = -\epsilon_{\infty} p_{11} \quad (5.16)$$

$$p_{11} = \frac{(n^2 - 1)(n^2 + 2)}{3n^4}(1 - \lambda). \quad (5.17)$$

Figure 5.2 shows a plot of literature values and calculated result by Eq. (5.17) of photo-elastic coefficients p_{11} in conventional EO materials vs. electron density in unit cell. The refractive index indicates a proportional relation to electron density in unit cell described as $n = \beta\rho$ where ρ is electron density in unit cell and β is proportional constant. In this chapter, we employed the electron density in unit cell ρ as the variables in Eq. (5.17) because of a lack of experimental data in the refractive index of the materials in Fig. 5.2. Good agreement indicated that the Eq. (5.17) is reliable therefore the photo-elastic coefficient indicates a proportionate relation to electron density in unit cell.

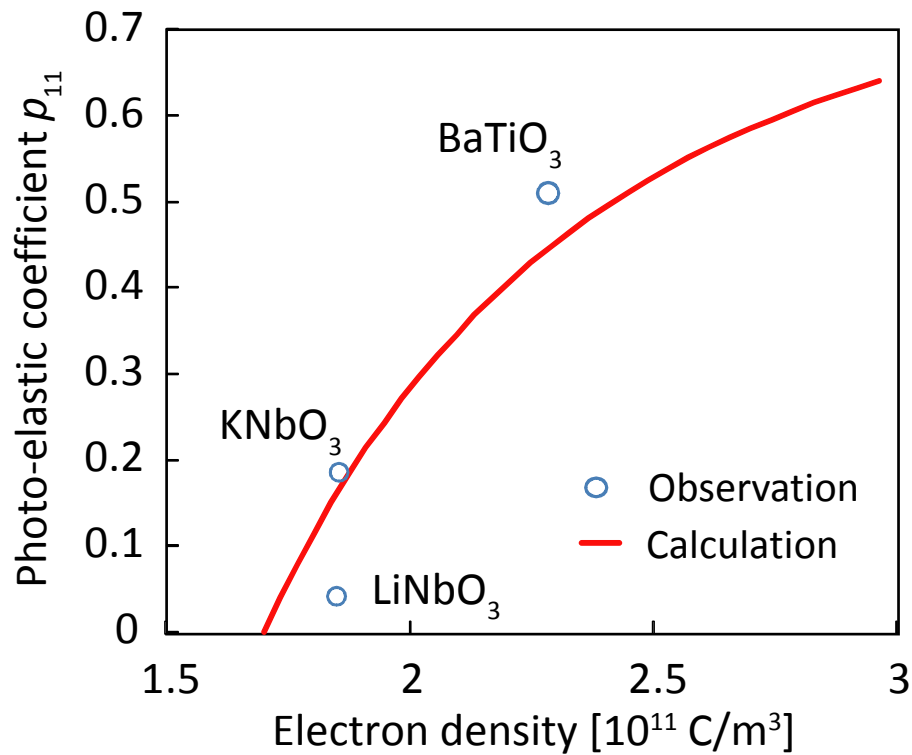


Fig. 5.2 Plots of literature values and calculated result by Eq. (5.14) of photo-elastic coefficients ρ_{11} in conventional EO materials (LiNbO $_3$, KNbO $_3$, BaTiO $_3$) vs. electron density in unit cell.

5.3.3.2 Calculation of photo-elastic coefficient by expanded equation

Equation (5.5) indicates the relation between the birefringence, photo-elastic coefficient, electrostrictive coefficient, and polarization. Therefore the photo-elastic coefficient can be calculated from Eq. (5.5) by the birefringence, electrostrictive coefficient, and polarization. If the calculated photo-elastic coefficient follows to the calculated result from Eq. (5.17), we can conclude that the expanded equation (5.5) is reliable.

Figure 5.3 shows the birefringence of PLZT10 with varying the strength of electric field -5 to 5 kV/cm. The birefringence of PLZT10 reached to 1.08×10^{-4} at 5 kV/cm with butterfly-type hysteresis. Figure 5.4 shows the strain with varying the strength of electric field 0 to 6 kV/cm. The strain of PLZT10 reached to 2.90×10^{-5} at 5 kV/cm. The electrostrictive coefficient is $3.2 \times 10^{-2} \text{ m}^4/\text{C}^2$ calculated by Eq. 5.1. Figure 5.5 shows a polarization P vs. electric field E curve of a PLZT10, where the polarization (P) was simply calculated as the charge divided by the electrode area. The polarization reached to $3.00 \text{ uC}/\text{cm}^2$ at 5 kV/cm. A slim hysteresis loop seen in the P vs. E curve. Although PLZT10 does not show anisotropy at room temperature, a butterfly-type hysteresis curve is observed. This may be caused by reorientation of PNRs.

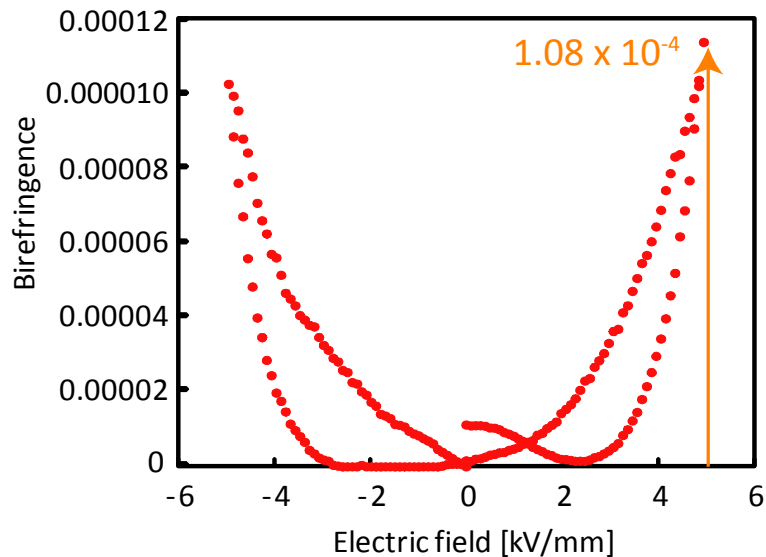


Fig. 5.3 Birefringence of PLZT10 with varying the strength of electric field -5 to 5 kV/cm.

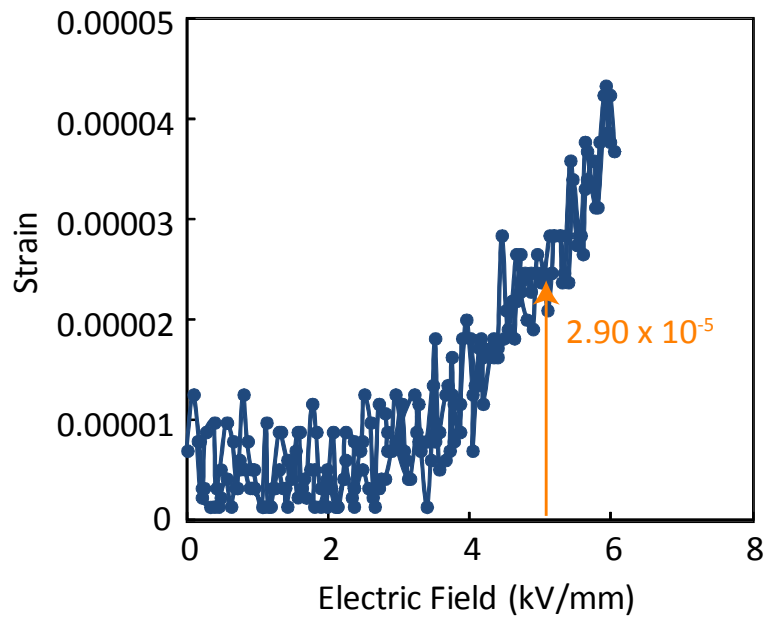


Fig. 5.4 Strain of PLZT10 with varying the strength of electric field 0 to 6 kV/cm.

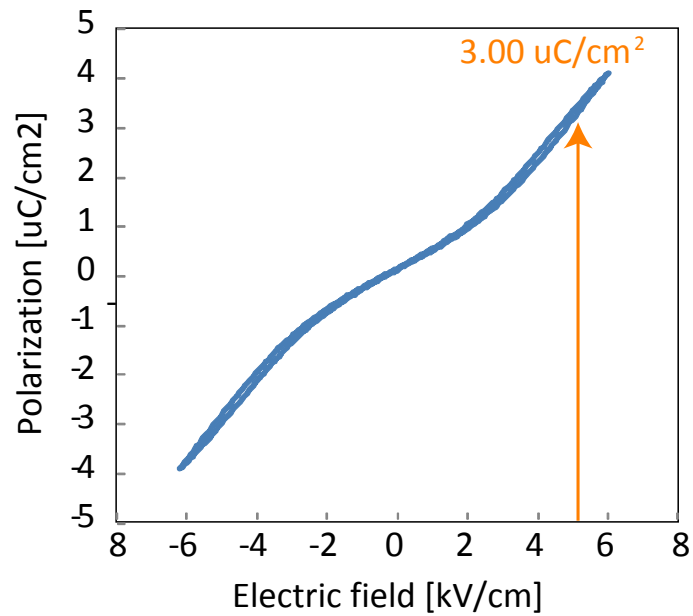


Fig. 5.5 Polarization P vs. electric field E curve of a PLZT10 at electric field -6 to 6 kV/cm.

The photo-elastic coefficient p_{11} of PLZT10 is 0.878 calculated by Eq. (5.6) from substituting the measured values. Note again that we estimated $S_3 \gg S_1, S_2$, so influence of S_1, S_2 were omitted. Figure 5.6 shows a plot of literature values, calculated result by Eq. (5.6), and Eq. (5.17) of photo-elastic coefficients p_{11} vs. the electron density in unit cell. The calculated photo-elastic coefficient of PLZT10 is followed to the calculated result from Eq. (5.17), this means the expanded equation (5.5) is reliable. Therefore the material with heavy ions, namely PLZT10, indicates high EO coefficient g because of their high photo-elastic coefficients. Further, the PLZT10 shows high permittivity, which means they show high polarization. Thus the PLZT10 shows high EO coefficients because of their high photo-elastic coefficients and high polarization.

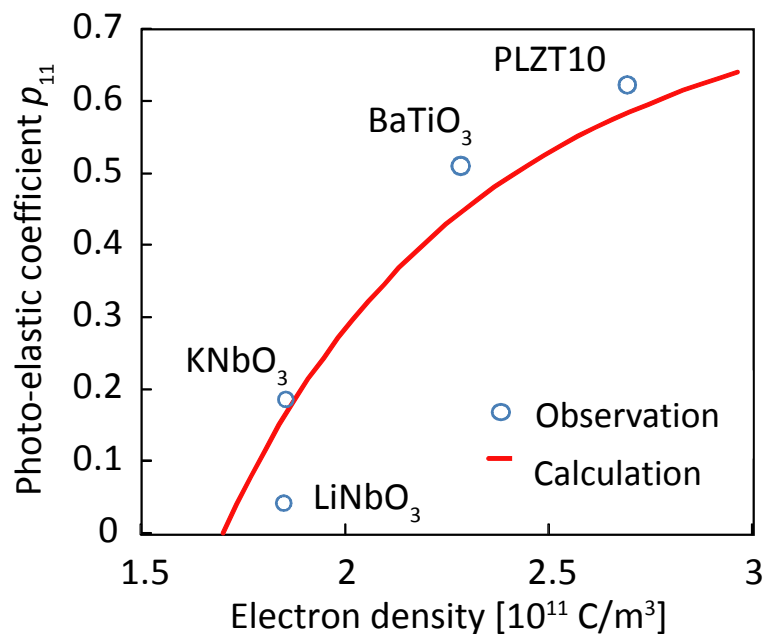


Fig. 5.6 Plots of literature values, calculated result by Eq. (5.5) and by Eq. (5.17) (solid line) of photo-elastic coefficients p_{11} vs. the electron density in unit cell. The plot of PLZT10 was calculated by Eq. (5.5).

5.3.3.3 Relation between electrostrictive coefficient and electron density

The electrostrictive coefficients are also important to EO coefficient g . However the electrostrictive coefficients were already reported that they were almost same in any materials as shown in Fig. 5.7. Therefore the tendency in photo-elastic effect and electron density can be applied in relation in EO coefficient g and electron density. Accordingly, the material including heavy ions indicate high EO coefficient g .

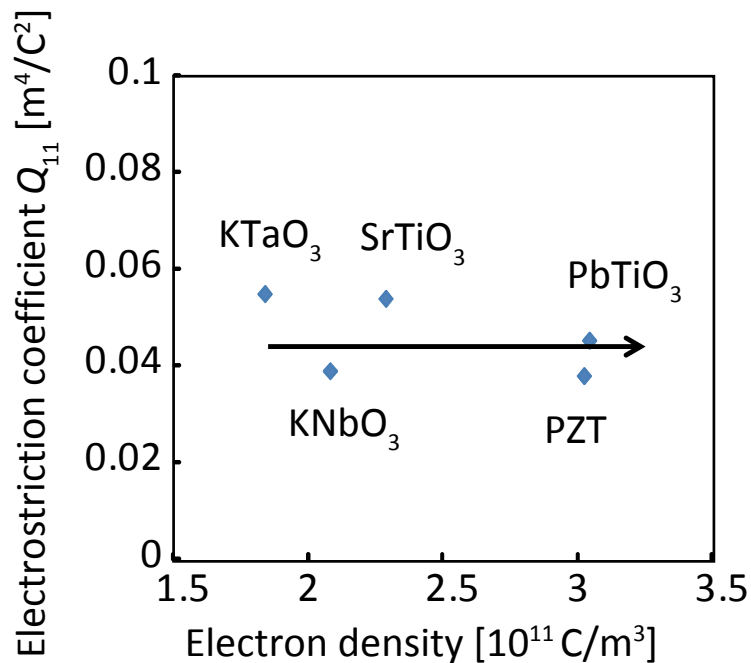


Fig. 5.7 Plots of literature values of electrostrictive coefficients vs. the electron density in unit cell.

5.4 Origin of EO effect and principle for development of material with high EO property

Here, the origin of EO effect was interpreted from the equation (5.5) as three effects: (i) the variation of polarization caused by application of electric field, (ii) the

lattice distortion induced by polarization, and (iii) the photo-elastic effect due to lattice distortion. As described in 5.3.3.3, the material including heavy ions indicate high EO coefficient g . This is the principle for development of material with high EO property derived from Eq. (5.5). It was considered the influence of frequency dependence and can be applied to relaxor materials because it was employed the EO coefficient g . Further it included the influence of strain because the photo-elastic coefficient was employed in Eq. (5.5). We concluded that this is the new principle by summarizing the results in chapter 2 to 4 and based on the origin of EO effect.

5.5 Summary of chapter 5

In this chapter, we elucidated the relation among the variation of polarization, lattice distortion and birefringence. We demonstrated the expanded equation for EO coefficients g including the contribution of the photo-elastic and electrostrictive coefficient. The Clausius-Mossotti relation indicated the tendency that the materials with heavy ions indicated high photo-elastic effect. The electrostrictive coefficients were already reported that they were almost same. Therefore the materials with heavy ions show high EO coefficients g because of their high photo-elastic effect. And finally, the origin of EO effect was interpreted as three effects: (i) the variation of polarization caused by application of electric field, (ii) the lattice distortion induced by polarization, and (iii) the photo-elastic effect due to lattice distortion.

References

- [1] M. Didomenico, S. Wemple, J. Appl. Phys. 40, 720 (1969)
- [2] S. H. Wemple, M. Didomenico, J. Appl. Phys. 40 735 (1969)
- [3] K. Chah, M. Aillerie, M. D. Fontana, G. Malovichko, Opt. Communications 176, 261 (2000)
- [4] J.D. Zook, D. Chen, G.N. Otto, Appl. Phys. Lett. 11,159 (1967)
- [5] E.H. Turner, Appl. Phys. Lett. 8, 303 (1966)
- [6] R. S. Weis, T. K. Gaylord, Appl. Phys. A 37, 191 (1985)
- [7] I. Kaminow, W. Jhonston, Phys. Rev. 160, 518 (1967)
- [8] F. Chen, J. Appl. Phys. 40, 3389 (1969)
- [9] R. Miller, A. Savage 9, 169 (1966)
- [10] K. Nakamura, J. Miyazu, M. Sasaura, K. Fujiura, Appl. Phys. Lett. 89, 131115 (2006)
- [11] K. Fujiura, K. Abe, ITE Technical Report 33, 7 (2009)
- [12] S. Toyoda, K. Fujiura, M. Sasaura, K. Enbutsu, A. Tate, M. Shimokozono, H. ushimi, T. Imai, K. Manabe, T. Matsuura, T. Kirihara Japanese J. Appl. Phys. 43, 5862 (2004)
- [13] J. Geusic, H. Levinstein, J. Rubin, S. Singh, L. Uitert, Appl. Phys. Lett. 11, 269 (1967)
- [14] S. Singh, D. Draegert, J. Geusic, Phys. Rev. 2, 1 (1970)
- [15] F. Wang, Phys. Rev. B 59, 9733 (1999)
- [16] G. Haertling, Ferroelectrics 75, 25 (1987)
- [17] H. Jiang, Z. Chen, K. Li, R. Zhang, Y. Wang, Trans. of Optoelectronic Devices and Integration (2005)

- [18] J. Dellis, *J. Phys.: Condens. Matter* 8, 7957 (1996)
- [19] V. Bovtun, J. Petzelt, V. Porokhonsky, S. Kamba, *J. Euro. Ceram. Soc.* 21, 1307 (2001)
- [20] M. Dambekalne, M. Antonova, M. Livinsh, B. Garbarz-Glos, W. Smiga, A. Sternberg, *J. Euro. Ceram. Soc.* 26, 2963 (2006)
- [21] B. Su, J. Holmes, C. Meggs, T. Button, *J. Euro. Ceram., Soc.* 23, 2699 (2003)
- [22] J. McAneney, L. Sinnamon, R. Bowman, J. Gregg, *J. Appl. Phys.* 94, 4566 (2003)
- [23] B. Su, J. Holmes, B. Cheng, T. Button, *J. Electroceramics* 9, 111 (2002)
- [24] A. Glazounov and A. Tagantsev, *Phys. Rev. Lett.* 85, 2192 (2000)
- [25] G. Smolensky, *J. Phys. Soc. Jpn.* 28, 26 (1970)
- [26] A. Levstik, Z. Kutnjak, C. Filipič and R. Pirc, *Phys. Rev. B* 57, 11204 (1998)
- [27] A. Glazounov and A. Tagantsev, *Appl. Phys. Lett.* 73, 856 (1998)
- [28] R. Sommer, N. Yushin, and J. Klink, *Phys. Rev. B* 48, 13230 (1993)
- [29] D. Viehland, S. Jang, L. Cross, and M. Wuttig, *J. Appl. Phys.* 68, 2916 (1990)
- [30] B. Vugmeister and H. Rabitz, *Phys. Rev. B* 57, 7581 (1998)
- [31] R. Pirc and R. Blinc, *Phys. Rev. B* 60, 13470 (1999)
- [32] C Kirkby, *Ferroelectrics* 37, 567 (1981)
- [33] P. D. Thacher, *J. Appl. Phys.* 41, 4790 (1970)
- [34] G. Haertling, *Ferroelectrics* 75, 25 (1987)
- [35] T. Fujii, T. Suzuki, Y. Fujimori, T. Nakamura, M. Moriwake, H. Takasu, *Jpn. J. Appl. Phys.* 45, 7520 (2006)

- [36] H. Hueller, Rhps. Rev. 47, 947 (1935)
- [37] M. Zgonik, R. Schlessler, I. Biaggio, E. Voit, J. Tscherry, P. Gunter, J. Appl. Phys. 74, 1287 (1993)
- [38] H. Mueller, Phys. Rev. 47, 947 (1935)
- [39] J. Shanker, P. Bakhshi, O. Sharma, Solid State Communications 24, 217 (1977)
- [40] H. Coker, J. Phys. Chem. Solids 40, 1079 (1979)
- [41] B. Singh, A. Ojha, S. Tripti, Physica B 350, 338 (2004)
- [42] E. Burstein, P. Smith, Phys. Rev. 74, 229 (1948)
- [42] K. Aggrawal, B. Szigeti, J. Phys. C3, 1097(1970)
- [43] T. Ikeda, *Fundamentals of Piezoelectric Materials*, (Ohmsha, Tokyo, 1984)

Chapter 6

Electro-optic effect of Bi-based relaxors

6.1 Introduction

6.1.1 Features for high EO property

Following is a principle derived in chapter 2 to 5: (i) The EO coefficients indicate the relaxation in high speed driving because of the relaxation of dielectric permittivity. The materials with high polarization show high EO coefficient but they show large relaxation. (ii) The relaxors with heavy ions show high EO coefficients g because of their high photo-elastic coefficients. The EO coefficients g remains constant with varying the frequency of applied electric field. Therefore, in order to develop the new EO materials using for high speed driving EO modulators, they must fulfill the two features: (i) low permittivity, and (ii) relaxors constituted by heavy ions. Furthermore, EO materials should be isotropic to prevent chirping that is wavelength shift by passing through the EO materials¹⁻³. And lead-free materials are better because they can prevent to a pollution of lead toxicity.

In this chapter, we focused on the Bi-based relaxer single crystals $(1-x)\text{Bi}_{0.5}\text{Na}_{0.5}\text{TiO}_3 - x\text{Bi}_{0.5}\text{K}_{0.5}\text{TiO}_3$ (BNT-BKT) as a new EO material. BNT-BKT single

crystals are studied as lead-free piezoelectric materials because of their attracted properties at morphotropic phase boundary⁴⁻⁸. They are constituted by heavy ion Bi, and they are isotropic in several compositions. The dielectric permittivity of BNT-BKT single crystals are low at all compositions moreover BNT-BKT single crystals show relaxor behavior. Therefore, BNT-BKT single crystals satisfy all demands for new EO materials with high EO properties but the EO properties of BNT-BKT single crystals were not reported yet.

We employed $67\text{Bi}_{0.5}\text{Na}_{0.5}\text{TiO}_3 - 33\text{Bi}_{0.5}\text{K}_{0.5}\text{TiO}_3$ (67BNT33BKT) single crystal as a sample in this study because they show the smallest spontaneous polarization in BNT-BKT group⁶. This means that the 67BNT33BKT single crystal is most isotropic in BNT-BKT group.

6.1.2 Objective

In this chapter, we aimed to evaluate the EO property of 67BNT33BKT single crystals. The EO coefficient g and high speed driving property of 67BNT33BKT were evaluated by using the method described in chapter 4 and 5.

6.2 Experimental procedure

6.2.1 Fabrication of 67BNT33BKT

BNT-BKT powder was synthesized by a solid-state reaction using high-purity

raw materials of Bi_2O_3 , TiO_2 , Na_2CO_3 , and K_2CO_3 . Stoichiometric powder was sintered at 1000°C for 4 hours. This heating treatment led to a single phase with perovskite-type crystal structure. Single crystals of 67BNT33BKT were grown by the top seed solution growth (TSSG) technique under oxygen atmosphere ($P_{\text{O}_2} = 0.9\text{Mpa}$) and high temperature (1070°C). This process provided 67BNT33BKT single crystals with a maximum $2 \times 2 \times 1 \text{ mm}^3$. The detailed fabrication procedure was described in Ref.9. Fabricated 67BNT33BKT single crystal was structurally characterized by x-ray diffraction. The dielectric permittivity was measured at 1kHz, 10kHz, 100kHz, and 1MHz as a function of temperature (room temperature to 650°C) using an impedance analyzer (4294A, Agilent Tech.) and a furnace for temperature control.

6.2.2 Measurement of EO effect

The EO coefficient of a rectangular transparent 67BNT33BKT single crystal with sample size of $1.7 \times 1.8 \times 0.9 \text{ mm}^3$ was measured with varying the strength of external electric field using the same measurement system described in chapter 2. The top and bottom gold planer electrodes were formed on the $1.7 \times 0.9 \text{ mm}^2$ surfaces by DC gold sputtering. We employed the Senarmont method to measure the EO effect with semi-conductive laser (Wavelength: $1.55 \text{ }\mu\text{m}$). The birefringence of samples were calculated by Eq. (2.4) with transmitted light intensity (I) normalized to the reference light intensity (I_0) (I / I_0) that is the same evaluation described in chapter 2. The incident light was induced in $1.7 \times 1.8 \text{ mm}^2$ face. Applied voltage was -800 to 800 V that

corresponds to the electric field of -4.3 to 4.3 kV/cm.

6.2.3 Measurement of Electrostrictive effect

The electrostrictive displacement of 67BNT33BKT single crystal was measured using mechanical strain gage with varying the strength of external electric field (0 to 7 kV/cm) as described in chapter 5. The electric field dependence of strain was fitted to Eq. (5.1) to evaluate electrostrictive coefficient.

6.2.4 Measurement of Polarization

Polarization (P) vs. electric field (E) curves of the 67BNT33BKT single crystal was measured using a ferroelectric tester (Radiant, RT6000) as described in chapter 5. Applied voltage was -800 to 800 V that corresponds to the electric field of -4.3 to 4.3 kV/cm. That is the same condition to measurement of EO effect.

6.2.5 Measurement of dielectric dispersion

From kHz to MHz, capacitance of rectangular 67BNT33BKT single crystal was measured with an impedance analyzer. Measured capacitance was converted to dielectric permittivity. Dielectric data up to 1GHz was determined using the micro-sized planar electrode method. Admittance between source and ground ports was measured with an impedance analyzer (E4991A, Agilent Tech.). The dielectric permittivity of

67BNT33BKT single crystal in the GHz range was then determined by fitting measured susceptance into that calculated using try-and-error method. The detailed evaluation procedure was described in chapter 4.

6.3 Result and discussion

6.3.1 Electric property of 67BNT33BKT

The fabricated 67BNT33BKT single crystal was transparent and yellow colored as shown in Fig. 6.1. Figure 6.2 (a) shows the x-ray diffraction (XRD) pattern of a 67BNT33BKT that exhibits a single phase crystalline. If 67BNT-33BNT has anisotropy, the separated peaks are observed in XRD pattern at high angle (57° to 60°). However the XRD pattern of 67BNT33BKT at high angle (Fig. 6.2 (b)) does not indicate two peaks clearly. Figure 6.3 shows the calculated and observed I / I_0 as a function of polarizer angles. The calculated result is indicated the result without birefringence. The observed results show good agreement with calculated result. The result from XRD pattern and measurement of birefringence indicated that the 67BNT33BKT crystal shows negligible initial birefringence at room temperature therefore the 67BNT33BKT is almost isotropic.

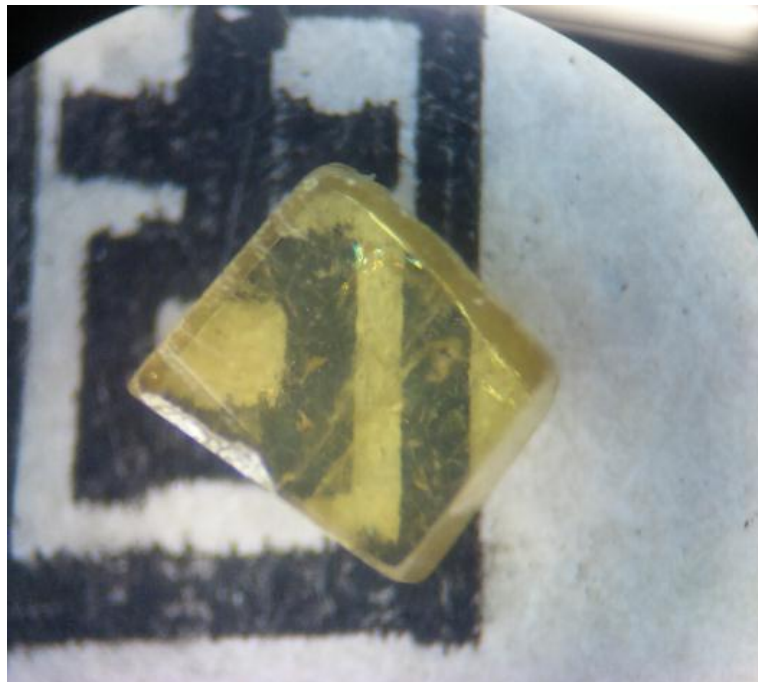
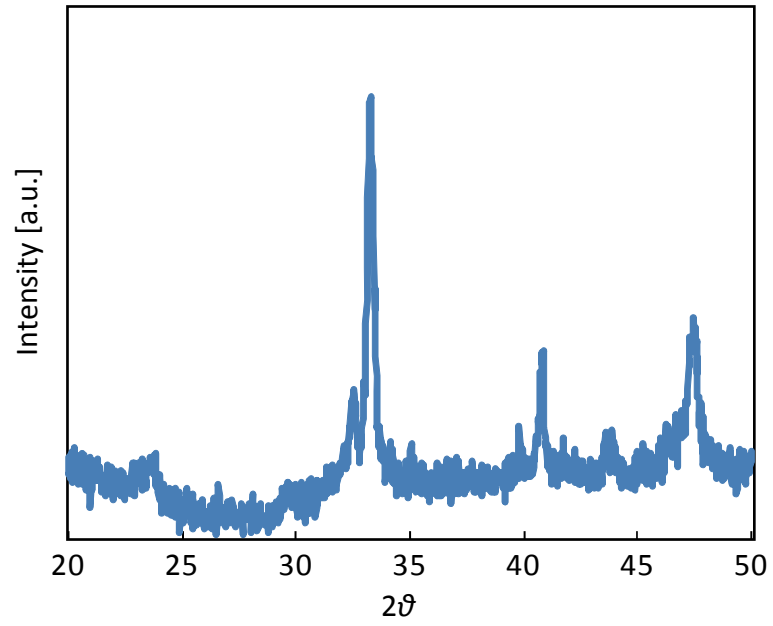
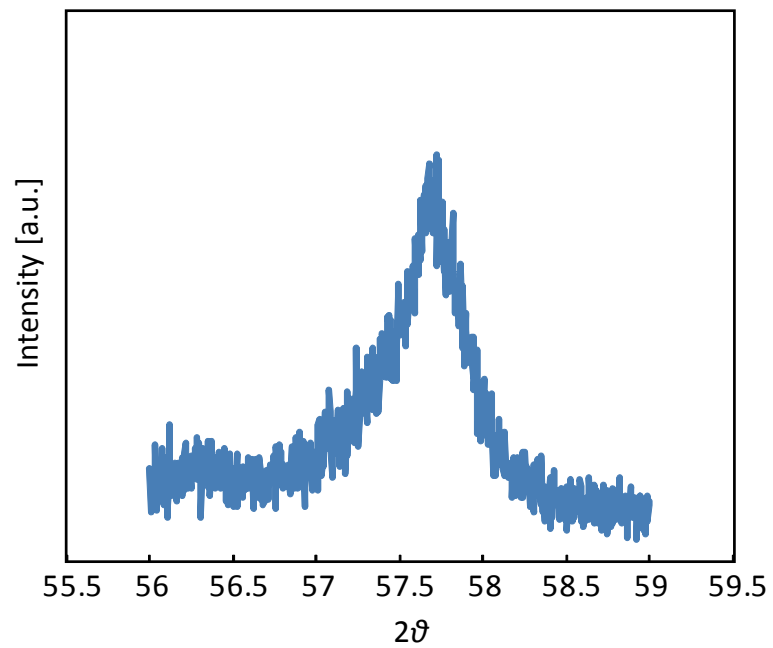


Fig. 6.1 Picture of 67BNT-33BKT



(a)



(b)

Fig. 6.2. The XRD pattern of 67BNT-33BKT single crystal observed at (a) wide angle (20° to 50°), (b) high angle (57° to 60°)

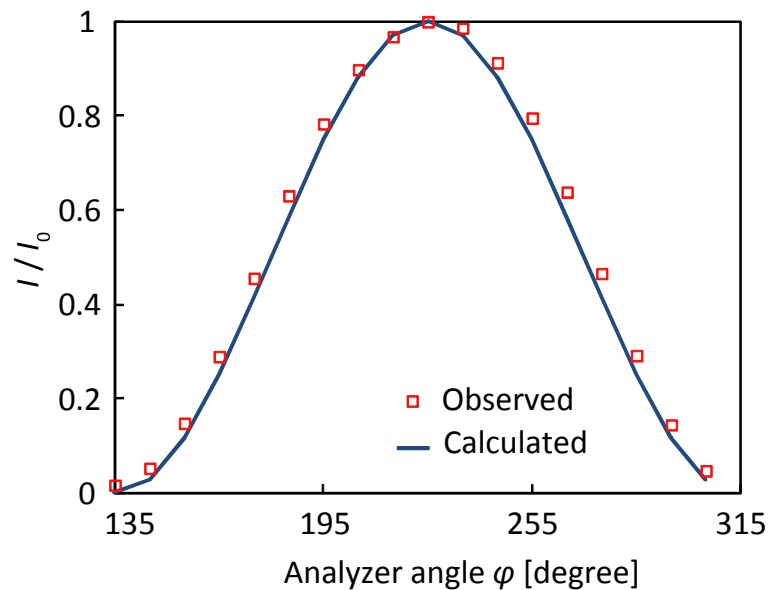


Fig. 6.3. Analyzer angle dependence of transmitted light intensity I normalized to the incident light intensity I_0 of 67BNT-33BKT.

The temperature dependence of the dielectric permittivity at different frequencies is shown in Fig. 6.4. It can be observed that first and second maximum (T_1 , T_2) exhibit a clearly dependency on frequency. T_1 gradually shifted toward higher temperature and T_2 gradually shifted toward lower temperature with increasing the frequency. ϵ_r shows a very strong dependence with frequency below T_1 , the dependence becomes weaker between T_1 and T_2 . However, the dependence becomes obvious again above T_2 . The character of the temperature dependence of ϵ_r shows behavior of ferroelectric relaxor²³. The dielectric permittivity at room temperature is about 2000 at 1kHz that is relatively lower than other materials.

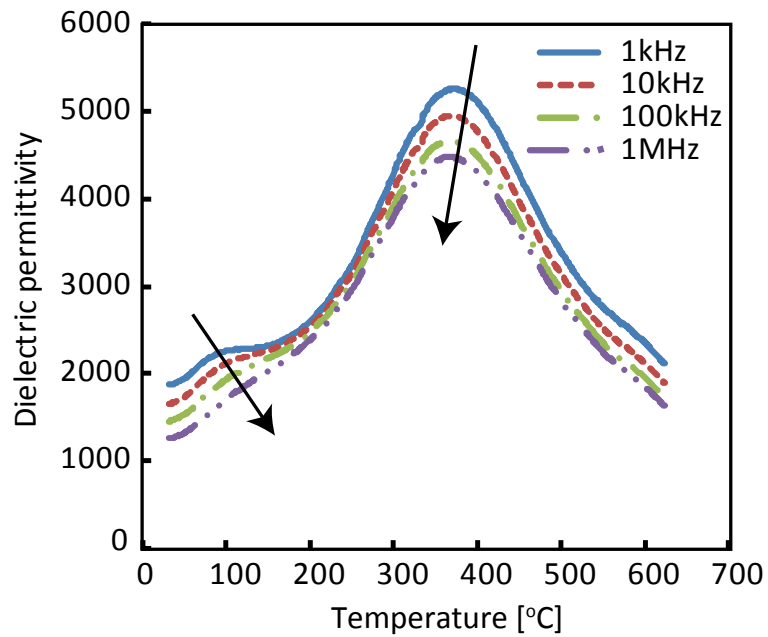


Fig. 6.4. The temperature dependence of dielectric permittivity of 67BNT-33BKT single crystal measured at 30°C to 650°C.

6.3.2 EO coefficients of 67BNT33BKT

Figure 6.5 indicates the change of birefringence as a function of electric field that is the quadratic EO behavior of the 67BNT33BKT. Although 67BNT33BKT does not show anisotropy at room temperature, a butterfly-type hysteresis curve is observed, that is similar to that of PLZT relaxor as described in chapter 4. From Fig. 6.5, the quadratic EO coefficient was calculated by Eq.(1) that is $1.6 \times 10^{-16} \text{ V}^2/\text{m}^2$.

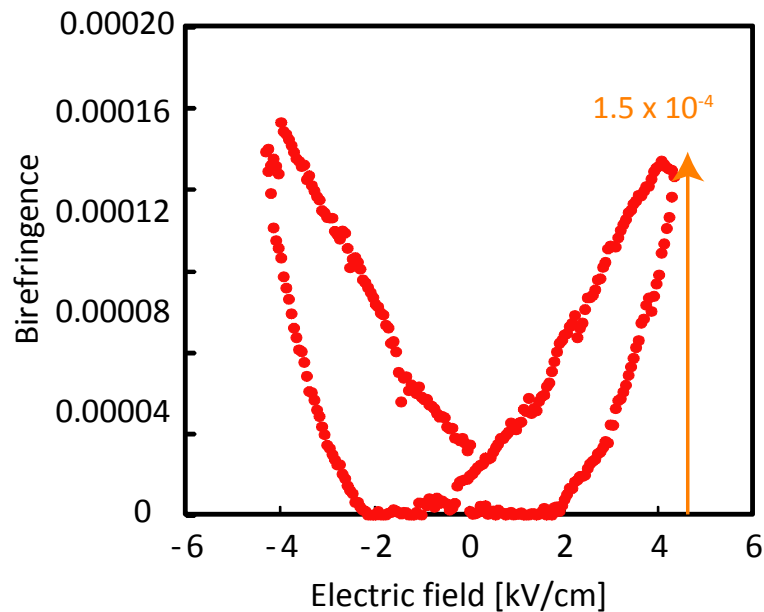


Fig. 6.5. The birefringence of 67BNT-33BKT single crystal as a function of electric field -4.2 to 4.2 kV/cm.

Table 1 shows the EO coefficient and dielectric permittivity at room temperature of 67BNT33BKT and other perovskite type dielectrics. This quadratic EO coefficient is higher than that of other lead-free perovskite type dielectrics¹⁰⁻²² except for Potassium tantalite niobate ($\text{KTa}_{0.65}\text{Nb}_{0.35}\text{O}_3$, KTN) single crystals. However, KTN single crystal needs high temperature (over 50°C) driving to show the high coefficients and to prevent from indicating initial birefringence. At high temperature, they indicate large dielectric permittivity that is disadvantage for high speed modulating. Therefore we decided the 67BNT-BKT indicated the highest quadratic EO constant in lead-free dielectrics at room temperature.

Table 6.1. The quadratic EO coefficients and dielectric permittivity of typical perovskite type EO crystals.

Material	EO coefficient [$10^{-17} \text{ m}^2/\text{V}^2$]	Dielectric Permittivity	Ref.
$\text{KTa}_{0.65}\text{Nb}_{0.35}\text{O}_3$	1000	30000	10-12
$(\text{Pb}_{0.91}\text{La}_{0.09})(\text{Zr}_{0.65}\text{Ti}_{0.35})\text{O}_3$ (PLZT9)	32	5000	13-16
$67\text{Bi}_{0.5}\text{Na}_{0.5}\text{TiO}_3 - 33\text{Bi}_{0.5}\text{K}_{0.5}\text{TiO}_3$ (67BNT-33BKT)	16	2000	This work
$(\text{Pb}_{0.9}\text{La}_{0.1})(\text{Zr}_{0.65}\text{Ti}_{0.35})\text{O}_3$ (PLZT10)	10.7	4500	13-16
$\text{Ba}_{0.5}\text{Sr}_{0.5}\text{TiO}_3$ (BST)	3.4	1300	17-22

6.3.3 Photo-elastic coefficients of 67BNT33BKT

The birefringence, polarization, and electrostrictive coefficient were measured in order to calculate the photo-elastic coefficient of 67BNT33BKT single crystal by Eq. (5.5). Figure 6.6 and 6.7 show the strain and polarization of 67BNT33BKT single crystal with varying the strength of electric field. 67BNT33BKT single crystal showed larger strain 6.7×10^{-5} than PLZT10 at 4.2 kV/mm and looks linear behavior. The electrostrictive coefficient is $4.7 \times 10^{-1} \text{ m}^4/\text{C}^2$ calculated by Eq. 5.1 in chapter 5. Therefore 67BNT33BKT single crystal indicated small anisotropy though their birefringence was negligible. A slim hysteresis loop was observed in the P vs. E curve of 67BNT33BKT single crystal, and the polarization was reached to $1.2 \text{ uC}/\text{cm}^2$ at 4.2 kV/mm.

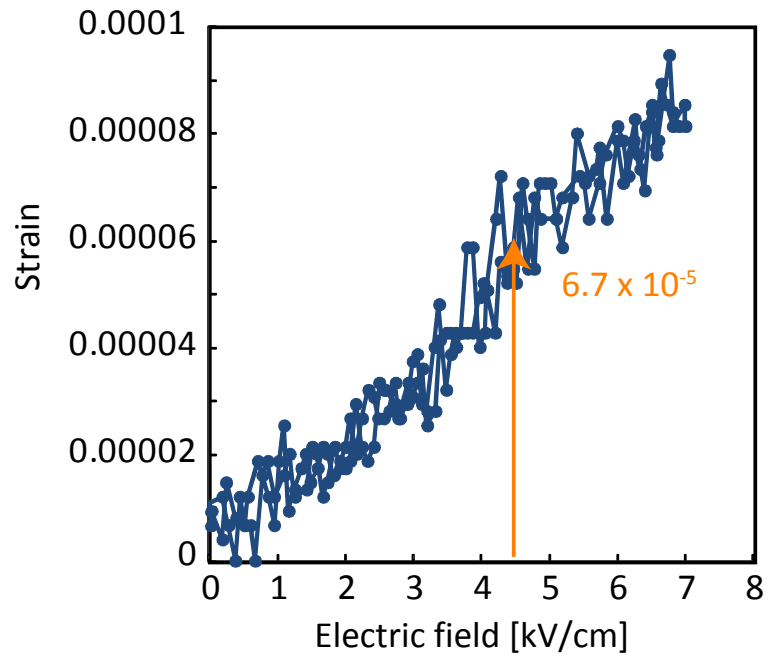


Fig. 6.6. The strain of 67BNT-33BKT single crystal as a function of electric field 0 to 7 kV/cm.

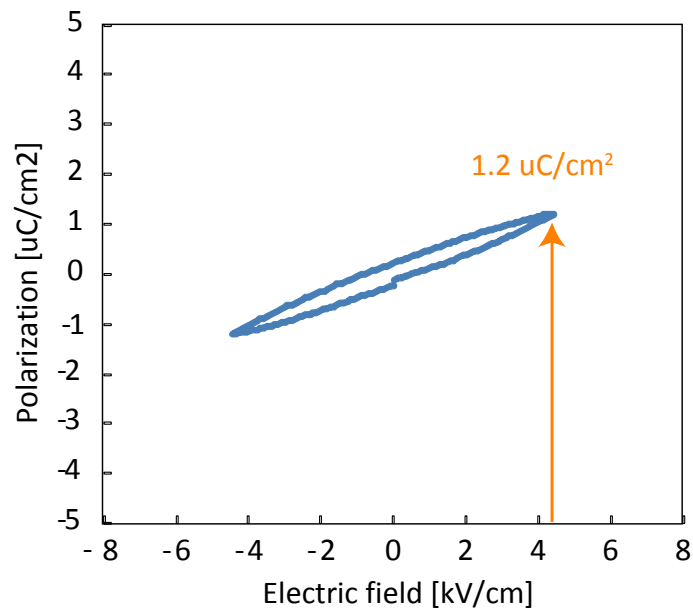


Fig. 6.7. Polarization P vs. electric field E curve of a 67BNT-33BKT single crystal at electric field -4 to 4 kV/cm.

The calculated photo-elastic coefficient p_{11} of 67BNT33BKT single crystal is 0.399. It is relatively high in EO materials as same as that of BaTiO₃ but lower than that of PLZT10. Figure 6.8 shows plots of photo-elastic coefficients p_{11} vs. the electron density in unit cell added a plot of 67BNT33BKT single crystal. The photo-elastic coefficient p_{11} of 67BNT33BKT indicated relatively low value though it is constituted by heavy ion Bi. An A site ion in 67BNT33BKT is Bi, Na, and K, so a content of Bi in A site is 1/2. On average the electron density of 67BNT33BKT, a weight of ions is not so heavy as compared to PLZT because sodium and potassium is not so heavy ions. Therefore the photo-elastic coefficient p_{11} of 67BNT33BKT is not show so high.

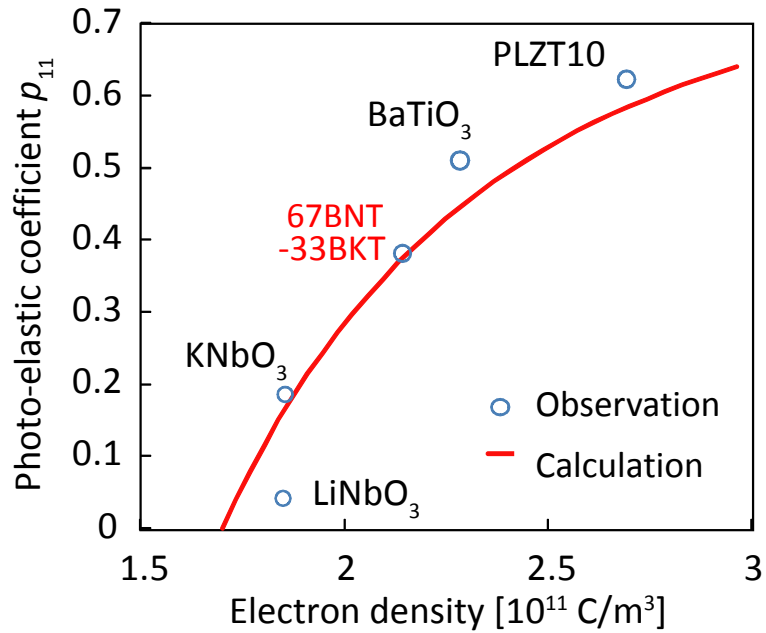


Fig. 6.8 Plots of literature values, calculated result by Eq. (5.5) and by Eq. (5.13) (solid line) of photo-elastic coefficients ρ_{11} vs. the electron density in unit cell where λ is 0.58. The plot of 67BNT-33BKT was calculated by Eq. (5.5).

6.3.4 Frequency dependence of EO coefficients of 67BNT33BKT

Figure 6.9 shows the dielectric dispersion of 67BNT33BKT up to 3GHz. It shows continuous relaxation until 3GHz, but decrement is smaller than that of PLZT9. The frequency dependence of EO coefficient R_c is calculated by Eq. (4.10) in chapter 4 as shown in Fig. 6.10. The result of PLZT9 was also plotted in Fig. 6.10 to compare with that of 67BNT33BKT. From comparison of these results, 67BNT33BKT shows high EO coefficient R_c as same as PLZT9 at 3GHz driving, though the EO coefficient R_c of PLZT9 is two times larger than that of 67BNT33BKT at low frequency. And we can estimate that

the EO coefficient R_c of 67BNT33BKT should get larger than that of PLZT9 in more high speed driving by extrapolating result shown in Fig 6.10 as broken lines. This result is due to a smaller relaxation of dielectric permittivity in 67BNT33BKT than that of PLZT9. Therefore, in high speed driving devices, such as optical modulator, 67BNT33BKT can be alternative new EO materials to PLZT9.

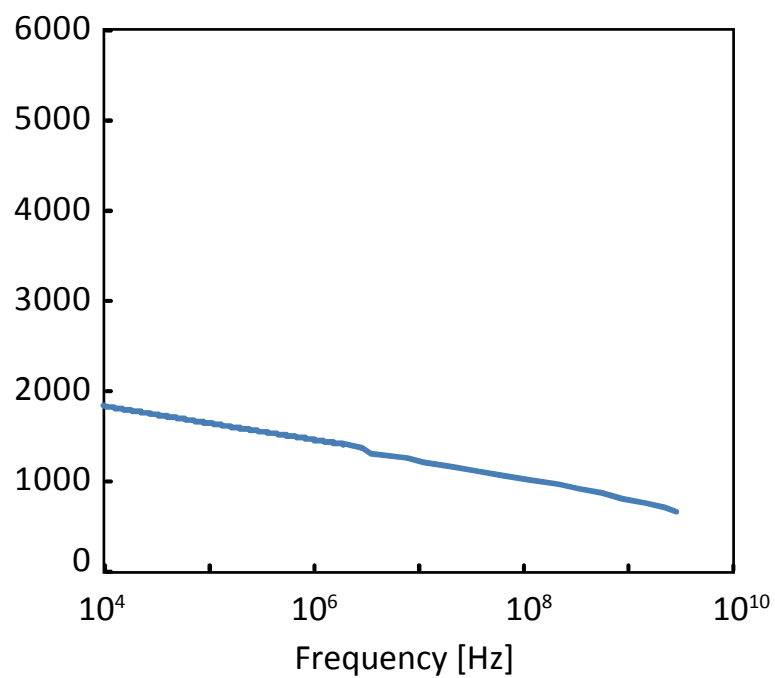


Fig. 6.9. Dielectric dispersion of 67BNT33BKT single crystal up to 3GHz.

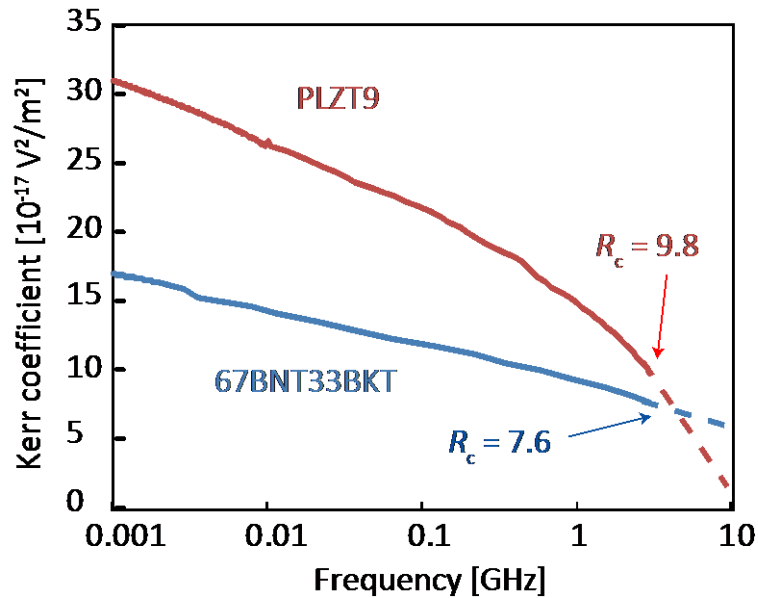


Fig. 6.10. Calculated results of frequency dependence of quadratic EO coefficient (Kerr coefficient) in PLZT9 ceramic and 67BNT-33BKT single crystal. Solid line is calculated result from observed values, broken line is extrapolated results from calculated result.

6.4 Summary of chapter 6

In this chapter, we demonstrated the EO property of lead-free 67BNT33BKT single crystal. 67BNT33BKT did not have initial birefringence. Relaxor behavior was observed in thermal dependence of dielectric permittivity. 67BNT33BKT indicated the highest EO coefficient of up to $1.6 \times 10^{-16} \text{ m}^2/\text{V}^2$ in lead-free materials in room temperature despite relatively low dielectric permittivity. This high EO coefficient R_c of 67BNT33BKT is due to relatively high photo-elastic coefficient. In high speed driving, 67BNT33BKT shows high EO coefficient R_c as same as PLZT9 at 3GHz driving, though

the EO coefficient R_c of PLZT9 is two times larger than that of 67BNT33BKT at low frequency. This result is due to a smaller relaxation of dielectric permittivity in 67BNT33BKT than that of PLZT9. We conclude that 67BNT33BKT can be alternative new EO materials to PLZT9 in high speed driving devices, such as optical modulators.

Reference

- [1] F. Koyama, K. Iga, J. Lightwave Tech. 6, 87 (1988)
- [2] T. Kawanishi, K. Kogo, S. Okikawa, M. Izutsu, Opt. Communications 195, 399 (2001)
- [3] A. Djupsjobacka, Photonics Tech. Lett. 4, 41 (1992)
- [4] S. Zhang, T. Shrout, H. Nagata, Y. Hiruma, T. Takedana, Trans. Ultrasonics, Ferroelectrics, and Frequency Control 54, 910 (2007)
- [5] Z. Yang, B. Liu, L. Wei, Y. Hou, Materials Research Bulletin 42, 81 (2008)
- [6] K. Yoshii, Y. Hiruma, H. Nagata, T. Takenaka, Japanese J. Appl. Phys. 45, 4493 (2006)
- [7] T. Yu, K. Kwok, H. Chan, Mat. Lett. 61, 2117 (2007)
- [8] W. Zhao, H. Zhou, Y. Yan, D. Liu, Key Eng. Mat. 368, 1908 (2008)
- [9] A. Morishita, Y. Kitanaka, M. Izumi, Y. Noguchi, M. Miyayama, Key Eng. Mat. 445, 7 (2010)
- [10] K. Nakamura, J. Miyazu, M. Sasaura, K. Fujiura, Appl. Phys. Lett. 89, 131115 (2006)
- [11] K. Fujiura, K. Abe, ITE Technical Report 33, 7 (2009)
- [12] S. Toyoda, K. Fujiura, M. Sasaura, K. Enbutsu, A. Tate, M. Shimokozono, H. Ushimi, T. Imai, K. Manabe, T. Matsuura, T. Kirihara Jpn J. Appl. Phys. 43, 5862 (2004)
- [13] C. Kirkby, Ferroelectrics 37, 567 (1981)
- [14] P. D. Thacher, J. Appl. Phys. 41, 4790 (1970)
- [15] G. Haertling, Ferroelectrics 75, 25 (1987)
- [16] T. Fujii, T. Suzuki, Y. Fujimori, T. Nakamura, M. Moriwake, H. Takasu, Jpn. J. Appl. Phys. 45, 7520 (2006)

- [17] D.Y. Wang, C. L. Mak, K. H. Wong, H. L. W. Chan, C. L. Choy, *Ceram. International* 30, 1745 (2004)
- [18] J. Li, F. Diewer, C. Gao, H. Chang, X. Xiang, *Appl. Phys. Lett.* 76, 769 (2000)
- [19] D. Kim, S. Moon, E. Kim, S. Lee, J. Choi, H. Kim, *Appl. Phys. Lett.* 82, 1455 (2003)
- [20] D. Wang, J. Wang, H. Chan, C. Choy, *Integrated Ferroelectrics* 88, 12 (2007)
- [21] J. Qiu, Q. Jiang, *J. Appl. Phys.* 102, 074101 (2007)
- [22] D. Wang, S. Li, H. Chang, C. Choy, *Appl. Phys. Lett.* 96, 061905 (2010)
- [23] A. Hussain, C. Ahn, J. Lee, A. Ullah, I. Kim, *Sensors and Actuators A* 158, 84 (2010)

Chapter 7

Summary

An origin of electro-optic effect was elucidated through the solution of three issues: conventional theory did not consider (i) the influence of strain, (ii) relatively high EO coefficient in relaxor materials, and (iii) the relaxation in frequency dependence of EO coefficient. Furthermore, the Bi-based relaxor was developed as novel EO material based on the principle derived in this study. The results obtained in this study are summarized as follows for each chapter.

In chapter 1, "Introduction"; from a literature survey, the background, the present problems and the objective were described.

In chapter 2, "Electro-optic effect and piezoelectric resonance"; the equation for apparent EO effect around piezoelectric resonance frequency was formularized. Good agreement was obtained between the observed and calculated results, this result indicated e formularized equation is reliable. We conclude that the apparent EO-coefficient is due to retardation from (i) clamped Pockels effect, (ii) change of light

path length, (iii) Photo-elastic effect, and contribution of phase lag between piezoelectric displacement and applying electric field. In these effects, the photo-elastic effect mainly contributed to EO effect that means the change of refractive index due to lattice distortion is notable contribution. Therefore we conclude that the photo-elastic coefficient must be considered as parameter for material search in order to solve the problem (iii).

In chapter 3, “Electric field dependence of birefringence and dielectric permittivity”; the electric field dependence of dielectric permittivity (dielectric tunability) and birefringence (electro-optic effect) were measured and the relation of polarization and birefringence variation with varying the electric field was discussed to figure out why the relaxor materials indicated relatively high electro-optic effect. We found out the polarization change gave rise to the change of birefringence from the different result of birefringence before and after electric field applying. But a material exhibiting a high dielectric tunability did not always exhibit a high EO effect that implied that the polarization change was only one factor to realize a high EO effect. We proposed that a weight of ions constituted EO materials is also one of key factors because the materials with heavy ions indicate high refractive indices. Nonlinear response appearing in the expansion series of susceptibility with respect to electric fields normally increases with linear susceptibility, which means that the nonlinear response giving rise to EO effect increases with refractive index.

In chapter 4, “Relaxation and frequency dependence of electro-optic

coefficient”; an equation for EO effect including an influence of dielectric permittivity was derived to elucidate the parameter determined the frequency dependence and relaxation of EO coefficient. The equation derived in chapter 4 indicated that the EO coefficients are a product of EO coefficient g , dielectric permittivity, and spontaneous polarization. From the comparison of calculated and observed results in the EO coefficient and dielectric permittivity at high speed driving, we conclude this expanded equation is reliable. We conclude that the relaxation of driving efficiency due to EO effect is mainly cause by the relaxation of dielectric permittivity due to relaxation of polarization. Thus, frequency dependence of EO effect was determined by the dielectric permittivity and spontaneous polarization. EO coefficient g remains constant with varying the frequency of applied electric field. Therefore we conclude that the EO coefficient g must be employed as parameter for material search in order to except the influence of frequency dependence and solve the problem (i).

In chapter 5, “Lattice distortion and variation of birefringence”; the EO coefficient g was determined as a product of the photo-elastic and electrostrictive coefficient from the equation formularized in this study. And the Clausius-Mossotti relation indicated the tendency that the materials with heavy ions indicated high photo-elastic effect. And the electrostrictive coefficients were already reported that they were almost same in any materials. Therefore the materials with heavy ions show high EO coefficients g because of their high photo-elastic effect. And finally, the origin of EO effect was interpreted as three effects: (i) the variation of polarization caused by

application of electric field, (ii) the lattice distortion induced by polarization, and (iii) the photo-elastic effect due to lattice distortion.

In chapter 6, “Electro-optic effect of Bi-based relaxor”; we demonstrated the EO property of lead-free 67BNT33BKT single crystal. As a result of chapter 2 to 5, we concluded that the EO materials must fulfill the two features: (i) low permittivity, and (ii) relaxors constituted by heavy atoms. Furthermore, EO materials should be isotropic to prevent chirping that is wavelength shift by passing through the EO materials. And lead-free materials are better because they can prevent to a pollution of lead toxicity. 67BNT33BKT single crystal is constituted by heavy ion Bi. The dielectric permittivity of 67BNT33BKT single crystal is low at all compositions. Moreover it shows relaxor behavior. Therefore, 67BNT33BKT single crystals satisfy all demands for new EO materials with high EO properties. 67BNT33BKT indicated the highest EO coefficient of up to $1.6 \times 10^{-16} \text{ m}^2/\text{V}^2$ in lead-free materials in room temperature despite relatively low dielectric permittivity. This high EO coefficient R_c of 67BNT33BKT is due to relatively high photo-elastic coefficient. In high speed driving, 67BNT33BKT shows high EO coefficient R_c as same as PLZT9 at 3GHz driving, though the EO coefficient R_c of PLZT9 is two times larger than that of 67BNT33BKT at low frequency. This result is due to a smaller relaxation of dielectric permittivity in 67BNT33BKT than that of PLZT9. We conclude that 67BNT33BKT can be alternative new EO materials to PLZT9 in high speed driving devices, such as optical modulators.

List of Publications

List of Reviewed Articles

- 1) Birefringence and Electro-optic effect in epitaxial BST thin films, K. Takeda, T. Muraishi, T. Hoshina, H. Kakemoto and T. Tsurumi, Mat. Sc. Eng. B, 161, (2008), pp61-65 (Chapter 3)
- 2) Dielectric tunability and electro-optic effect of $Ba_{0.5}Sr_{0.5}TiO_3$ thin films, K. Takeda, T. Hoshina, H. Takeda and T. Tsurumi, J. Appl. Phys., 107, (2010), pp074105-074111 (Chapter 3)
- 3) Electro-optic effect of Lithium Niobate in piezoelectric resonance, K. Takeda, T. Hoshina, H. Takeda and T. Tsurumi, Submitted to J. Appl. Phys., (Chapter 2)
- 4) Relation between electro-optic effect and dielectric permittivity of $Ba_{0.5}Sr_{0.5}TiO_3$ thin films, K. Takeda, T. Hoshina, H. Takeda and T. Tsurumi, Submitted to Key Eng. Mat., (Chapter 3, 5)
- 5) High electro-optic Kerr effect in Bi-based relaxor single crystals, K. Takeda, T. Hoshina, H. Takeda and T. Tsurumi, Submitted to Jpn J. Appl. Phys., (Chapter 6)
- 6) Role of photo-elastic constant in electro-optic effect of ferroelectric and related materials, K. Takeda, T. Hoshina, H. Takeda and T. Tsurumi, To be submitted to Appl. Phys. Lett., (Chapter 5)

List of Presentation at International Conferences

1. K.Takeda, T.Muraishi, T.Hoshina, H.Kakemoto, and T.Tsurumi " Correlation between electro-optical coefficient and dielectric permittivity of BST thin film" 17th International Symposium on Applications of Ferroelectrics (ISAF2007) (2007, Feb.)

List of Publications

2. K.Takeda, T.Muraishi, T.Hoshina, H.Kakemoto and T.Tsurumi "Electro-optic effect and dielectric tunability of BST thin film" 2nd International Conference on Science and Technology for Advanced Ceramics and the 1st International Conference on Science and Technology of Solid Surface and Interface (STAC2-STSI1) (2008, May)
3. K.Takeda, T.Hoshina and T.Tsurumi "Piezoelectric Constant and Electro-optic Coefficient of LN Single Crystal at Resonance Frequency" International Union of Material Research Society-International Conference in Asia 2008 (IUMRS-ICA2008) (2008, Dec.)
4. K. Takeda, T. Hoshina, H. Takeda and T. Tsurumi " Analysis of Electro-optic Effect Originated from Piezoelectric Displacement in LiNbO₃ Single Crystal near Resonance Frequency" The IMF-ISAF-2009, a joint meeting of 12th International Meeting on Ferroelectricity and 18th IEEE International Symposium on Applications of Ferroelectrics(ISAF2009) (2009, Aug.)
5. K.Takeda, T.Hoshina, H.Takeda and T.Tsurumi "Electro-optic Effect around Piezoelectric Resonance Frequency" The 10th Russia/CIS/Baltic/Japan Symposium on Ferroelectricity(RCBJSF10) (2010, Apr.)
6. K.Takeda, T.Hoshina, H.Takeda and T.Tsurumi "Correlation between the Electro-optic Effect and Piezoelectric Effect around Resonance Frequency" Ceramic Interconnect and Ceramic Microsystems Technologies 2010(CICMT2010) (2010, Apr.)
7. K.Takeda, T.Hoshina, H.Takeda and T.Tsurumi "Analysis in the frequency dependence of electro-optic effect" The 3rd China-Japan Meeting on Ferroelectric Materials and Their Applications(China-Japan FMA-3) (2011, Nov.)

Acknowledgement

I would like to thank my advisor, Professor Takaaki Tsurumi, for providing me the opportunity to work on this exciting field of electro optic effect. I remember being challenged and inspired by Prof. Tsurumi from the first day I met him. Prof. Tsurumi's genuine optimism reminded me to think positively and not to give up too early, which will be an invaluable attitude if one day I start an entrepreneurial journey myself. I could not be more grateful to Prof. Tsurumi as he understood my struggles and conflicts during the years at TITech and tried to help whenever possible.

I am greatly honored to have acquaintances with many authority researchers in this research field such as associate Professor Hiroaki Takeda of Tokyo institute of Technology, assistant professor Takuya Hoshina of Tokyo institute of Technology, Professor Clive A. Randall of Pennsylvania State University, Professor Satoshi Wada of Yamanashi University, Dr. Takashi Teranishi of Okayama University, Dr. Naohiro Horiuchi of Tokyo Medical and Dental University, and so on. They gave me invaluable suggestions and advices as much as their heartfelt encouragement. I sincerely express my gratitude to their mentorship.

I wish to express my sincere gratitude to my family. My parents have always loved me and encouraged me with generous assist and great hope. My grandparents have always been side with me and watching my growth. I'm proud of being their son.

Jan. 5, 2012

Kotaro Takeda